UiT
THE ARCTIC UNIVERSITY OF NORWAY

Faculty of science and technology

Metamorphic conditions in the Coastal-Punta del Este Terrane of the Kaoko-Dom Feliciano Belt in Namibia and Uruguay

—

Ida Grindal Skagseth

Master thesis in geology, GEO-3900

June 2016

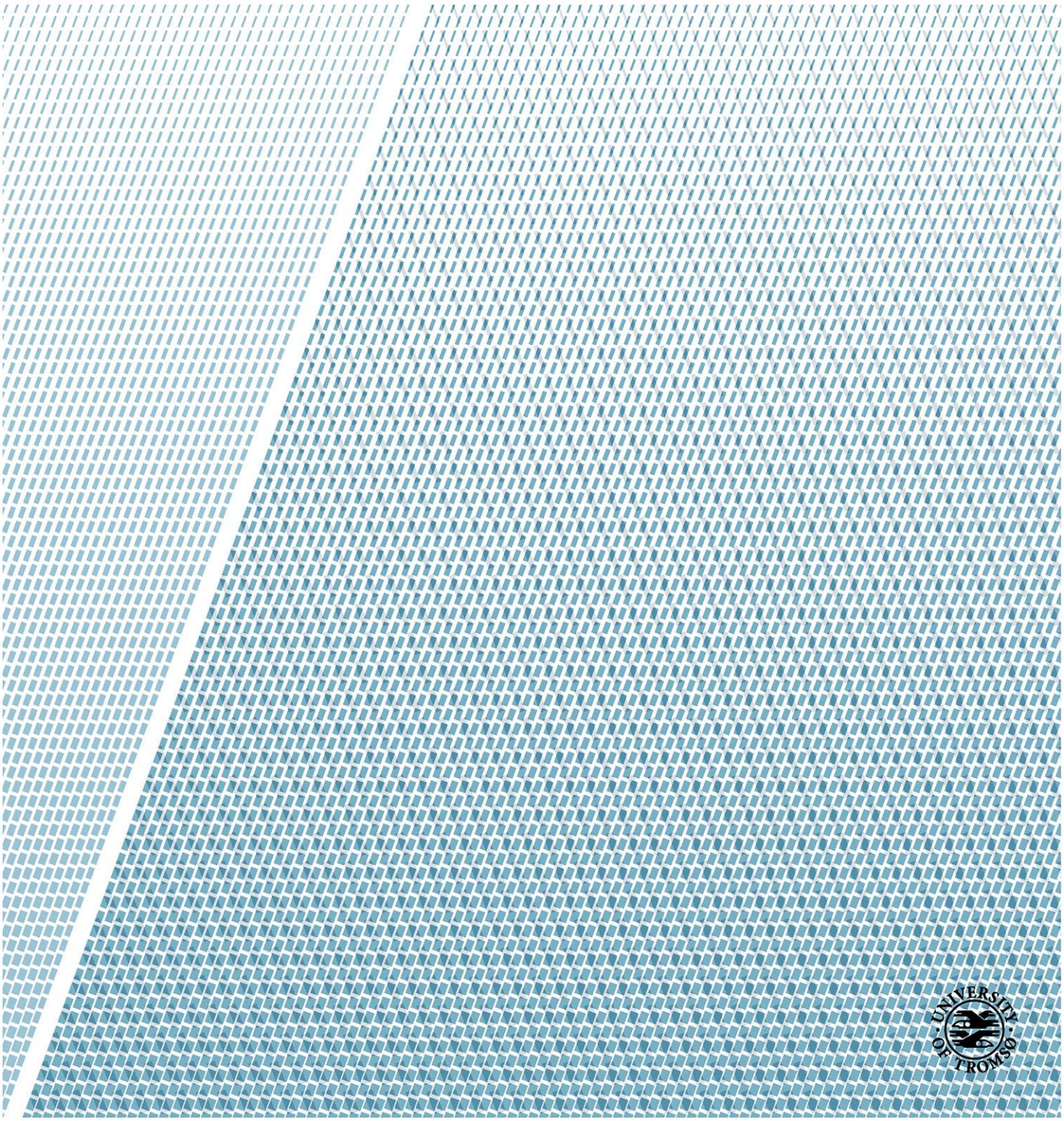

Acknowledgments

First, I would like to thank my supervisor Jiří Konopásek for being a fantastic help to me. You been so patient with me throughout this project, and given me many good advices. To the staff at the lab at the Institute for Geology in Tromsø, thank you for all the help. Thanks to Muriel at UiO for helping me with the microprobe analysis. A special thanks to Carly Faber for helping me at the end.

To my friends in Tromsø, you have made these years here some of the best. Carina, we have shared an office and managed to abstain from killing each other despite all the frustration, I call that a win. To Heidi for all the laughs and fun Sundays. Tonje, you rock.

To my friends back home. No matter where we are, when we meet up after ages apart, it is as if no time had passed. Thank you for being you.

Mamma, thank you for being the best mom. Pål, I am happy that you are my brother, and thanks for the help with my computer problems.

Pappa, I wish you were here.

Ida Grindal Skagseth

Tromsø, June.2016

Abstract

The metasediementary rocks of the Coastal Terrane in the Kaoko Belt (Namibia) and the meta-igneous rocks of the Punta del Este-Terrane in the Dom Feliciano Belt (Uruguay) both share one high-grade metamorphic event at approximately the same time of c. 650-630 Ma.

Metamorphic conditions of this high-grade event were estimated in four samples from the Punta del Este Terrane and two samples from the Kaoko Belt. The P-T conditions recorded in the Punta del Este Terrane yielded temperatures of c. 830-860°C and pressure of c. 7,5-10,5 kbar in one sample, whereas other two gave temperatures of c. 630-800°C and pressure of c. 3,0-4,5 kbar. One sample suggests temperatures of c. 780-790C and pressures lower than 2,8 kbar. The samples from the Kaoko Belt yielded P-T conditions of c. 580-640 and c. 2,5-7,5 kbar.

It was previously suggested that the Punta del Este Terrane in Uruguay and the Coastal Terrane in Namibia represent one tectonic unit dissected by the Atlantic Ocean. The P-T conditions of the samples from the Coastal Terrane indicate that this unit could represent its upper crustal part of the same tectonic unit as the middle- to lower-crustal samples from Punta del Este Terrane.

Contents

1 Introduction and aim of the work

(Porada, 1979) provided the first correlation of the Pre-Mesozoic geology of southeastern Brazil/Uruguay and Namibia when describing the similarities between the Dom Feliciano, Kaoko and Gariep belts based on the geological evolution of these units (Fig 1). The Coastal Terrane of the Kaoko Belt was correlated with the Punta del Este Terrane in the Dom Feliciano Belt by Gross et al. (2009), Oyantçabal et al. (2009) and Lenz et al. (2011). This was based on the presence of igneous rocks with an age of ca. 800-770 Ma that are present in both terranes and were metamorphosed in the granulite facies at ca. 650-630 Ma. Such temporal and tectonic evolution is unique to the Dom Feliciano-Kaoko-Gariep orogenic system, and thus provides a good basis for the spatial correlation of the units across the Atlantic Ocean (Goscombe et al., 2008; Konopásek et al., 2016).

The lithology of the Coastal Terrane of the Kaoko Belt in Namibia is represented by metamorphosed volcano-sedimentary rocks, which probably represented the upper-crustal rocks of the Coastal-Punta del Este Terrane during its high-grade metamorphism at 650-630 Ma. The Punta del Este Terrane (PET) crops out in the easternmost part of the Dom Feliciano Belt in Uruguay. It is comprised mostly of meta-igneous rocks such as granulitic gneisses and granulites, which suggest a middle- to lower-crustal position during metamorphism.

The aim of this project was to analyse samples collected from both parts of the Coastal–Punta del Este Terrane and establish the metamorphic conditions for the northern (Kaoko) and the southern (PET) part of the unit. The estimated metamorphic conditions allowed comparison of apparent thermal gradients that existed during metamorphic peak in the northern and southern part of the unit, as well as in different depth levels of the crust.

With the use of optical microscopy on available samples from the Coastal Terrane and the Punta del Este Terrane, several samples were chosen for further analysis. The samples selected were analysed with electron microprobe and SEM (Scanning Electron Microscope) to identify mineral composition, compositional zoning across minerals and chemical differences between similar minerals that occupy different textural positions. P-T pseudosections were calculated from the whole-rock chemical data by using the software package Perple_X (Connolly, 2005; 2009).

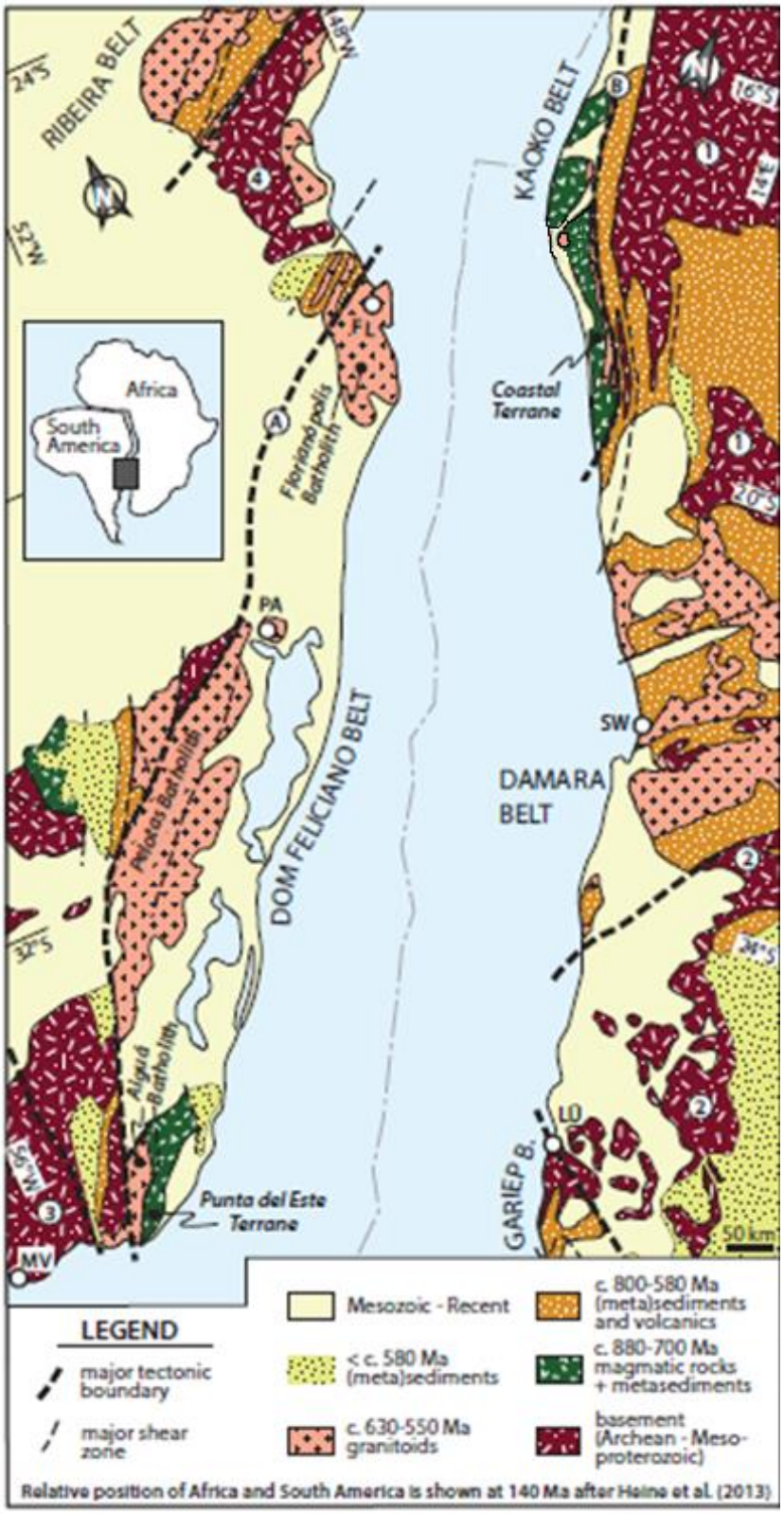

Fig 1. Simplified geological map of the Dom Feliciano, Ribeira Damara and Kaoko belt, (modified after Gross et al., 2011) Meta(cratonic domains: 1-Congo Craton; 2-Kalahari Craton; 3-Rio de la Plata Craton; 4-Luis Alves Terrane. A-Sierra Ballena-Dorsal Cangucu-Major Gercino shear zone; B-Village-Three Palm shear zone system. MV-Montevideo; Pa-Porto Alegre; FL-Florianópolis; LÜ-Lüderitz; SW-Swakopmund. Modified from Konopasek et al. (2016).

2 Regional Geology

2.1 Geological History

At the breakup of the Rodinia supercontinent in the Neoproterozoic, a north-trending narrow rift basin formed between the Rio de la Plata and the Congo cratons (Fig 2.3.1). The basin filled with eroded continental crust and syn-sedimentary volcanic rocks dated at c. 800 Ma. Based on the age of the intrusions, the rift-phase took place approximately between c. 830-710 Ma and the setting changed from extensional to compressional at around c. 650-630 Ma (Konopásek and Sláma 2016).

The supercontinent Gondwana was formed by numerous continental collisions in late Neoproterozoic. It was fully assembled at the end of Neoproterozoic time (c. 550 Ma) and comprised mostly of present-day South America, Africa, India, Australia and Antarctica (Meert et al., 1997).The Neoproterozoic linear orogenic belts formed by the same tectonic processes that occur at the present day. Such tectonic processes include seafloor spreading, ophiolite obduction, subduction and continental collision (Woodcock et al., 2009).

The Ribeira and Dom Feliciano belts (Fig 2.3.1) in South America represent the result of the Neoproterozoic orogeny that happened between the Congo/São Francisco, Paranapanema, Rio de la Plata and Kalahari cratons. In the area of southeast South America and southwestern Africa, the Brasiliano/Pan African (620-900 Ma) and Rio Doce (530-620 Ma) orogenies are documented by metamorphic belts and remnants of magmatic arcs. These can be found in the Ribeira and Dom Feliciano Belts (Basei et al., 2000). On the other side of the South Atlantic, the equivalent African belts are the Kaoko, Damara, Gariep and Saldania (Basei et al., 2010).

South America

2.2 The Rio de la Plata Craton

The Rio de la Plata Craton (Fig 2.3.1), located in South America, is the western cratonic foreland of the Dom Feliciano Belt and is divided into two terranes, the Piedra Alta Terrane and the Nico Pérez Terrane (Fig 2.3.1). These two terranes are separated by the Sarandi del Yi Shear Zone. West of the shear zone is the Piedra Alta Terrane, which is a juvenile Palaeoproterozoic terrane dominated by granitic rocks with the presence of two small low- to medium grade volcano-sedimentary belts. The age of the Piedra Alta Terrane is early Palaeoproterozoic and it was not affected by the Neoproterozoic events. The Nico Pérez Terrane is located between the Sarandi del Yi and Sierra Ballena Shear Zones. This terrane is of Archaean to Palaeoproterozoic age; it was reworked during the Neoproterozoic and can be considered as a metacraton. It comprises several basement blocks of gneisses and granulitic rocks covered by a metasedimentary platform successions and foreland basin deposits of the Dom Feliciano Belt (Oyhantcabal et al., 2009).

2.3 The Dom Feliciano Belt

The Dom Feliciano Belt (Fig 2.3.1) is located east of the Rio de la Plata Craton in the south-eastern part of Brazil and the northern part of Uruguay, and is a product of successive subductions and collisions. It is a broad region, 1200 km long and 150 km wide, and it strikes sub-parallel to the southern Brazilian and Uruguayan coastline (Basei et al., 2011). The basement of the Dom Feliciano Belt was affected by metamorphic processes and intruded by granitic batholiths during the Neoproterozoic. The Dom Feliciano Belt can be divided into three units representing three crustal segments, from east to west, the Granite Belt, the Schist Belt and the Foreland Belt (Fig 2.3.1)(Basei et al., 2000).

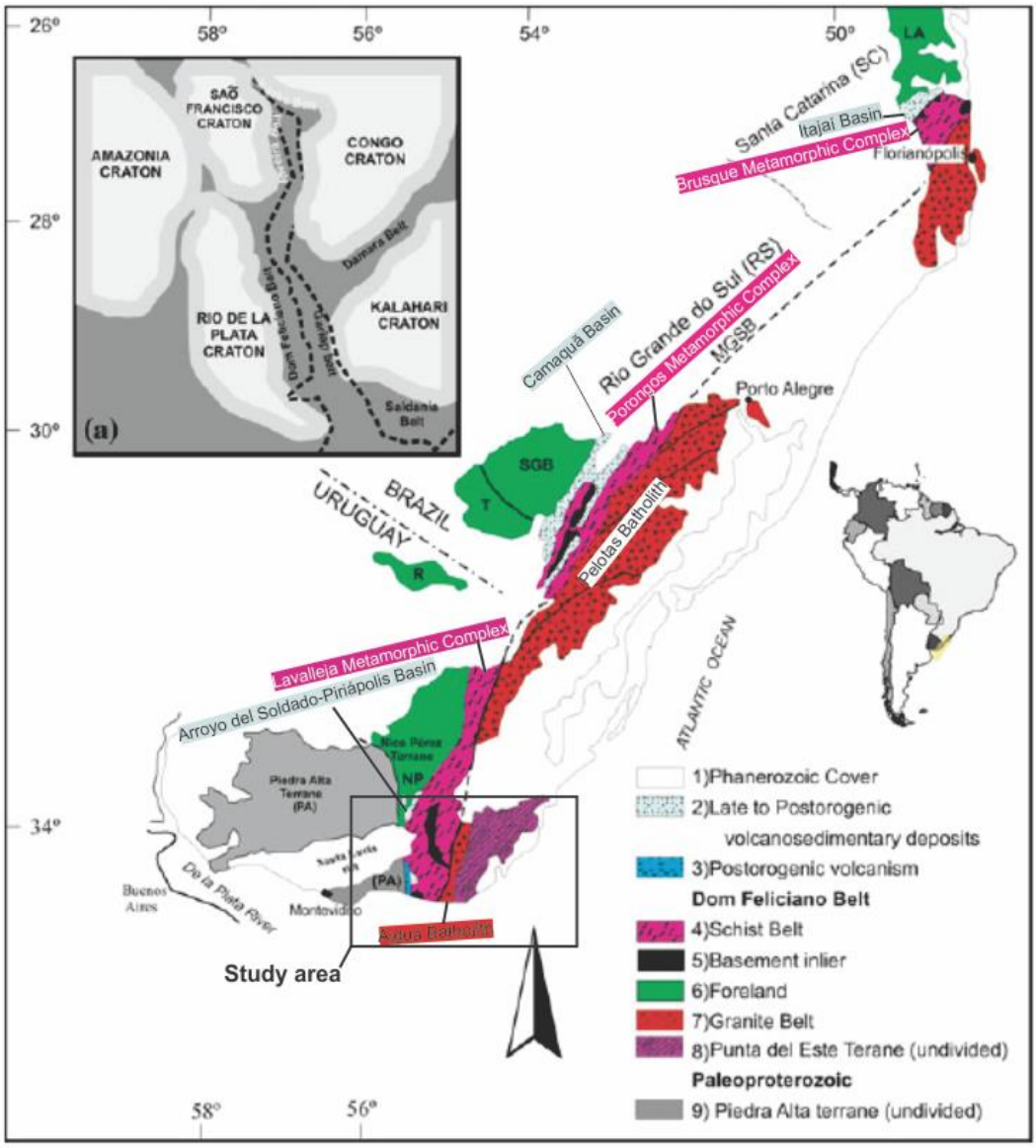

Fig 2.3.1. a) Paleogeographic outline showing the arrangement of the major orogenic belts and cratons. b) Geological sketch of Southern Brazil and Uruguay. Study area is shown in the box. (Modified from Basei et al. 2010)

2.3.1 The Granite Belt

The Granite Belt (Fig 2.3.1) is divided into three units located in the Santa Catarina state (Brazil), Rio Grande do Sul state (Brazil), and in Uruguay (Oyhantcabal et al., 2009). They are named from north to south as the Florianópolis, Pelotas and Aiguá batholiths, respectively (Preciozzi et al., 2001). They are dominated by post-tectonic alkaline granites that are intrusive into calk-alkaline orogenic granitoids The Granite Belt is interpreted as the result of post-collisional magmatism during transcurrent deformation or as the roots of a magmatic arc (Oyhantcabal et al., 2009).

2.3.1.1 Aiguá Batholith

The Aiguá Batholith (Fig 2.3.1) is located in Uruguay and it is built of granitoid rocks of Neoproterozoic age that can be correlated to the Pelotas Batholith. The two granitoids in the south of the Batholith (Cañas region) are of monzogranitic composition comprised of biotite and amphiboles in a quartz-rich matrix (Basei et al., 2000).

2.3.2 The Schist Belt

The Schist Belt (Fig 2.3.1) covers the Nico Pérez Terrane in Uruguay, and is represented by low-grade supracrustal rocks called the Lavalleja Complex in Uruguay, and it continues into Brazil where it is known as the Porongos and Brusque Metamorphic Complexes. These complexes comprise metasediments and metavolcanic rocks of greenschist to lower-amphibolite facies metamorphic conditions. The age of these three sequences are Neoproterozoic (Oyhantcabal et al., 2009).

2.3.2.1 Lavalleja Metamorphic Complex

The Lavalleja Metamorphic Complex (Fig 2.3.1) is located in Uruguay in the southernmost part of the Schist Belt and can be divided into three supracrustal units, from east to west, Zanja del Tigre, Fuente del Puma and Minas Formations. There is a decrease in the metamorphic grade from east to west, from low amphibolite, greenschist to very low (anchimetamorphic) grade in the northwestern region (Basei et al., 2000; Preciozzi et al., 2001). The Lavalleja Complex is separated from the Porongos and Brusque Complexes by the NNW-trending Sarandi del Yi-Pirípolis mega Shear Zone and in the eastern domain the complex is marked by the transcurrent NE-trending strike slip Sierra Ballena Shear Zone (Lenz et al., 2011). The Zanja del Tigre Formation is overlain by the metavolcano-sedimentary Fuente del Puma formation, and corresponds to a metavolcano-sedimentary sequence that is made of gabbros and amphibolites, hosted by mica schists and marbles (Basei et al., 2000). The upper Minas Formation is comprised solely of sedimentary rocks like metapelites, quartzites and arkoses, with limestones that include stromalitic units (Basei et al., 2000).

2.3.3 The Foreland Belt

Oyhantcabal et al. (2009) described the Foreland Belt (Fig 2.3.1) as comprised of several successions of sedimentary and volcano-sedimentary rocks. The Foreland Belt is made up of several foreland basins that form a narrow belt with a parallel trend the Dom Feliciano Belt, the basins are named north to south, Itajaí, Camaquã and El Soldado-Piriápolis (Basei et al., 2000). Based upon their sedimentary characteristics, these basins may have been interlinked during the Vendian-Cambrian (650- 485 Ma) by a sea opening southwestward (Basei et al., 2000).

Arroyo del Soldado-Piriápolis Basin:

The basins in Uruguay do not represent a typical transitional between the metamorphic-deformational climax of the adjacent metasedimentary belts and the installation of large Paleozoic intracratonic basins, but the Arroyo del Soldado Group has many of these characteristics. This Group is located in Uruguay and was deposited in the Proterozoic-Phanerozoic transition period. It is comprised of marine sediments deposited in shallow waters, resting as an angular unconformity on a metasedimentary basement and is approximately 5000 m thick (Basei et al., 2000).

Africa

2.4 Congo Craton

De Waeler et al. (2008) described the Congo Craton (Fig 2.4.1) as comprised of various Archean and Palaeoproterozoic blocks, flanked or truncated by orogenic belts. The Palaeproterozoic Rusizian, Ubendian and Usagaran belts consist of greenstone belts, granitoid gneisses, metasedimentary rocks and high-pressure eclogite facies rocks. The Mesoproterozoic Kibaran and Irumide belts are comprised of deformed basement metasedimentary units and granitoids, with volcanic rocks and felsic to mafic amphibolite-facies metavolcanic rocks. The Archean and Palaeoproterozoic blocks are magmatic complexes of orthogneisses and metasedimentary quartzites and schists (De Waele et al., 2008).

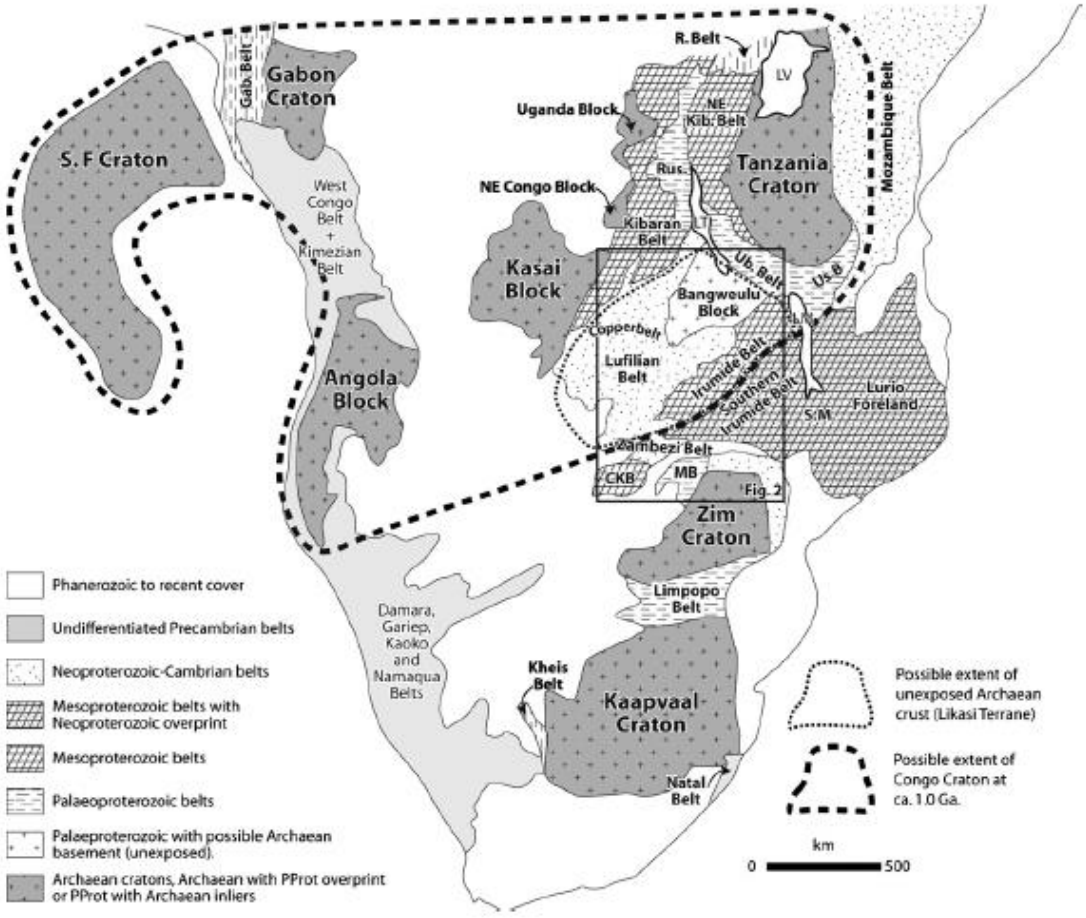

Fig 2.4.1. Simplified geological map of Sub-Saharan Africa. CKB: Choma Kalomo Block; Gab. Belt: Gabon Belt; LM: Lake Malawi; LT: Lake Tanganyika; LV: Lake Victoria; MB: Magondi; NE Kib Belt: Northeastern Kibaran Belt; R.Belt: Ruwenzori Belt; Rus: Rusizian; SF: São Francisco Craton; S.M.: Southern Malawi; Ub Belt: Ubendian Belt; Ub. Belt: Usagaran Belt. Waele et at (2008).

2.5 The Kaoko Belt

The Kaoko Belt (Fig 2.5.1) is a 400 km long Neoproterozoic belt extending from the borders of Angola in the north to the Ugab Zone in the south with a NNW-trend along the Atlantic coast. The belt has a basement of Archean, Paleoproterozoic and Mesoproterozoic metamorphic and igneous complexes (Jung et al., 2014). It is a result of a collision between the Congo and Kalahari Cratons in Africa, and the Rio de la Plata Craton in South America (Damara Orogeny) (Porada, 1979). Miller (1983) divided the Kaoko Belt into three zones based on tectono-stratigraphic observations; the Eastern Kaoko zone, the Central Kaoko zone and the Western Kaoko zone (Fig 2.5.1). Based on the age of the metamorphism of the Coastal Terrane, Goscombe et al. (2005) subdivided the Western Kaoko Zone into two units, the Orogen Core and the Coastal Terrane. The metamorphism increases from east to west, with lower greenschist facies in the Eastern Kaoko Zone to granulite (low-pressure, high temperature) facies in the Coastal Terrane. Konopasek et al. (2005) recognized three deformation events in the Kaoko Belt, the first two phases developed under ductile conditions, while the third phase occurred under brittle-ductile conditions. The Congo Craton basement is exposed in both the Eastern and Central Kaoko Zones and also in the Orogen Core, but it is missing in the Coastal Terrane.

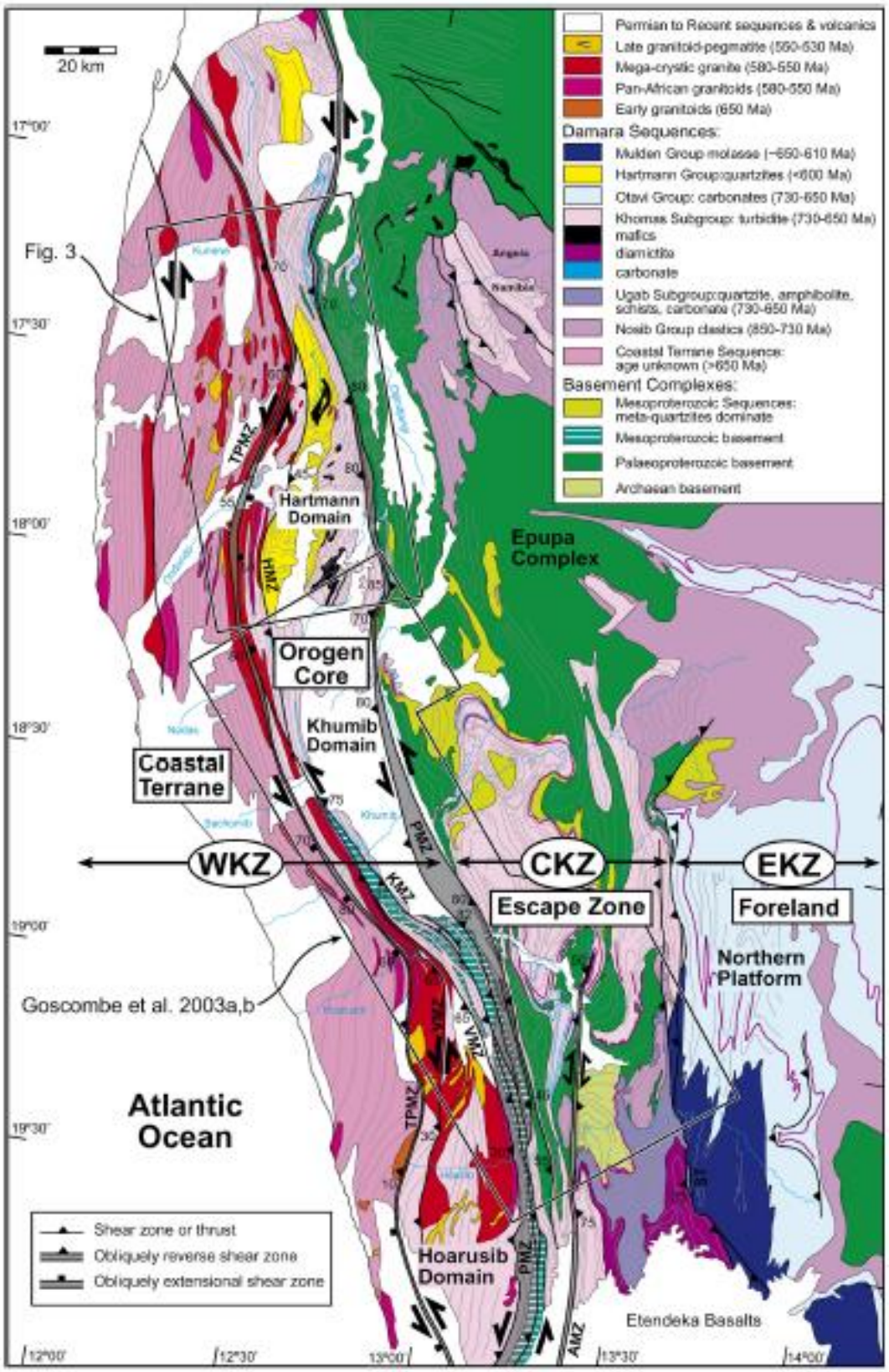

Fig 2.5.1. Geological and structural map of the Kaoko Belt showing outcrop traces of the major shear zones (bold lines) and traces of the dominant foliation (fine lines). EKZ: Eastern Kaoko Zone; CKZ: Central Kaoko Zone; WKZ: Western Kaoko Zone; TPMZ: Three Palms Mylonite Zone; HMZ: Hartmann Mylonite Zone; AMZ: Ahub Mylonite Zone; KMZ: Kuhib Mylonite Zone; PMZ: Puros Mylonite Zone. Map is from Goscombe and Grey (2008)

Damara Sequence (cover)

Goscombe et al. (2008) determined that the marine Damara sequence was deposited on top of the Congo Craton between approximately >770 and <600 Ma as a passive margin deposits and consists of the basal Nosib group and the Otavi Group. The Nosib Group is comprised of Neoproterozoic siliciclastics and has the minimum age of 750 Ma. The Otavi Group overlays the Nosib Group and is dominated by carbonates (in the Eastern Kaoko Zone), tubiditic meta-pelite, meta-greywacke and quartz-muscovite and mafic schists, calcsilicate and quartzite (in the Central and Western Kaoko Zones). The deposition was terminated by the orogenic phase that started at c. 580 Ma. The Damara Sequence was folded and overlain by the Mulden Group, which is a siliclastic molasse.

2.5.1 The Easter Kaoko Zone (EKZ)

Goscombe et al. (2008) named the Eastern Kaoko Zone (Fig 2.5.1) the Foreland and it is comprised of sub–greenschist, low-strain, Damara Sequence platform carbonates (Jung et al., 2014). These carbonates were deformed into upright folds and steep thrusts by east-west shortening during the Pan-African orogeny (Goscombe et al., 2008; Jung et al., 2014). Konopásek et al (2008) described that Eastern Kaoko Zone is representing the folded autochtonous sedimentary cover of the passive Congo Craton margin. The shallow dipping Sesfontein Thrust that formed under brittle conditions in the late Damara Orogeny marks the western margin of this zone where the metamorphic rocks of Kaoko Belt are thrust over the Congo Cratons unmetamorphosed sedimentary cover (Jung et al., 2014; Kröner, 2005). Goscombe et al. (2008) described the Sesfontein Thrust as a strand of an anastomosing and discontinuous network of thrusts that coincides with the transition to slope facies and interpreted it as a reactivated growth faults in the passive margin.

2.5.2 The Central Kaoko Zone (CKZ)

The Central Kaoko Zone or the Escape Zone (Fig 2.5.1) as named by Goscombe et al. (2003a), represents a fold-and-thrust-belt with a well-developed Barrovian metamorphic zonation with metamorphic grade ranging from lower-greenschist in the east to upper-amphibolite grade in the west (Jung et al., 2014; Konopásek et al., 2008). A prominent shear zone, the Purros Mylonite Zone (PMZ) runs the entire length of the Kaoko Belt west of the Central Zone (Jung et al., 2014). The Congo Craton basement is included in highly strained antiformal nappes or appears as broad low-strain basement windows variably reworked during the Pan-African orogeny (Goscombe et al., 2008).

The Puros Mylonite Zone

The Puros Mylonite Zone (Fig 2.5.1) represents the boundary between the Central and Western Kaoko Zones. The shear zone is continuous for at least 620 km, it extends the entire length of the Kaoko Belt, and ranges 1-5 km in width, with a heterogeneous network of several meters wide utlramylonitic shear zones that trend parallel with the main foliation (Konopásek et al., 2005).

2.5.3 The Western Kaoko Zone (WKZ)

The Western Kaoko Zone (Fig 2.5.1) is an area of shear zone-bounded amphibolite- to granulite-facies Damara Sequence rocks and Neoproterozoic granitoids that show a high degree of partial melting (Jung et al., 2014). Goscombe et al. (2005) divided this zone into two units: the Coastal Terrane and the Orogen Core (the margin of the Congo Craton). The Western Kaoko Zone stretches from the Atlantic Ocean in the west to the Puros Shear Zone in the east. Its western part is the Coastal Terrane that experienced high-temperature/low-pressure metamorphism during c. 650-630 Ma with a sinistral strike-slip deformation refolding an earlier metamorphic fabric (Konopásek et al., 2005). The eastern part of the Western Kaoko Zone is the Orogen Core unit showing silimanite- and cordierite-bearing low-pressure mineral assemblages in metasedimentary lithologies (Konopásek et al., 2005).

2.5.3.1 The Orogen Core

The Orogen Core (Fig 2.5.1) is a unit of shear zone-bounded panels of strongly deformed and migmatized deep water facies of the Damara sequence, Pan-African granitoids and antiformal Paleo-Mesoproterozoic basement slivers (Goscombe et al., 2008). It is ca. 20-40km wide and composed of three domains that have distinct lithostratigraphy and structural and metamorphic style. They are named from north to south: The Hartmann Domain, the Khumib Domain and the Hoarusib Domain (Goscombe et al., 2005b).

Hartmann Domain

The Hartmann domain (Fig 2.5.1*)* is located in the north of the Orogen Core and consists of three longitudinally aligned convex domains with distinct tectono-metamorphic character (Goscombe et al., 2008). This domain is made of Damara Sequence meta-turbidites, meta-greywacke, quartzites, meta-arkose, amphibolite and carbonate units where there is almost no basement exposed, and the sheared Pan-African granitiods are dominated by megacrystic granitic orthogneisses (Goscombe et al., 2008). The metamorphic grade ranges from upper amphibolite to granulite facies and the domain was intensely deformed by isoclinal folding, steep penetrative foliations and shear zones with sub-horizontal stretching lineations (Goscombe et al., 2005b).

Khumib Domain

The Khumib domain (Fig 2.5.1) is located in the central part of the Orogen Core. Goscombe et al. (2008) described the domain as consisting entirely of a monotonous sequence of turbiditic chevron folded Damara sequence meta-greywacke with meta-psammite and calc-silicate bands of lower amphibolite facies and minor carbonate units. The western part of this unit include the Khumib and Hartman Mylonite Zones.

Hoarusib Domain

The Hoarusib domain (Fig 2.5.1) is located in the southern part of the Orogen Core and consists of upper amphibolite to granulite grade gneisses in a narrowing elongated domain. Isoclinal folding, steep penetrative foliations and shear zones with sub-horizontal stretching lineations intensively deformed this domain. High-grade Damara Sequence meta-greywackes with minor mafic and carbonate units dominate the domain, with 40% being sheared Pan-African granitoids that form segregations, sills and map-scale lenticular plutons. The Hoarusib domain is bounded by the crustal-scale Puros Shear Zone to the east and the Three Palms Mylonite Zone to the west (Goscombe et al., 2005b; Goscombe et al., 2008).

3 Areas of interest

The areas of interest in the thesis are the Punta del Este- and the Coastal Terrane. These terranes have several similarities in both lithology and metamorphism. The Cerro Bori Gneisses of the Punta del Este Terrane show a high-grade metamorphic event that took place between c. 676±10 Ma and 666±1 Ma, while the migmatites in the Coastal Terrane of the Kaoko belt experienced metamorphism and partial melting at c. 650-630 Ma (Konopásek et al., 2008; Lenz et al., 2011). Two magmatic events have been recognised in these terranes, one older at ca. 700-800 Ma, and one younger at c. 580-550 Ma.

3.1 Punta del Este Terrane

The Punta del Este Terrane (Fig 3.1.1) is located in the easternmost part of the Dom Feliciano Belt, east of the Sierra Ballena Shear Zone. The Terrane is subdivided into two main units, the Cerro Olivo Complex and the Rocha group. The Punta del Este Terrane is also named the Cuchilla Dionísio Terrane (Gross et al., 2009; Lenz et al., 2011). It has been interpreted to be an allochtonous block that was accreted to the Rio del Plata Craton during the Cambrian (Lenz et al., 2011). The Punta del Este Terrane is comprised of orthogneisses, paragneisses, amphibolites and migmatites, and is considered as pre-Brasiliano basement (Oyhantcabal et al., 2009). Some of the granitic rocks of the Aiguá Batholith are emplaced into the Cerro Olivo Complex (Masquelin et al., 2012). The foliation in the gneisses is predominantly E-W to NW-SE and it is crosscut by both the Cordillera Shear Zone and the Alférez Shear Zone (Masquelin et al., 2012). Oyhantçabal et al. (2009) recognized three major events in the Punta del Este Terrane: (1) magmatic event at c. 850-750 Ma; (2) a high-grade metamorphism at c. 650 Ma; (3) magmatic event at c. 590-560 Ma.

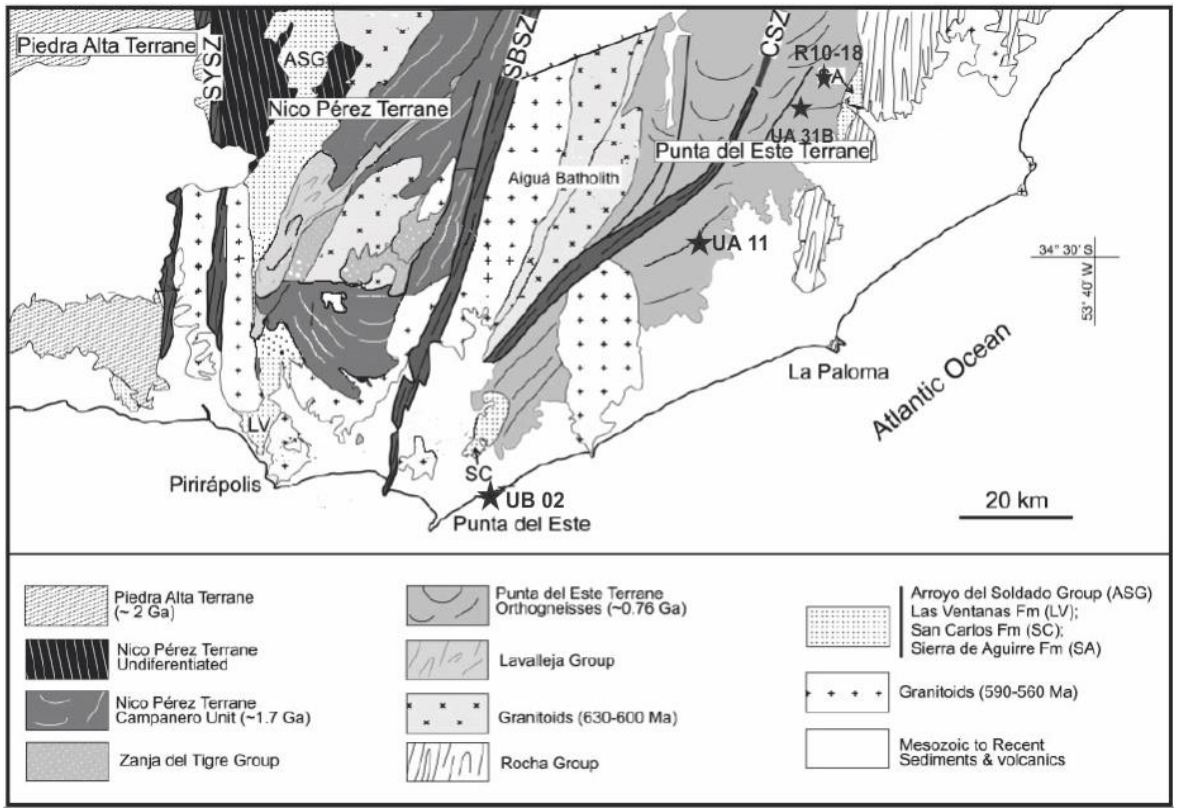

Fig 3.1.1. Geological map of the study area showing the main geological units and location of the studied samples (marked with stars)(modified from Oyhancabal et al. (2009).

3.1.1 Cerro Olivo Complex

The Cerro Olivo Complex (Fig 3.1.2) is a part of an older and reworked lower-crustal metamorphic complex that is the host rock for the Pelotas-Aiguá Batholith. Based on the age of zircons from the Cerro Bori orthogneisses, Lenz et al. (2011) concluded that the high-grade metamorphic event took place at c. 676-666 Ma. The older magmatic zircons (1.0-1.3 Ga) represents an old crustal material (cratonic sediments) that was involved in the partial melting before the collisional event (Masquelin et al., 2012). The Cerro Olivo Complex is subdivided into five units, four metamorphic and one plutonic named the Cerro Bori orthogneisses, the Centinela augen gneisses, the Manantiales gneisses, the Chafalote paragneisses, and the Piriz granodiorite (Masquelin et al., 2012).

3.1.2 The Cerro Bori orthogneisses

Masquelin et al. (2012) suggested that the Cerro Bori orthogneisses (Fig 3.1.2) may have been derived from tonalitic or granodioritic protoliths. They are medium-grained, dark to light grey foliated quartz-feldspathic rocks with a low volume of accompanying mafic/ultramafic rocks. The mineral assemblage of the tonalitic orthogneisses is plagioclase (20-50%), orthopyroxene (15-30%), microcline (5-10%), quartz (10-20%), and biotite (1-5%), with minor occurrence of

garnet, zircon, apatite and opaque minerals such as ilmenite, Ti-magnetite and pyrite. Veins of trondhjemite and pegmatite have injected this unit and they are often slightly deformed. Trondhjemite veins crosscut, or are parallel to, the foliation in the main biotite orthogneisses, and these orthogneisses are partially affected by low-temperature deformation that is represented by ribbon/lamellae of quartz and biotite selvages. Isolated boudins or massive lenses of mafic rocks are composed of fine (< 3mm) to coarse-grained (>1cm) foliated mafic granulites, with injections of thin leucocratic veins. The two main mafic mineral assemblages are: clinopyroxene, hornblende, plagioclase, or ±garnet, orthopyroxene, clinopyroxene, hornblende and a poikilitic/sympectite texture (Masquelin et al., 2012).

3.1.3 The Centinela augen gneisses

Masquelin et al. (2012) described the Centinela augen gneisses (Fig 3.1.2) as predominantly partially molten augen gneiss that is exposed in the Centinela Hill and the Punta del Este Peninsula. They are light pink, fine to coarse-grained felsic granitoids. The foliation is flat lying and coarse in texture with 5 cm wide mantled porphyroblasts with asymmetry that suggest a top to E-SE shear direction. The texture of this rock is porphyroblastic, and contains almandine porphyroblasts, subdiomorph plagioclase, and microperthitic K-feldspar or microcline. There is little chloritized-biotite and secondary muscovite in epitactic growth, and the gneiss also contains garnet porphyroblasts that are rounded and show resorbed grain boundaries. Other accessory minerals are rutile, apatite and zircon.

3.1.4 The Manantiales gneisses

These are high temperature mylonitic gneisses that crop out on the Atlantic coast of Manantiales and contain altering light- and dark-grey layers. The light-grey layers contain microperthitic K-feldspar, plagioclase, and flattened quartz lenses, while the dark-grey layers contain K-feldspar, quartz, garnet, biotite, and sillimanite (Masquelin et al., 2012).

3.1.5 The Chafalote paragneisses

This Chafalote paragneisses (Fig 3.1.2) are migmatitic metasedimentary rocks that intercalate with massive and layered mafic rocks. The most common lithotypes are quartzites, Grt-Bt-Pl semipelitic gneisses, Grt-Crd-Sp semipelitic layers, Grt-Sil-Crd-Bt semi-pelitic gneisses, Di-Wo calc-silicate gneisses, Ti-hornblende amphibolites, and Grt-bearing mafic granulites (Masquelin et al., 2012). According to Gross et al. (2009) this suite is less abundant than the Piriz and Centinela suites and is characterized more like as roof-pendants and xenoliths. The Chafalote paragneisses in the Rocha District can be divided into three compositional groups:

pelitic migmatites, semi-pelitic migmatites, and mafic granulites. The politic migmatites have a mineral assemblage made of mainly quartz-deficient layers with Grt+Crd+Bt+Spl+Sil+Pl+Ilm and interleaved with layers that are quartz-rich and bear mineral assemblage Grt+Crd+Bt+Qtz+Sil+Pl+Kfs+Ilm and garnet-bearing leucosomes. The semi-pelitic migmatites are biotite-rich layers with mineral assemblage Opx+Grt+Pl+Bt+Qtz with subordinate mafic granulites. These layers are interlayered with biotite-poor layers that include Grt+Pl+Qtz with minor Opx+Bt and lenticular Grt+Opx leucosomes. Dark, massive, fine grained mafic granulites occur interlayered with Grt+Bt and sillimanite-rich pelitic migmatites in the central areas and are characterized by the mineral assemblage Grt+Opx+Cpx+Pl+Qtz±Bt±Ilm (Gross et al., 2009).

3.1.6 The Piriz granodiorite

The Piriz granodiorite (Fig 3.1.2) cross-cuts the Cerro Bori orthogneisses. It is pale-grey medium-grained with a hypidiomorphic texture consisting of idiomorphic feldspar phenocrysts and a quartz-rich matrix composed of plagioclase and few microperthitic K-feldspars as phenocrysts, abundant quartz, biotite, muscovite, cordierite, and garnet (as xenocrysts, with sillimanite inclusions), with accessory minerals such as zircon, apatite, opaque minerals, monazite, and titanite (Masquelin et al., 2012).

3.1.7 Rocha Group

The Rocha Group (Fig 3.1.2) is a ca. 120 km long and 20-30 km wide, NE-trending belt that consists of metasedimentary rocks, predominantly metapelites to metapsammites that was mostly affected by greenschist facies metamorphism with locally occurring biotite schists. The area experienced a polyphase folding and displays NW-plunging structures and an eastward tectonic transport. Primary structures are preserved in the domains of lower metamorphic grade, such structures consist of cross and plane-parallel bedding, cross stratification, mud drapes and arenitic levels with graded bedding, and climbing ripples (Basei et al., 2010).

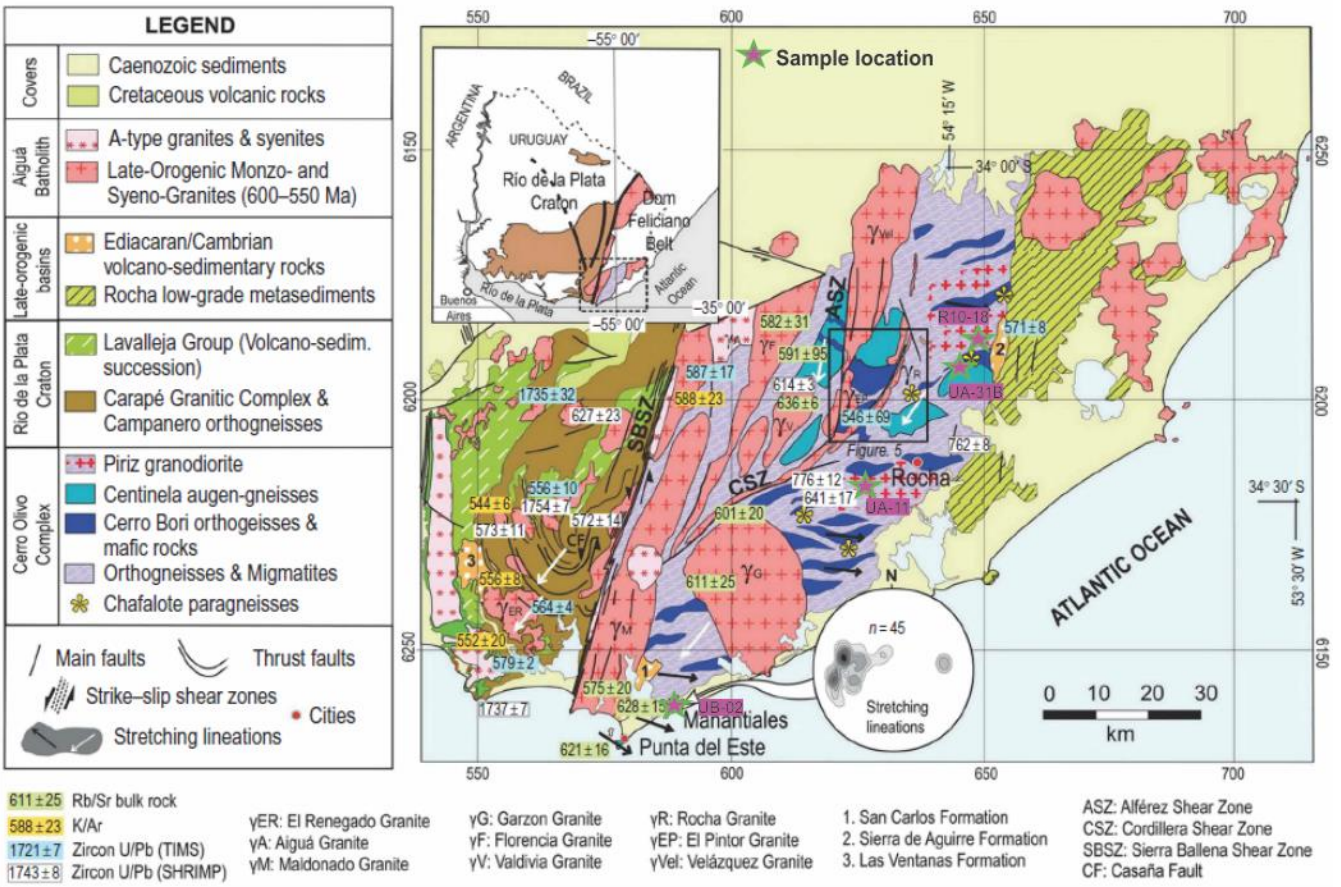

Fig 3.1.2. Geological map of the Dom Feliciano Belt in South-Eastern Uruguay. Left: Rio de la Plata Craton and Lavelleja-Porongos schist Belt; center: the Aiguá Batholith and the Cerro Olivo Complex; right: the Eastern schist Belt. Location of samples is marked with a star. Modified from Masquelin et al (2011).

3.2 The Coastal Terrane

The Coastal Terrane (Fig 3.2.1) is exposed in the wersternmost Kaoko Belt. It trends parallel to the Atlantic coast and it is separated from the Orogen Core by the Three Palm Mylonite Zone. The metasedimentary rocks of the Coastal Terrane are different from the rest of the Kaoko Belt. They are devoid of meta-pelites, carbonates and quartzites, but contain metamorhopsed feldspathic psammites and arkoses with greywackes and minor psammopelites (Goscombe et al., 2007). The rocks are of Neoproterozoic age, but reached partial melting conditions at c. 650-630 Ma, i.e. c. 80-100 Ma earlier than the underlying deformed cratonic margin (Goscombe et al., 2007). Konopasek et al. (2008) recognized three periods of magmatic activity in the Coastal Terrane. The earliest magmatic event is preserved as metamorphosed synsedimentary volcanics and plutonic bodies or their fragments, with ages older than c. 700 Ma. C. 650-630 Ma granitoid bodies define the second magmatic event associated with the peak of high-grade metamorphism in this unit. Granitoid bodies with ages of c. 580-550 Ma represent the final magmatic period, and these are temporally associated

with metamorphism and melting of the eastern part of the Western Kaoko Zone (Goscombe et al., 2008). Goscombe et al. (2005a) and Kröner (2005) concluded that the Coastal Terrane may represent an exotic terrane juxtaposed to the rest of the belt prior to the 580-550 Ma collision, based on the different ages of metamorphism between the Orogen Core and the Coastal Terrane, while Goscombe et al. (2008) suggested that the Coastal Terrane could possibly have represented a back-arc basin.

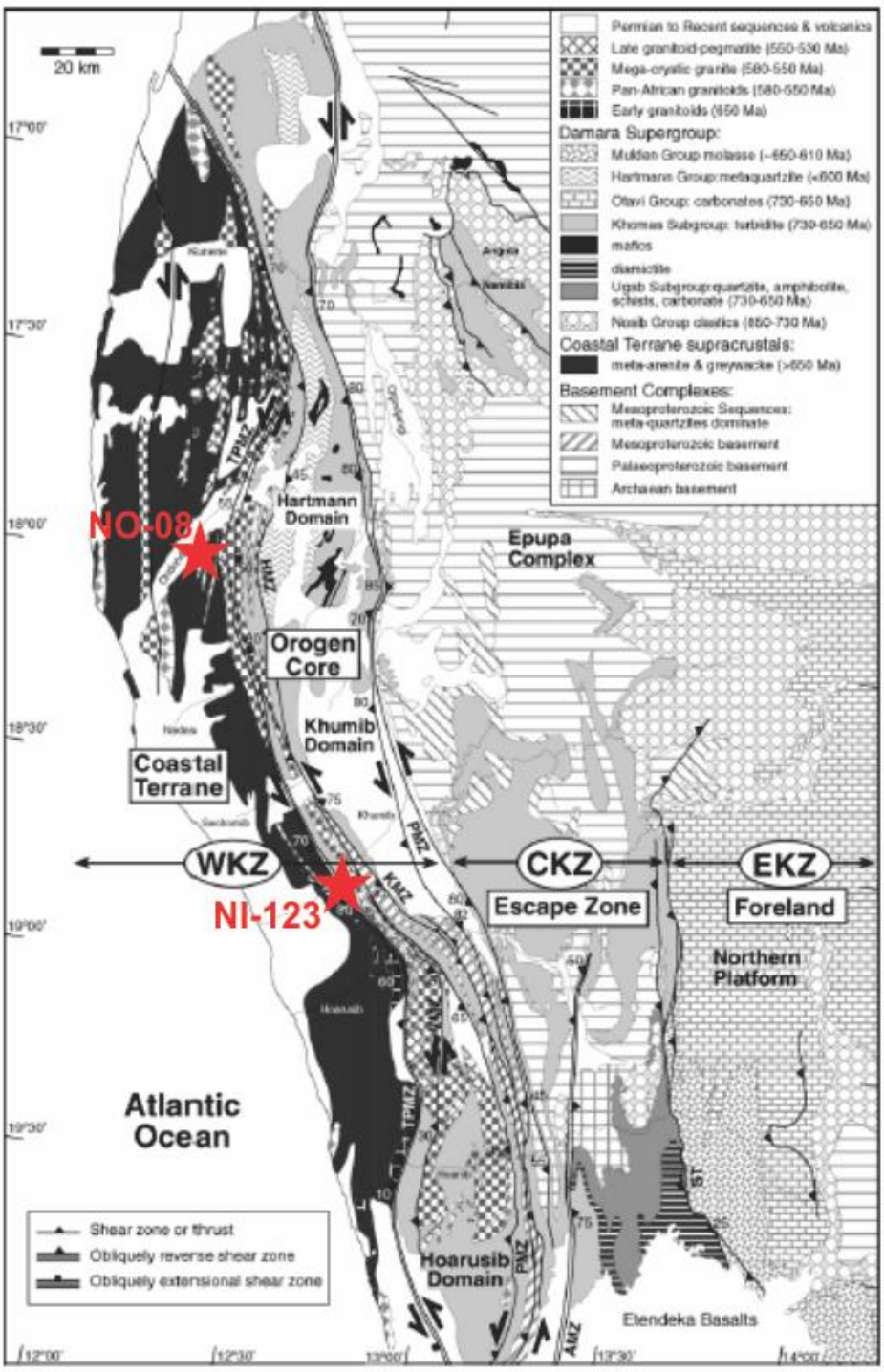

Fig 3.2.1. Geological map of the Kaoko Belt showing the location of the samples (marked with red stars) (modified from Goscombe et al.2007)

4 Methods

4.1 Sample collection

The samples were collected in Uruguay and Namibia, four from the Punta del Este Terrane in Uruguay (UA-11,-31B, UB-02 and R10-18), and two in the Kaoko Belt in Namibia (NI-123 and NO-08). Fig 3.1.2 and Fig 3.2.1 show the locations from where the samples were collected. The UB-02 was collected from the Manantiales gneisses and the other samples from Uruguay were collected from the Chafalote paragneisses.

4.2 Petrographic thin sections

With a diamond saw, a part of each sample was cut off, labelled and given to the laboratory technicians to make standard thin sections. The thin sections were polished so that they could be analysed with an electron microprobe.

4.3 Crushing, milling and LOI determination

Four of the samples were crushed with a jaw crusher (Fig 4.6.1) to a gravel size, put in bags and marked. Due to a lack of equipment at the University of Tromsø, the samples were sent to the University of Bergen to be milled to the analytical grain size. To determine the loss of volatiles ca 2,5g of the rock powder was put into a ceramic crucible and weighed, the crucible was ignited (to eliminate contaminants) and weighed beforehand. The crucibles with the samples were heated up to ca 1000°C in an oven for approximately 2-3 hours and weighed again after cooled. The loss of ignition (LOI) is the difference in weight of the sample before and after heating, and represents the general loss of volatiles. Samples UA-02 and R10-18 were analysed by the company Veritas in Vancouver, Canada.

4.4 Glass tablet preparation

0.8000g of rock powder was mixed together with 5.600g of Flux powder (spectromelt A-10, lithium tetraborate, $Li_2B_4O_7$). The flux powder lowers the melting temperature of the rock and also mixes the samples to a homogeneous mix. The samples were mixed and then transferred to platinum crucibles and mounted in a xrFuse 2 furnace, with platinum collection plate underneath to catch the melted mixture. The furnace could only take two samples at the time. The procedure included a melting stage, shaking stage (for homogenization of the sample) and a cooling stage.

4.5 Major element analysis

The analysis of the whole-rock major element concentrations was conducted by a standard X-ray fluorescence spectroscopy (XRF). The results of the analysis were not satisfactory and the Uruguayan samples UA-31B and UA-11, and the Namibian samples NI-123 and NO-08 were analysed in the Czech Republic in the laboratories of the Czech Geological Survey in Prague.

4.6 Mineral analysis

The six samples were analysed by a Cameca SX100 Electron microprobe at the department of Geoscience in Oslo. The electron microprobe operated under 15KeV acceleration voltage with a beam current of 15 nA and a focus beam.

Table 4.6.1. Overview of other methods.

Methods/Software	Aim
Optical microscopy	Identification of mineral assemblages.
SEM	Detection of micro textures, image acquisition.
Perple_X (Connolly, 2005;2009)	Modelling of the PT conditions at which the determined mineral assemblages formed.
Gabbrosoft, mineral formula recalculation spread sheets.	Recalculating mineral formulas from the analyzed mineral composition.
Corel Draw	Redrawing of the output postscript files from Perple_X.

Fig 4.6.1 a) jaw crusher located in the Emilbua at the University in Tromsø. b) SEM located at the department of medicine at the University of Tromsø.

5 Petrography and mineral chemistry

5.1 Whole Rock Chemistry

The whole-rock chemical analyses and results of effective bulk composition calculations for the spinel-bearing domains (described further in the text) are shown in the table below (Table 5.1.1)

Table 5.1.1: Whole rock chemistry from each respective sample.

Wt %	UB-02	UA-31B	UA-11	R10-18	NI-123	NO-08	Moles	UA-31B	UA-11
SiO2	74,03	60,46	67,71	49,84	67,28	60,34		1,9932	1,4775
TiO2	0,30	1,37	0,87	1,17	0,64	0,92		0,1110	0,7072
Al2O3	13,51	17,99	15,56	16,65	15,35	16,45		0,7957	0,7279
Fe2O3	2,48	10,19	7,38	13,07	4,98	8,57	**FeO**	0,6071	1,1169
MgO	0,57	2,67	2,06	8,45	1,64	3,04		0,4794	0,3568
MnO	0,03	0,15	0,145	0,25	0,139	0,191		0,0050	0,0046
CaO	0,97	1,19	0,79	8,40	1,88	2,92		0,0215	0,0063
Na2O	1,69	1,14	0,86	0,83	2,17	3,08		0,0093	0,0005
K2O	5,45	2,87	3,35	0,70	3,8	2,47		0,0119	0,0035
P2O5	0,14	0,071	0,038	0,08	0,117	0,088			
Cr2O3				0,054					
LOI	0,7	0,61	0,39	0,20	1,47	1,23	**H2O**	0,0070	0,0000
Total	99,87	98,92	99,33	99,69	99,68	99,52			

SAMPLE DESCRIPTION

Based on mineral composition six samples, two samples from Namibia and four from Uruguay were selected for estimation of metamorphic conditions. The samples from Uruguay named UA- (11, 31B), UB 02, and R10-18, and from Namibia named NI-123 and NO-08 (Table 5.1.2) are described on a textural and compositional basis.

Table 5.1.2. Rock classification, metamorphic assemblage and location of the studied samples. PET: Punta del Este Terrane; Pl: plagioclase; Bt: biotite; Qtz: quartz; Grt: garnet; Ksp: K-feldspar; Sill: sillimanite; Spl: spinel; Crd: cordierite; Ilm: Ilmenite; Ru: rutile; Opx: orthopyroxene; Amp: amphibole;Mu: muscovite

Sample name	Rock classification	Metamorphic assemblages	Location/coordinates
UA-11	Felsic granulite	Pl+Bt+Qtz+Grt+Ksp+Sill+Spl+Crd+Ilm	PET, Uruguay 34°30'15.9"S/54°25'05.8"W
UA-31B	Intermediate granulite	Pl+Bt+Qtz+Grt+Ksp+Sill+Spl+Crd+Ilm	PET, Uruguay 34°17’06.7’’S /54°13’36.8’’W
UB-02	Felsic granulite	Pl+Bt+Qtz+Grt+Ksp+Sill+Ru+Ilm	PET, Uruguay 34°54'28.8"S/54°49'32.3"W
R10-18	Mafic granulite	Pl+Bt+Qtz+Opx+Amp	PET, Uruguay 34°14’23.4’’S /54°10’36.6’’W
NI-123	Migmatitic gneiss	Pl+Bt+Qtz+Grt+Ksp+Mu	Kaoko Belt, Namibia 18°00’09.4’’S /12°05’08.3’’E
NO-08	Migmatitic gneiss	Pl+Bt+Qtz+Grt+Mu	Kaoko Belt, Namibia 18°44’54.4’’S /12°35’21.7’’E

5.2 UB-02 Felsic granulite

This sample is composed of garnet porphyroblasts in a feldspar and quartz rich matrix (Fig 5.2.1). The garnets (ca 5-10% of total thin section area) are fractured and there are small grains of sillimanite. Biotite is not very abundant (~1%), and small, around 250 µm, which is a little larger than the minerals of the matrix and it is consuming garnet and sillimanite. The matrix consists of mostly quartz (30%), plagioclase (15%) and potassium feldspar (20%). There is some small occurrence of rutile and ilmenite.

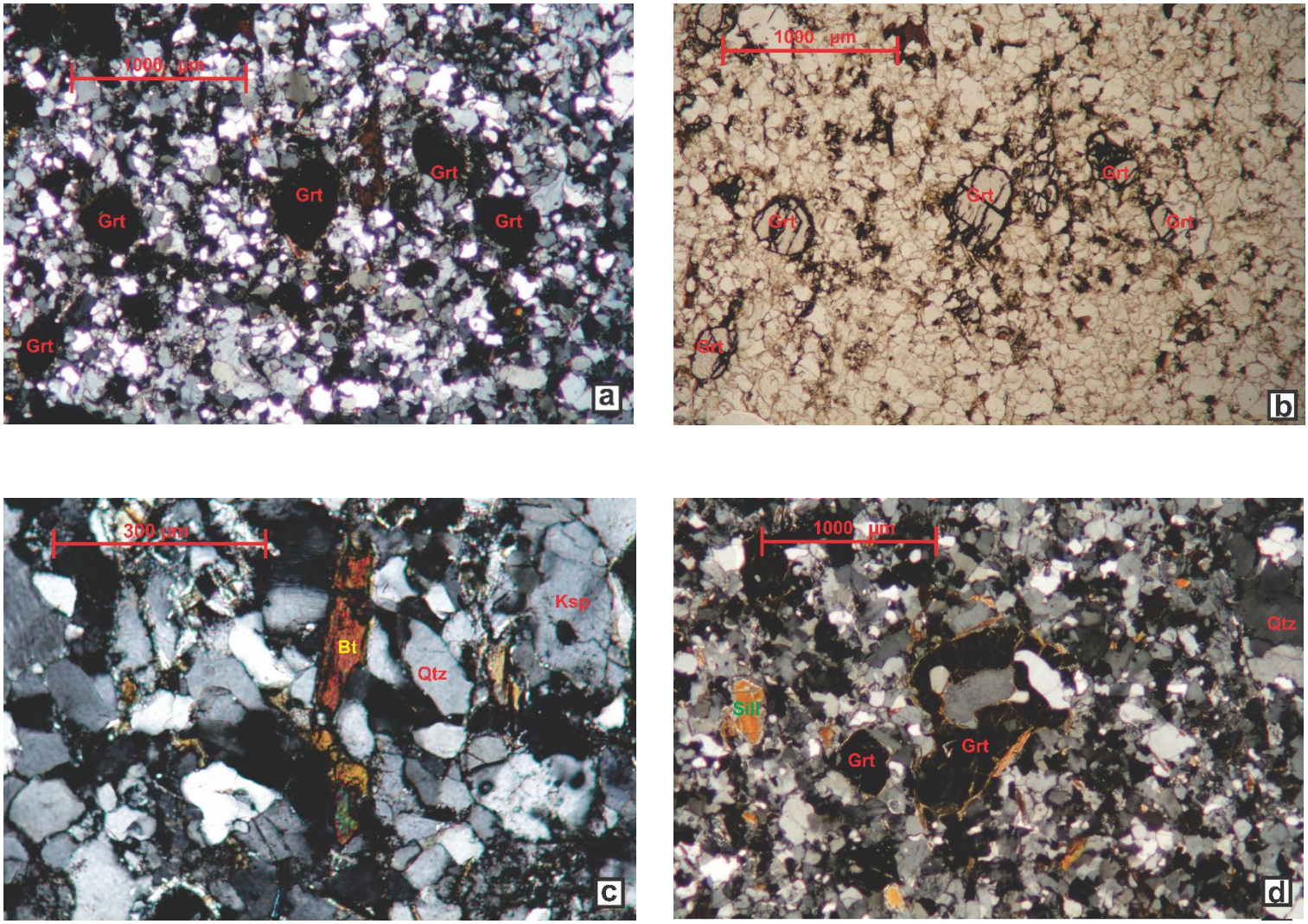

Fig 5.2.1a) Garnets in feldspar and quartz rich matrix. b) Lightly to highly fractured garnets in feldspar and quartz rich matrix. c) Small biotite in quartz and feldspar matrix. d) biotite consuming garnet and sillimanite.

Table 5.2.1. Representative electron microprobe analyses in wt%. recalculated to structural formulas with indicated number of oxygens. The formulas were recalculated using excel sheets listed in Table 4.6.1. Grt: Garnet; Bt:Biotite; Plag: Plagioclase; Ksp: K-feldspar.

Sample:	**UB-02**											
Position	Core	Rim	Rim		Core							
Mineral	Grt	Grt	Grt	Grt	Grt	Bt	Bt	Bt	Plag	Ksp	Ksp	Plag
Data set/ point	66 / 1 .	67 / 1 .	72 / 1 .	73 / 1 .	74 / 1 .	78 / 1 .	79 / 1 .	85 / 1 .	68 / 1 .	69 / 1 .	71 / 1 .	75 / 1 .
SiO2	38,036	37,964	37,896	37,466	37,624	37,495	37,896	37,539	59,119	64,116	64,236	58,620
TiO2	0,053	0,028	0,042	0,009	0,029	5,290	4,807	4,857	0,002	0,052	0,045	0,045
Cr2O3	0,000	0,024	0,002	0,052	0,051	0,000	0,017	0,002	0,015	0,000	0,000	0,023
Al2O3	21,418	21,427	21,540	21,310	21,376	15,502	15,635	15,415	25,274	18,630	18,740	25,778
FeO	32,791	32,165	32,833	33,304	33,493	15,559	13,130	15,271	0,044	0,047	0,048	0,037
MnO	0,630	0,575	0,680	0,638	0,690	0,015	0,036	0,033	0,010	0,000	0,000	0,021
MgO	6,537	6,552	5,661	5,803	5,968	11,621	12,588	11,972	0,000	0,006	0,006	0,000
CaO	0,907	0,958	0,995	0,978	0,897	0,012	0,000	0,000	7,617	0,185	0,229	7,612
Na2O	0,005	0,041	0,000	0,007	0,017	0,109	0,110	0,064	7,481	1,308	2,473	7,371
K2O	0,000	0,000	0,005	0,006	0,006	9,900	9,802	10,057	0,324	15,209	13,386	0,181
Total	100,376	99,733	99,653	99,574	100,151	95,502	94,020	95,210	99,885	99,553	99,162	99,686
No.O	12,000	12,000	12,000	12,000	12,000	11,000	11,000	11,000	8,000	8,000	8,000	8,000
Si	2,984	2,992	3,006	2,975	2,969	2,914	2,960	2,918	2,638	2,961	2,960	2,622
Ti	0,003	0,002	0,002	0,001	0,002	0,309	0,282	0,284	0,000	0,002	0,002	0,002
Cr	0,000	0,001	0,000	0,003	0,003	0,000	0,001	0,000	0,001	0,000	0,000	0,001
Al	1,980	1,991	2,014	1,995	1,988	1,420	1,440	1,413	1,329	1,014	1,018	1,359
Fe3+	0,046	0,026	0,000	0,052	0,070	0,000	0,000	0,000	0,002	0,002	0,002	0,001
Fe2+	2,104	2,093	2,178	2,160	2,141	1,011	0,858	0,993	0,000	0,000	0,000	0,000
Mn	0,042	0,038	0,046	0,043	0,046	0,001	0,002	0,002	0,000	0,000	0,000	0,001
Mg	0,764	0,770	0,669	0,687	0,702	1,346	1,465	1,387	0,000	0,000	0,000	0,000
Ca	0,076	0,081	0,085	0,083	0,076	0,001	0,000	0,000	0,364	0,009	0,011	0,365
Na	0,001	0,006	0,000	0,001	0,003	0,016	0,017	0,010	0,647	0,117	0,221	0,639
K	0,000	0,000	0,000	0,001	0,001	0,981	0,977	0,997	0,018	0,896	0,787	0,010
Total	8,000	8,000	8,000	8,000	8,000	8,000	8,002	8,004	5,000	5,000	5,000	5,000
X_{Mg}	0,262	0,266	0,235	0,237	0,241	0,571	0,631	0,583				
Py	0,248	0,253	0,221	0,222	0,225			**An**	0,354	0,009	0,011	0,360
Alm	0,684	0,687	0,718	0,700	0,686			**Ab**	0,628	0,115	0,217	0,630
Grss	0,025	0,027	0,028	0,027	0,024			**Ksp**	0,018	0,877	0,772	0,010
Spss	0,014	0,013	0,015	0,014	0,015							

MINERAL COMPOSITION FOR UB-02:

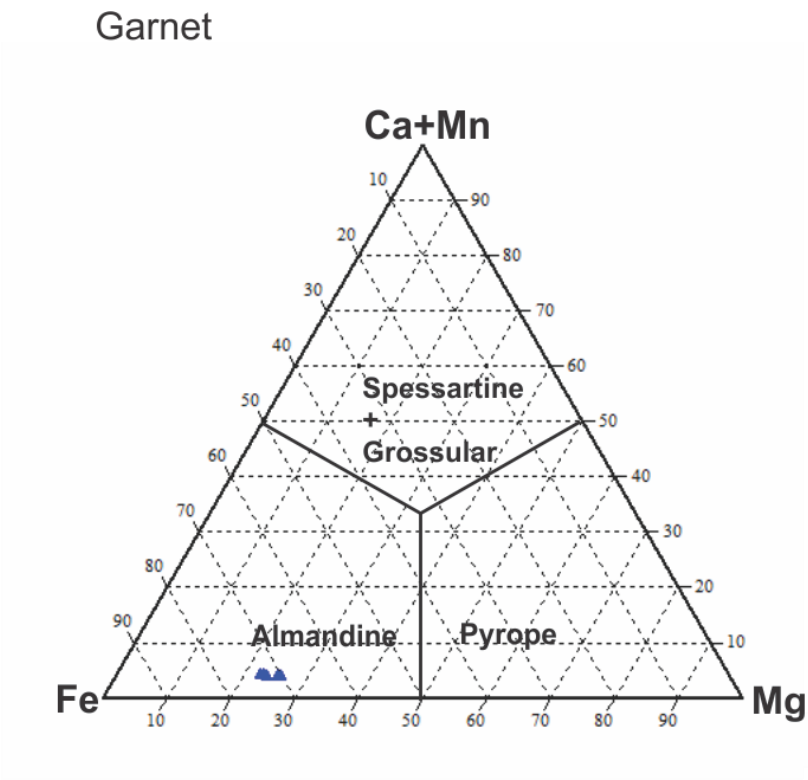

Fig 5.2.2. Ternary diagram of mol% of the endmembers almandine, pyrope and spessartine+grossular in ganret from the sample UB-02.

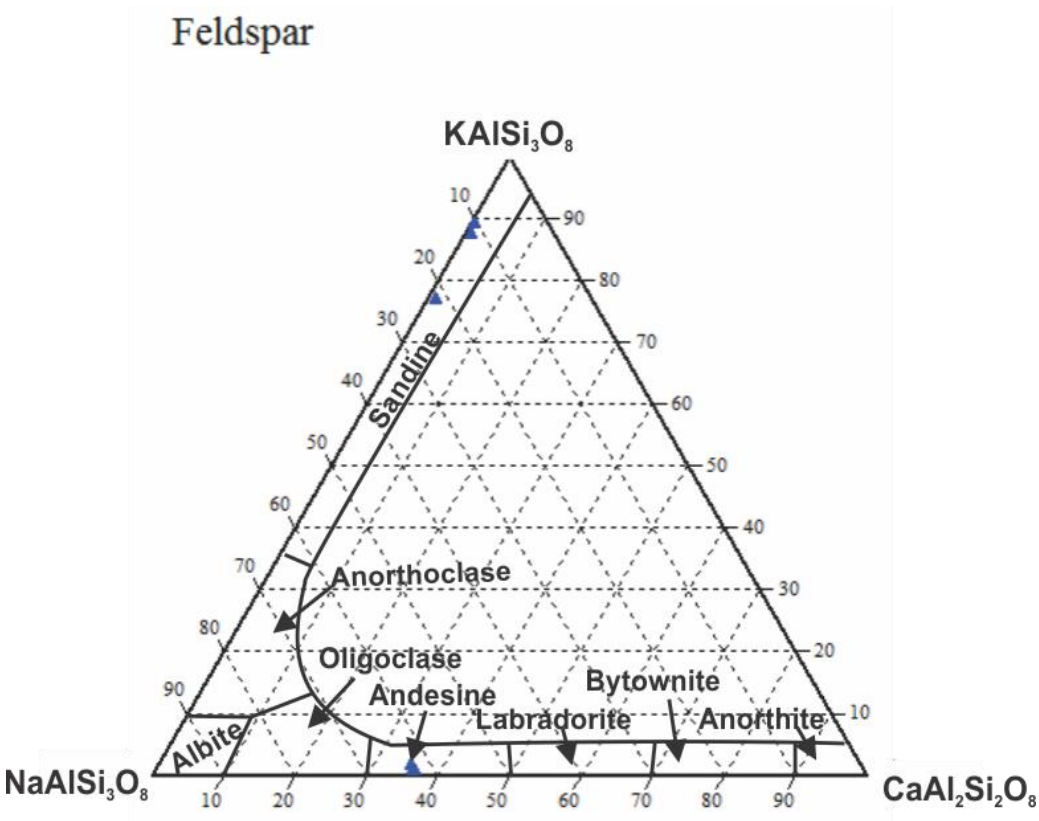

Fig 5.2.3. Ternary diagram of mol% content of the feldspars with respect to an, ab and ksp endmembers.

Garnet

Fig 5.2.2 shows a ternary diagram of the garnet composition in sample UB-02. All analyses plot in a cluster with a composition of Alm_{68-72} Py_{22-26} $Grss_{2,4-2,8}$ and $Spss_{1,3-1,5}$. The analysis of both the rim and the core of the garnet showed no difference in composition (see also Table 5.2.1)

Feldspar

The feldspars in this sample are represented by plagioclase with ca 35-37% anorthite, ca. 63% albite and K-feldspar with 77-90% K-feldspar component and 0,8-18% albite. The ternary diagram in Fig 5.2.3, shows that the feldspars in this sample can be classified as andesine and sandine.

Silimanite

The sillimanite that appear in this sample, are small prismatic crystals homogenously distributed in the thin section.

Biotite

The biotite for this sample has X_{Mg} (X_{Mg}=Mg/Mg+Fe) of 0,571-0,664, with a Si and Al content of 2,9-3 and 1,4-1,45 a.p.f.u. respectively (Table 5.2.1)

5.3 UA-11 Felsic granulate

This sample is comprised mainly of garnet (10%), K-feldspar (20%), plagioclase (20%) and quartz (25%). While these are the most abundant minerals seen in optical microscope, other minerals such as biotite (3%), silimanite (4%), spinel (2%) and corderite (15%) are present (Fig 5.3.1). The garnet crystals are large (ca 300µm-2mm) and fractured with some fine grained biotite growing in the fractures. K-feldspar is sometimes partially replaced by myrmekite. Spinel grows completely enclosed in cordierite, which the sillimanite appears to do as well. Ilmenite is accessory mineral (<1%).

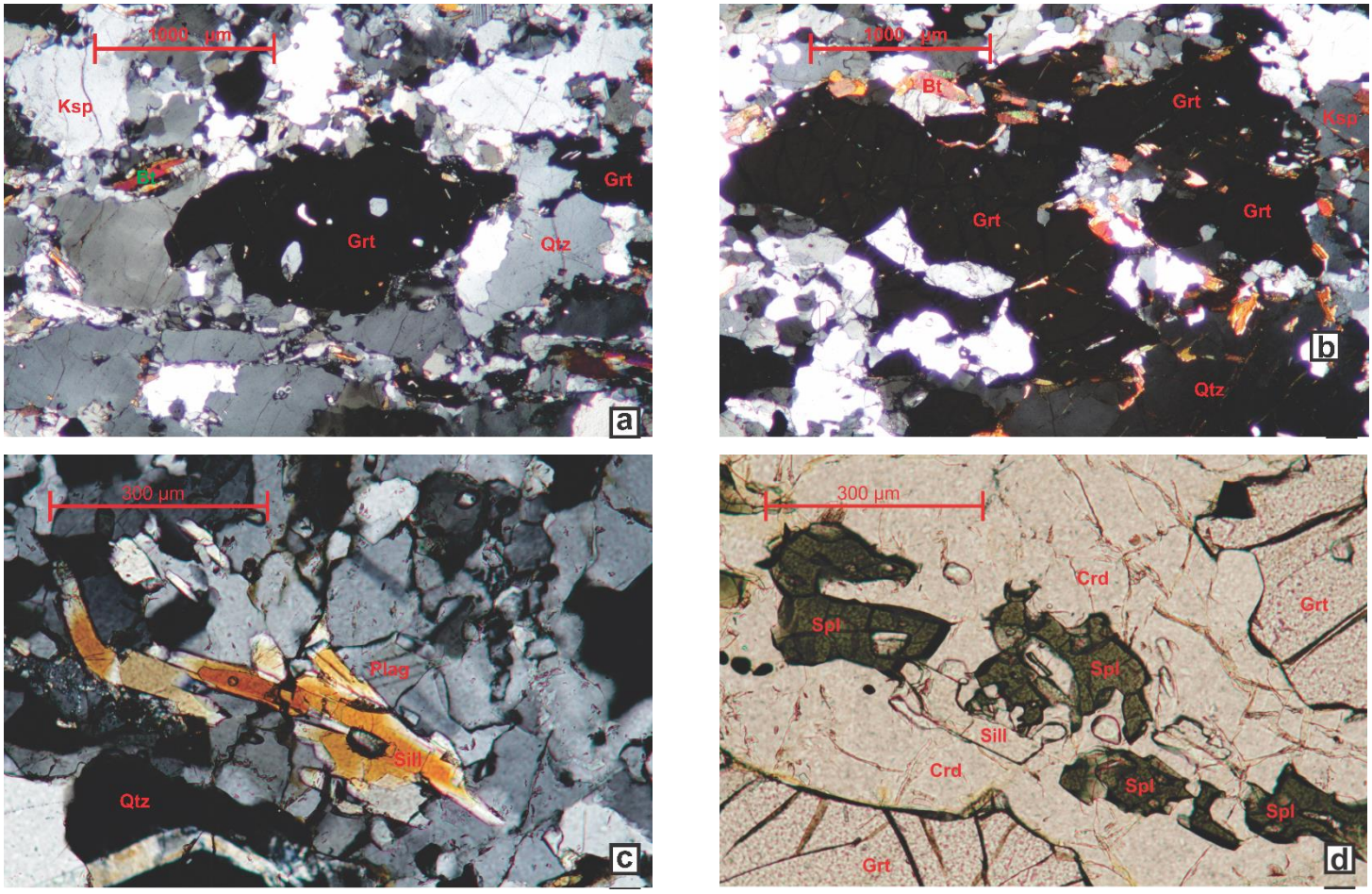

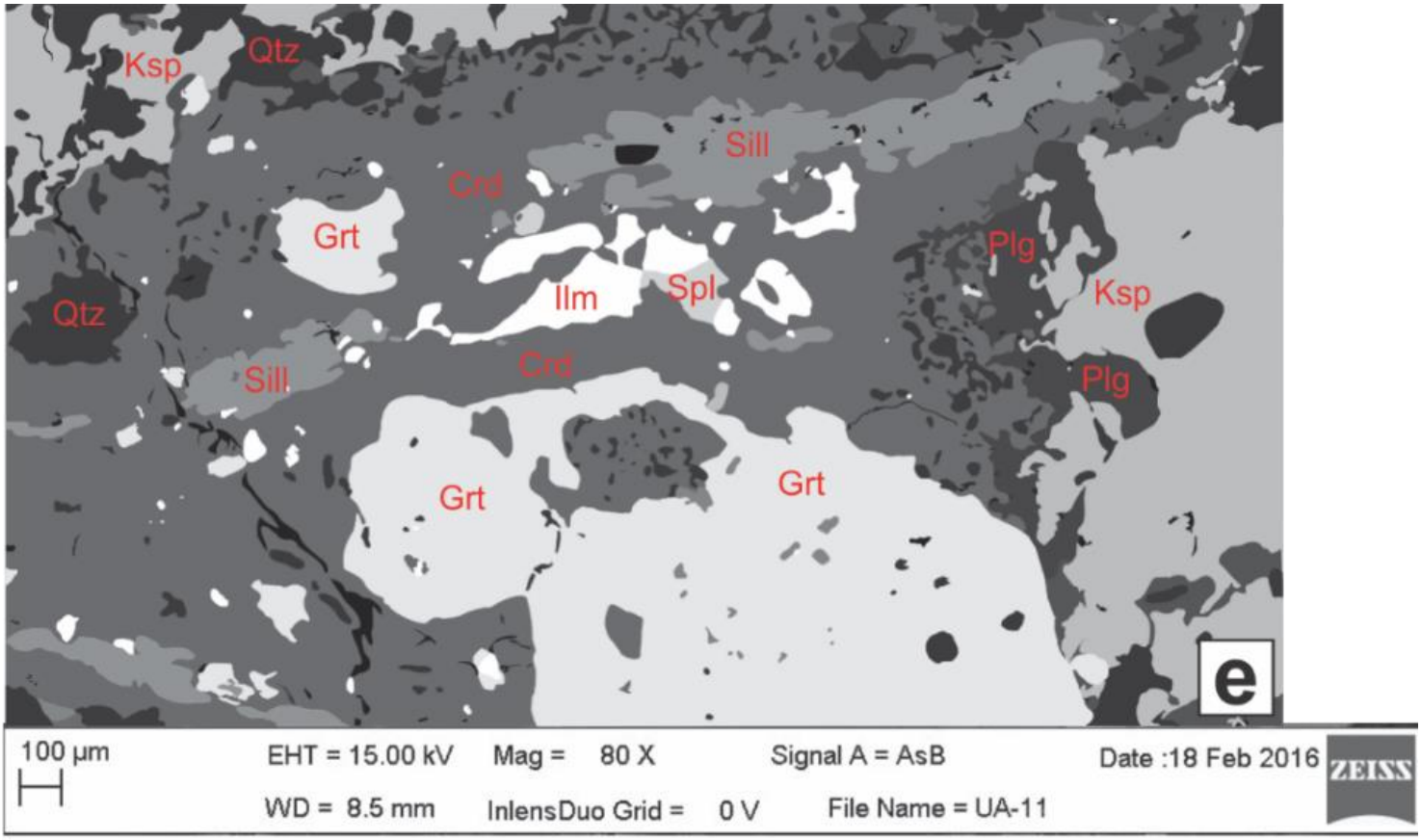

Fig 5.3.1. a) Large garnet, quartz and feldspar crystals, with smaller biotite and sillimanite. b) Biotite grow close to or on garnet crystals. c) Sillimanite surrounded by feldspar and quartz. d) Spinel in cordierite zone. e) Electron microprobe image of spinel enclosed in cordierite.

Table 5.3.1. Representative electron microprobe analyses in wt%. recalculated to structural formulas with indicated number of oxygens. Grt: Garnet; Bt: Biotite; Plag: Plagioclase; Ksp: K-feldspar; Spl: Spinel; Crd: Cordierite.

Sample:	**UA-11**											
Position	Rim	Core			Rim	Core						
Mineral	Grt	Grt	Crd	Crd	Sp	Sp	Bt	Bt	Ksp	Plag	Ksp	Plag
Data set/point	40 / 1 .	42 / 1 .	46 / 1 .	48 / 1 .	47 / 1 .	62 / 1 .	45 / 1 .	55 / 1 .	50 / 1 .	58 / 1 .	59 / 1 .	60 / 1 .
SiO2	37,909	38,065	48,942	48,887	0,000	0,000	35,420	36,235	64,586	58,147	65,261	56,949
TiO2	0,029	0,053	0,093	0,094	0,000	0,000	5,702	5,109	0,024	0,000	0,024	0,019
Cr2O3	0,023	0,006	32,806	32,850	57,018	57,018	0,122	0,107	0,020	0,000	0,000	0,000
Al2O3	21,542	21,447	0,011	0,009	0,006	0,006	16,744	16,617	18,630	26,566	18,496	27,051
FeO	32,629	32,446	0,022	0,030	0,000	0,000	19,150	17,599	0,114	0,016	0,036	0,047
MnO	0,997	1,128	0,004	0,055	0,027	0,027	0,000	0,000	0,007	0,025	0,000	0,000
MgO	6,024	6,050	8,816	8,238	34,300	34,300	9,055	10,164	0,000	0,000	0,019	0,000
CaO	1,131	1,167	0,099	0,087	0,101	0,101	0,000	0,000	0,031	8,652	0,029	9,523
Na2O	0,007	0,000	8,635	8,772	4,416	4,416	0,134	0,120	1,259	6,881	2,068	6,334
K2O	0,012	0,002	0,000	0,011	0,891	0,891	9,769	9,740	15,089	0,170	13,924	0,125
Total	100,303	100,364	99,429	99,031	96,758	96,758	96,097	95,691	99,759	100,456	99,856	100,047
No.O	12,000	12,000	18,000	18,000	4,000	4,000	11,000	11,000	8,000	8,000	8,000	8,000
Si	2,982	2,993	4,978	4,983	0,000	0,000	2,786	2,836	2,979	2,589	2,996	2,554
Ti	0,002	0,003	0,018	0,018	0,000	0,000	0,337	0,301	0,001	0,000	0,001	0,001
Cr	0,001	0,000	3,933	3,946	1,952	1,952	0,008	0,007	0,001	0,000	0,000	0,000
Al	1,998	1,988	0,001	0,001	0,000	0,000	1,552	1,533	1,013	1,394	1,001	1,430
Fe3+	0,035	0,019	0,002	0,003	0,000	0,000	0,000	0,000	0,004	0,001	0,001	0,002
Fe2+	2,112	2,115	0,000	0,004	0,001	0,001	1,260	1,152	0,000	0,000	0,000	0,000
Mn	0,066	0,075	0,131	0,098	0,026	0,026	0,000	0,000	0,000	0,001	0,000	0,000
Mg	0,706	0,709	0,619	0,604	0,807	0,807	1,062	1,186	0,000	0,000	0,001	0,000
Ca	0,095	0,098	0,009	0,007	0,002	0,002	0,000	0,000	0,002	0,413	0,001	0,458
Na	0,001	0,000	1,309	1,333	0,191	0,191	0,020	0,018	0,113	0,594	0,184	0,551
K	0,001	0,000	0,000	0,000	0,020	0,020	0,980	0,972	0,888	0,010	0,815	0,007
Total	8,000	8,001	11,001	10,999	3,000	3,000	8,005	8,005	5,000	5,001	5,001	5,001
X_{Mg}	0,248	0,249	0,686	0,679	0,181	0,192	0,457	0,507				
Py	0,231	0,234						**An**	0,427	0,002	0,406	0,001
Alm	0,690	0,697						**Ab**	0,565	0,112	0,584	0,184
Grss	0,031	0,032						**Ksp**	0,008	0,886	0,010	0,815
Spss	0,022	0,025										

MINERAL COMPOSITION FOR UA-11

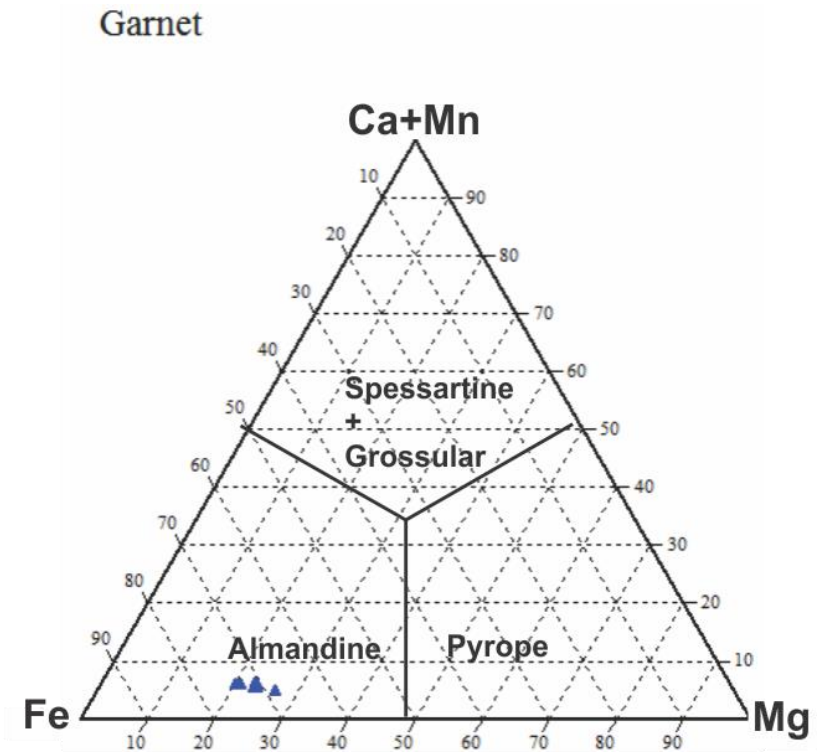

Fig 5.3.2. Ternary diagram of mol% of the endmembers almandine, pyrope and spessartine +grossular in garnet from the sample UA-11.

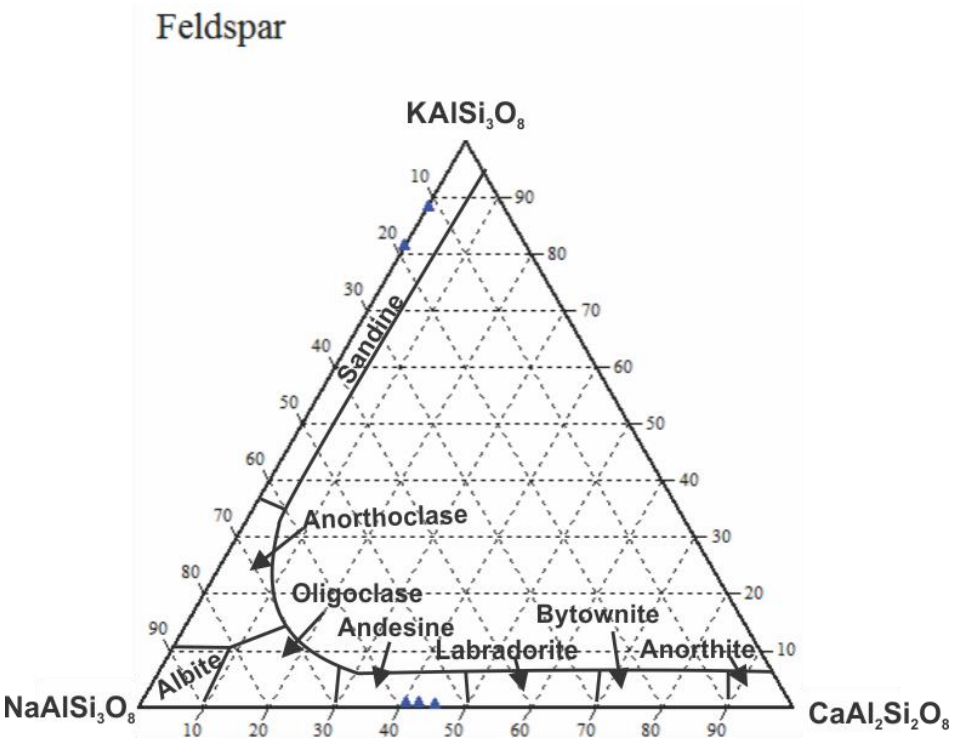

Fig 5.3.3. Ternary diagram of mol% content of the feldspars with respect to an, ab and ksp endmembers.

Garnet

The garnets have a X_{Mg} of 0,217-0,281 (Table 5.3.1) and an overall composition $Alm_{65-72}Py_{20-26}Grss_{2,8-3,6}$ and $Spss_{2-2,8}$ (Fig 5.3.2). The analyses of rims and cores show no major difference in composition.

Feldspar

The plagioclase has an endmember proportion of ca 40-45% anorthite and 54-59% albite. The K-feldspars have a proportion of endmembers K-feldspar component and albite of 81-89 % and 11-19% respectively. Fig 5.3.3 shows the feldspars plotted in a ternary diagram. The feldspars are classified as andesine and sandine.

Cordierite

The cordierite in this sample has a X_{Mg} of 0,657-0,688 (Table 5.3.1).

Spinel

The spinels has X_{Mg} of 0,181-0,192 (Table 5.3.1).

Biotite

The biotite in this sample has X_{Mg} of 0,457-0,569, with a Si and Al content of 2,78-2,89 and 1,52-1,55 a.p.f.u. respectively (Table 5.3.1).

5.4 UA-31B Intermediate granulite

This sample is composed of large garnet crystals with smaller quartz and feldspar making up the most abundant mineral assemblage (Fig 5.4.1). The garnets are elongated, ca. 0,1-1mm and appears in bands, with smaller and thinner bands of sillimanite running parallel with the garnet bands. The quartz and feldspars ranges from very small to larger crystals, ca. 10µm-500µm. The plagioclase sometime appears as myrmekite (vermicular inclusion of quartz). Smaller amounts of ilmenite and biotite is present. Cordierite has a poikiloblastic texture, and in the quartz deficient layers contains inclusions of spinel, sillimanite, biotite, K-feldspar and ilmenite. The spinel is always completely isolated from quartz and surrounded by cordierite.

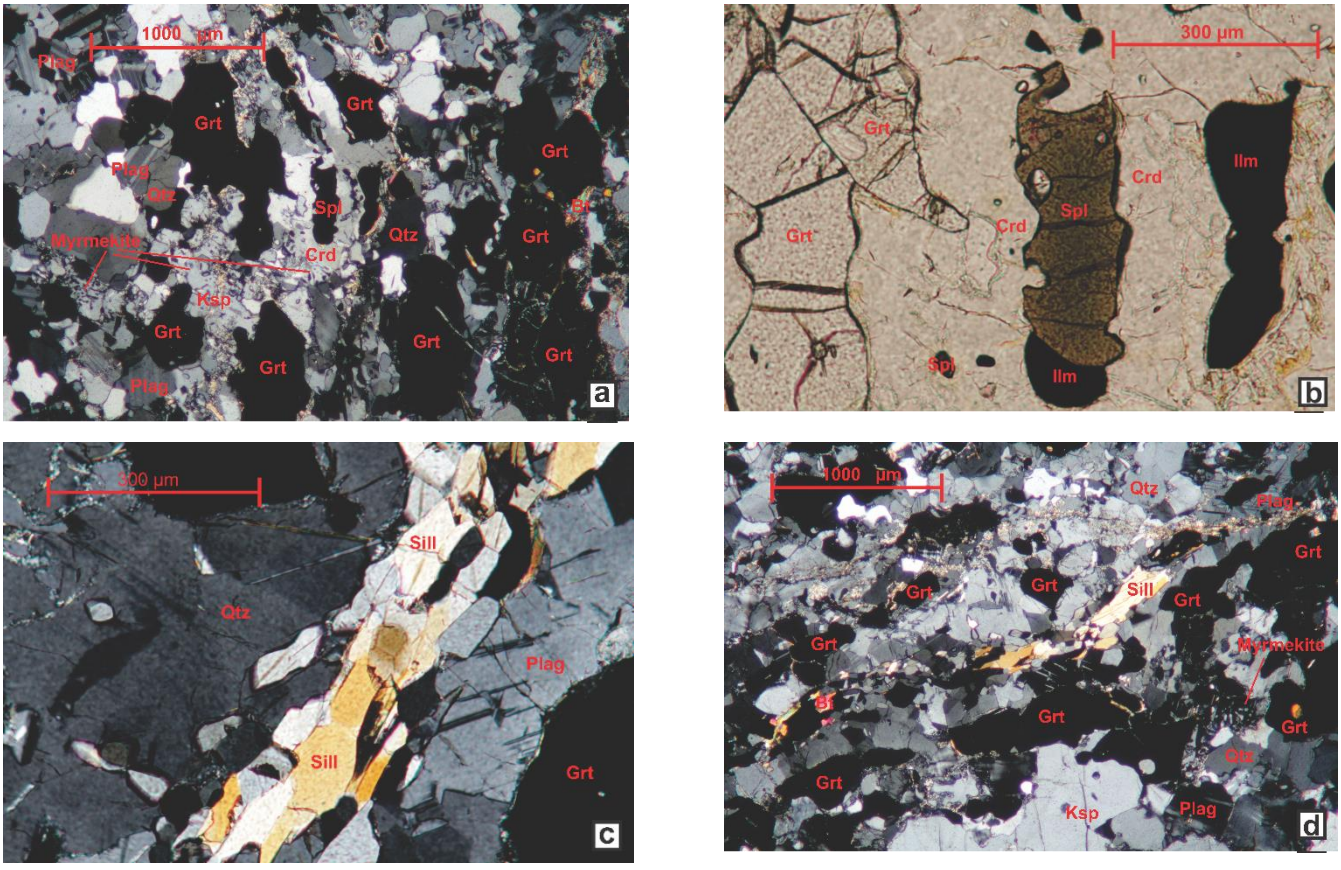

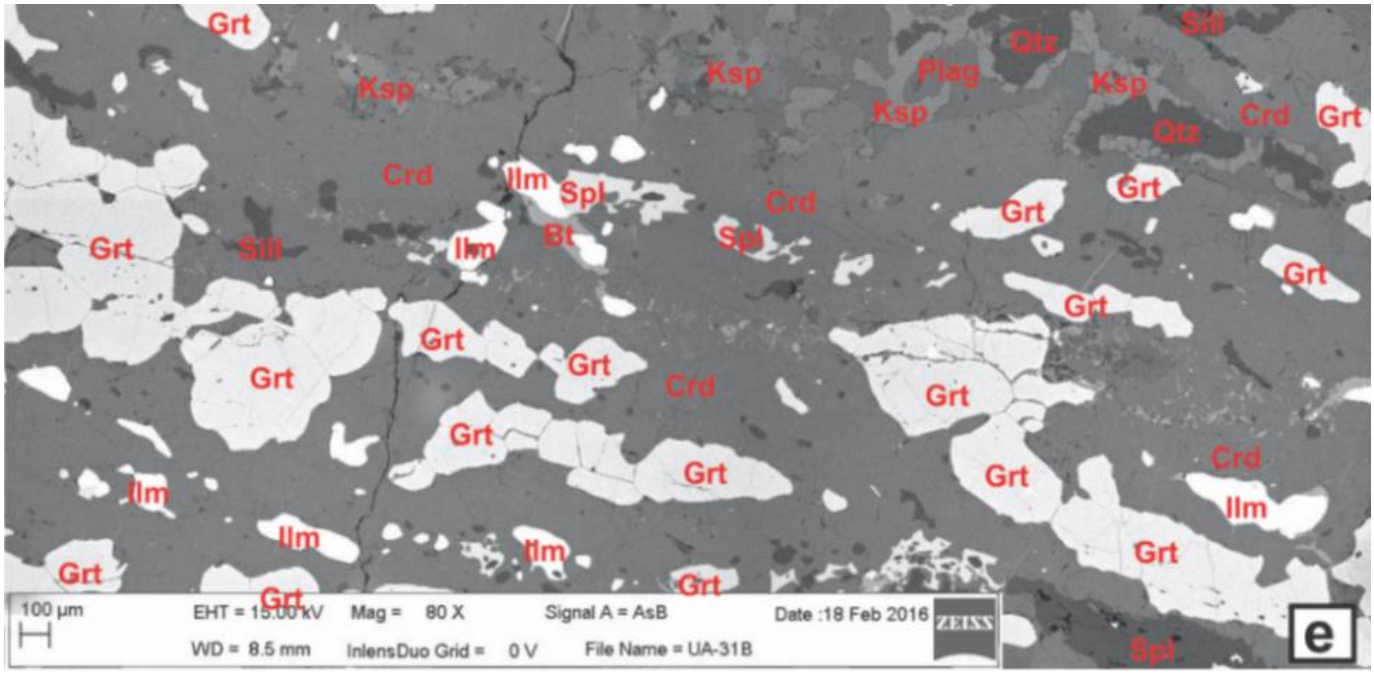

Fig 5.4.1. a) Large garnet surrounded by quartz, plagioclase, quartz, very little biotite. b) Spinel enclosed by cordierite. c) Layer of sillimanite. d) Sillimanite and garnet "bands. Garnet is elongated. e) Microprobe image of spinel surrounded by cordierite. Garnet is elongated in bands, some occurrences of ilmenite.

Table 5.4.1. Representative electron microprobe analyses in wt%. recalculated to structural formulas with indicated number of oxygens. Grt: Garnet; Bt: Biotite; Plag: Plagioclase; Ksp: K-feldspar; Spl: Spinel; Crd: Cordierite.

Sample:	**UA-31B**											
Position	Core	Rim					Core	Core				
Mineral	Grt	Grt	Crd	Crd	Bt	Bt	Spl	Spl	Plag	Plag	Ksp	Ksp
Data set/ point	1 / 1 .	2 / 1 .	27 / 1 .	35 / 1 .	13/1.	14/1.	8 / 1 .	9 / 1 .	18 / 1 .	19 / 1 .	20 / 1 .	21 / 1 .
SiO2	37,536	37,351	49,060	48,779	34,876	35,398	0,033	0,000	57,962	57,653	64,286	64,655
TiO2	0,039	0,048	0,135	0,135	2,669	2,605	0,000	0,000	0,022	0,004	0,036	0,037
Cr2O3	0,000	0,024	33,161	32,863	0,074	0,059	56,896	56,706	0,026	0,014	0,000	0,015
Al2O3	21,418	21,427	0,004	0,016	20,195	19,834	0,010	0,000	26,349	26,416	18,547	18,681
FeO	32,520	32,165	0,016	0,026	15,704	15,592	0,000	0,000	0,076	0,040	0,016	0,060
MnO	0,603	0,681	0,000	0,016	0,017	0,029	0,044	0,019	0,000	0,025	0,000	0,000
MgO	6,890	6,669	7,296	8,230	11,437	11,253	34,629	34,023	0,000	0,000	0,024	0,000
CaO	1,030	1,012	0,037	0,038	0,000	0,000	0,098	0,061	8,429	8,767	0,026	0,045
Na2O	0,001	0,016	9,043	8,658	0,121	0,111	4,031	3,963	6,945	6,712	1,293	1,417
K2O	0,000	0,042	0,000	0,000	9,792	9,966	0,701	0,653	0,197	0,168	14,905	14,828
Total	100,036	99,433	98,751	98,760	94,885	94,848	96,443	95,425	100,007	99,798	99,134	99,738
No.O	12,000	12,000	18,000	18,000	11,000	11,000	4,000	4,000	8,000	8,000	8,000	8,000
Si	2,947	2,951	4,996	4,985	2,692	2,735	0,001	0,000	2,592	2,586	2,983	2,980
Ti	0,002	0,003	0,027	0,027	0,155	0,151	0,000	0,000	0,001	0,000	0,001	0,001
Cr	0,000	0,001	3,980	3,958	0,004	0,004	1,958	1,970	0,001	0,000	0,000	0,001
Al	1,982	1,996	0,000	0,002	1,837	1,807	0,000	0,000	1,389	1,397	1,014	1,015
Fe3+	0,119	0,101	0,002	0,003	0,000	0,000	0,000	0,000	0,003	0,002	0,001	0,002
Fe2+	2,017	2,025	0,000	0,001	1,014	1,008	0,001	0,000	0,000	0,000	0,000	0,000
Mn	0,040	0,046	0,058	0,100	0,001	0,002	0,022	0,013	0,000	0,001	0,000	0,000
Mg	0,806	0,785	0,563	0,603	1,316	1,296	0,824	0,825	0,000	0,000	0,002	0,000
Ca	0,087	0,086	0,003	0,003	0,000	0,000	0,002	0,002	0,404	0,421	0,001	0,002
Na	0,000	0,002	1,373	1,319	0,018	0,017	0,175	0,174	0,602	0,584	0,116	0,127
K	0,000	0,004	0,000	0,000	0,964	0,982	0,016	0,015	0,011	0,010	0,882	0,872
Total	8,000	8,000	11,001	11,002	8,002	8,002	3,000	3,000	5,002	5,001	5,001	5,000
X_{Mg}	0,274	0,270	0,709	0,686	0,565	0,563	0,176	0,174				
Py	0,252	0,248						**An**	0,397	0,415	0,001	0,002
Alm	0,631	0,638						**Ab**	0,592	0,575	0,116	0,127
Grss	0,027	0,027						**Ksp**	0,011	0,009	0,882	0,871
Spss	0,013	0,014										

MINERAL COMPOSITION FOR UA-31B

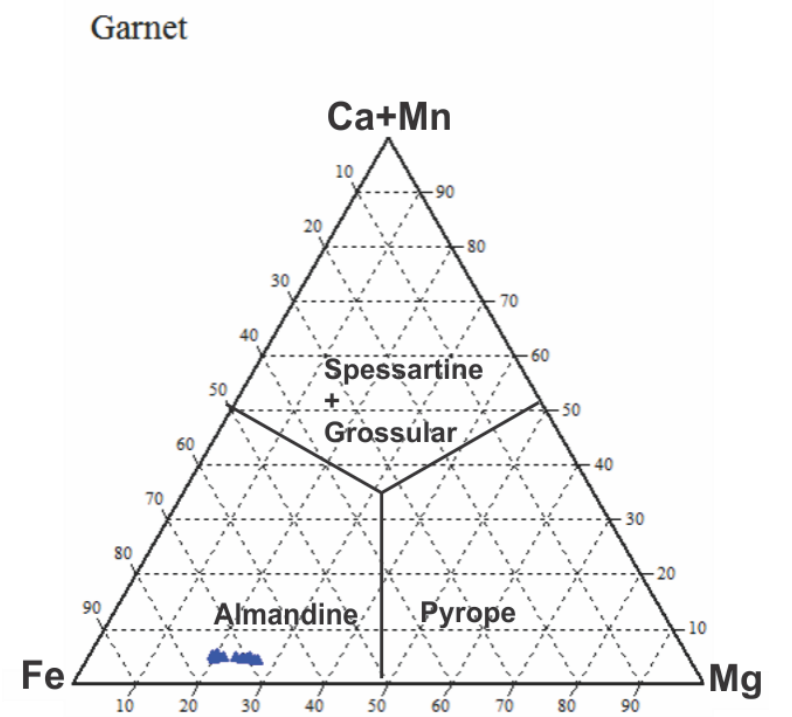

Fig 5.4.2. Ternary diagram of mol% of the endmembers almandine, pyrope and spessartine+grossular in garnet from the sample UA-31B.

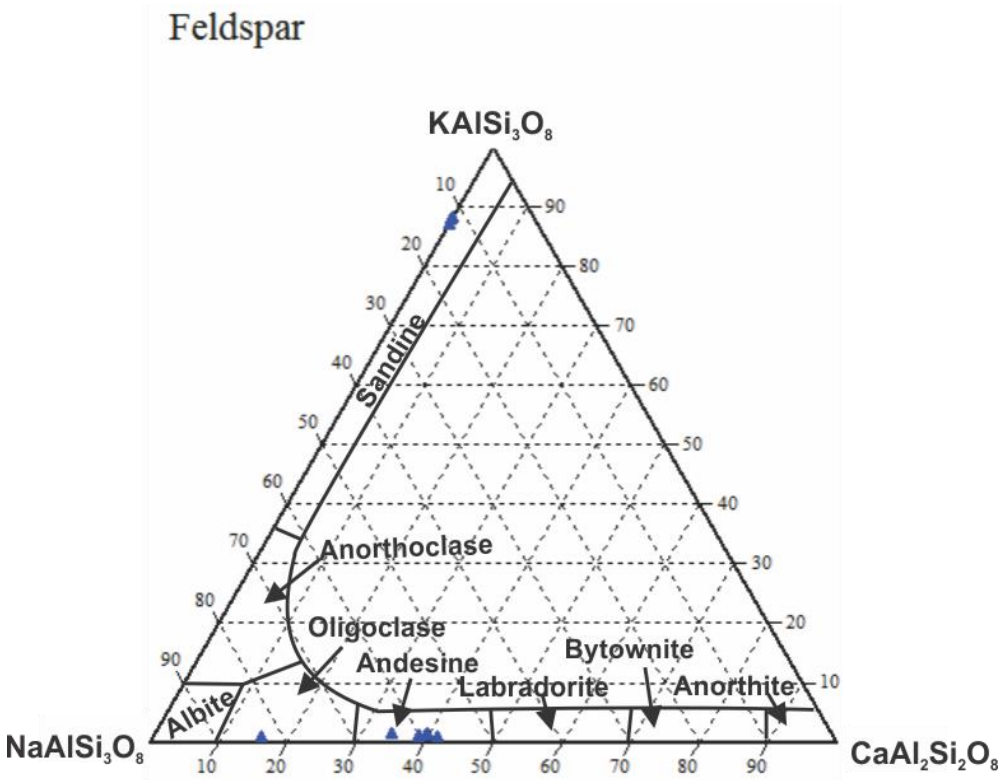

Fig 5.4.3. Ternary diagram of mol% content of the feldspars with respect to an, ab and ksp endmembers.

Garnet

The garnets are essentially an almandine-pyrope solid solution with minor components of spessartine and grossular (Table 5.4.1). Composition of the garnet measured in this sample is shown in Fig 5.4.2, suggesting the proportion of the garnet endmembers is Alm_{63-74} Py_{19-25} $Grss_{2,5-3}$ and $Spss_{1,5-2}$. There garnets show no chemical zoning. The X_{Mg} of the garnets is 0,208-0,286. The large gap in X_{Mg} could be related to the fact that the analysis was done in different zones, one zone has garnet with X_{Mg}=0,280-0,286, the second zone has garnets with X_{Mg}=0,208-0,213, the last zone has garnets with X_{Mg}=0,248-0,267.

Feldspar

In this sample the feldspars are composed of plagioclase with endmembers anorthite and albite of ca 16-42% and 57-64% albite respectively. Less than 2%of the K-feldspar component was present in the plagioclase. The K-feldspars have an endmember proportion of 11-13% albite and 87-88% K-feldspar component. The feldspars are classified as andesine and sandine, with one classified as oligoclase (Fig 5.4.3).

Corderite

This sample has cordierite with X_{Mg} of 0,661-0,709 (Table 5.4.1) and show no significant compositional variation. The analytical totals at 97,5-99,5 wt.% may indicate presence of some H_2O.

Spinel

The spinels occur as green spinels and have X_{Mg} of 0,172-0,187 (Table 5.4.1).

Biotite

The biotite in this sample has X_{Mg} = 0,554-569 and the Si and Al content are 2,63-2,74 and 1,8-1,96 a.p.f.u. respectively (Table 5.4.1).

5.5 R10-18 Mafic granulite

This sample is composed of large crystals of orthopyroxene (35%), feldspar (35%), biotite (9%),quartz (20%) and brown amphibole (<1%) (Fig 5.5.1). Two different types of orthopyroxene can be distinguished: (1) medium (ca. 1mm) porphyroblasts; (2) small (<1mm) vermiform grains intergrown with biotite, quartz and feldspar.

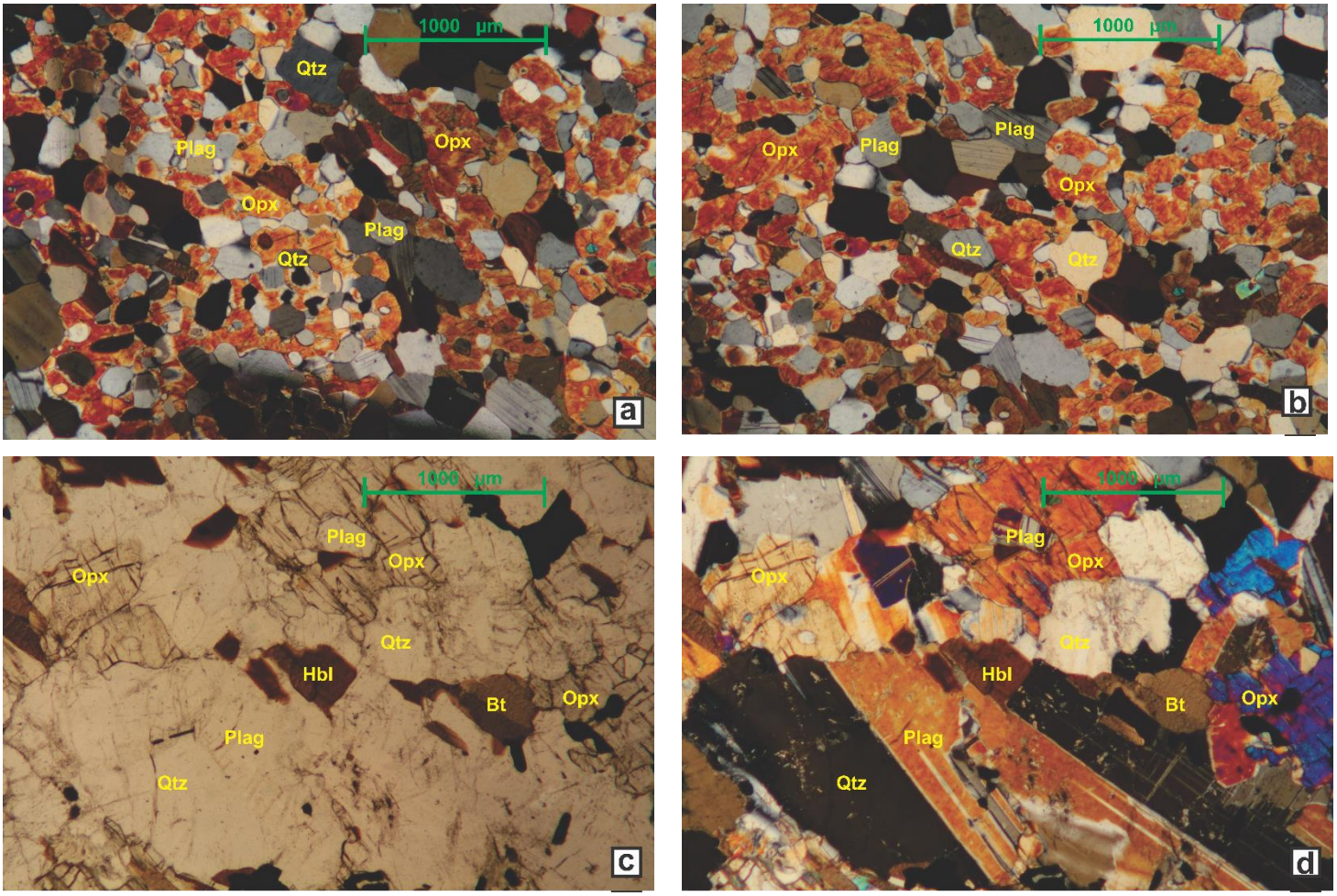

Fig 5.5.1. a) small orthopyroxene inergrown with feldspar and quartz. b) small orthopyroxene intergrown with quartz and feldspar. c) Plan polarized view of brown amphibole and biotite surrounded by feldspar, quartz and orthopyroxene. d) Medium orthopyroxene, quartz and feldspar surrounding smaller amphibole and biotite.The thin section was made thicker than what is standard and the colors are therefore different than usual.

Table 5.5.1. Representative electron microprobe analyses in wt%. recalculated to structural formulas with indicated number of oxygens. Plag: Plagioclase; Oamp: Orthoamphibole; Amp: Amphibole; Opx: Orthoamphibole; Bt: Biotite.

Sample:	**R10-18**											
Position					Core	Rim	Rim	Core	Core			
Mineral	Plag	Plag	Plag	Oamp	Amp	Amp	Opx	Opx	Opx	Bt	Bt	Bt
Data set/ point	89 / 1 .	90 / 1 .	98 / 1 .	88 / 1 .	91 / 1 .	92 / 1 .	150 / 1 .	151 / 1 .	152 / 1 .	97 / 1 .	101 / 1 .	104 / 1 .
SiO2	46,858	46,430	47,653	55,201	46,063	52,043	51,948	51,963	51,546	37,518	37,109	37,668
TiO2	0,000	0,021	0,022	0,068	1,731	0,680	0,076	0,107	0,130	5,683	5,334	4,688
Cr2O3	0,010	0,000	0,000	0,064	0,280	0,116	0,043	0,095	0,019	0,312	0,349	0,349
Al2O3	33,830	33,487	33,860	0,370	9,211	4,473	0,684	0,676	0,753	14,252	14,274	14,489
FeO	0,147	0,333	0,096	22,069	12,816	11,697	26,563	26,264	26,812	15,403	15,186	15,304
MnO	0,000	0,007	0,008	0,550	0,189	0,205	0,730	0,666	0,722	0,057	0,042	0,078
MgO	0,000	0,010	0,000	18,940	13,447	16,518	19,218	19,500	19,125	13,508	13,643	14,048
CaO	18,064	17,568	17,659	0,705	11,530	11,503	0,781	0,793	0,793	0,000	0,000	0,000
Na2O	1,516	1,726	1,715	0,036	1,008	0,424	0,000	0,015	0,000	0,201	0,178	0,162
K2O	0,016	0,033	0,038	0,007	0,829	0,244	0,004	0,012	0,001	9,615	9,691	9,520
Total	100,441	99,615	101,049	98,009	97,104	97,901	100,047	100,091	99,900	96,548	95,805	96,304
No.O	8,000	8,000	8,000	22,000	22,000	22,000	3,000	3,000	3,000	11,000	11,000	11,000
Si	2,147	2,141	2,168	6,975	6,701	7,315	1,986	1,965	1,965	2,872	2,856	2,876
Ti	0,000	0,001	0,001	0,006	0,189	0,072	0,003	0,004	0,004	0,327	0,309	0,269
Cr	0,000	0,000	0,000	0,006	0,032	0,013	0,001	0,001	0,001	0,019	0,021	0,021
Al	1,827	1,820	1,816	0,055	1,579	0,741	0,028	0,034	0,034	1,286	1,295	1,304
Fe3+	0,006	0,013	0,001	2,332	0,575	0,849	0,000	0,028	0,028	0,000	0,000	0,000
Fe2+	0,000	0,000	0,003	0,000	0,984	0,526	0,827	0,827	0,827	0,986	0,977	0,977
Mn	0,000	0,000	0,000	0,059	0,023	0,024	0,021	0,023	0,023	0,004	0,003	0,005
Mg	0,000	0,001	0,000	3,567	2,916	3,460	1,098	1,087	1,087	1,541	1,565	1,598
Ca	0,887	0,868	0,861	0,095	1,797	1,732	0,035	0,032	0,032	0,000	0,000	0,000
Na	0,135	0,154	0,151	0,009	0,284	0,116	0,001	0,000	0,000	0,030	0,026	0,024
K	0,001	0,002	0,002	0,001	0,154	0,044	0,000	0,000	0,000	0,939	0,951	0,927
Total	5,002	5,000	5,003	13,105	15,235	14,891	4,001	4,000	4,000	8,000	8,000	8,000
X_{Mg}				0,605	0,652	0,716				0,610	0,616	0,621
An	0,867	0,847	0,849			**Enst**	0,545	0,552	0,543			
Ab	0,132	0,151	0,149			**Ferr**	0,417	0,408	0,413			
Ksp	0,001	0,002	0,002									

MINERAL COMPOSITION FOR R10-18

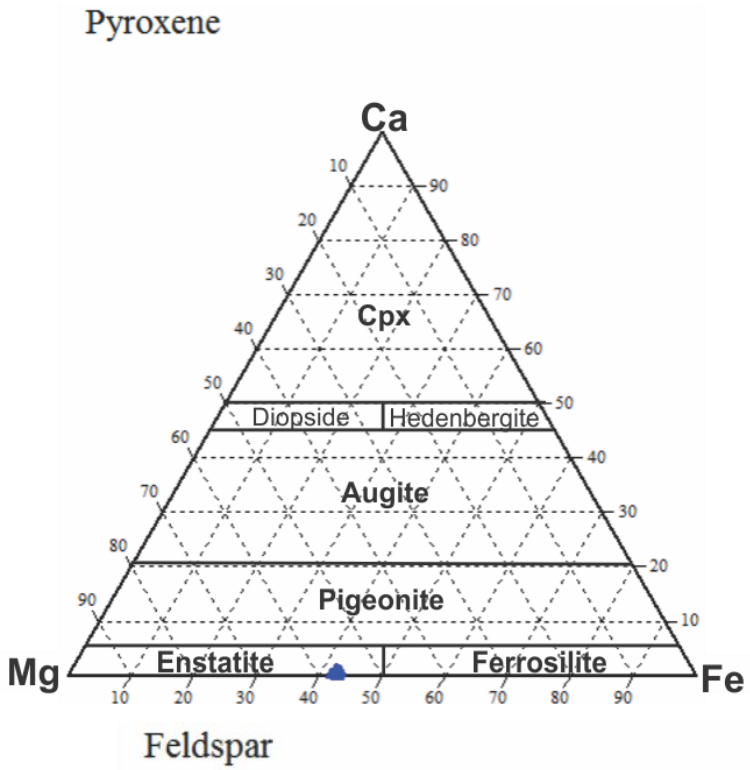

Fig 5.5.2. Ternary diagram of mol% content of the pyroxene with respect to enst and ferr endmembers, and cpx.

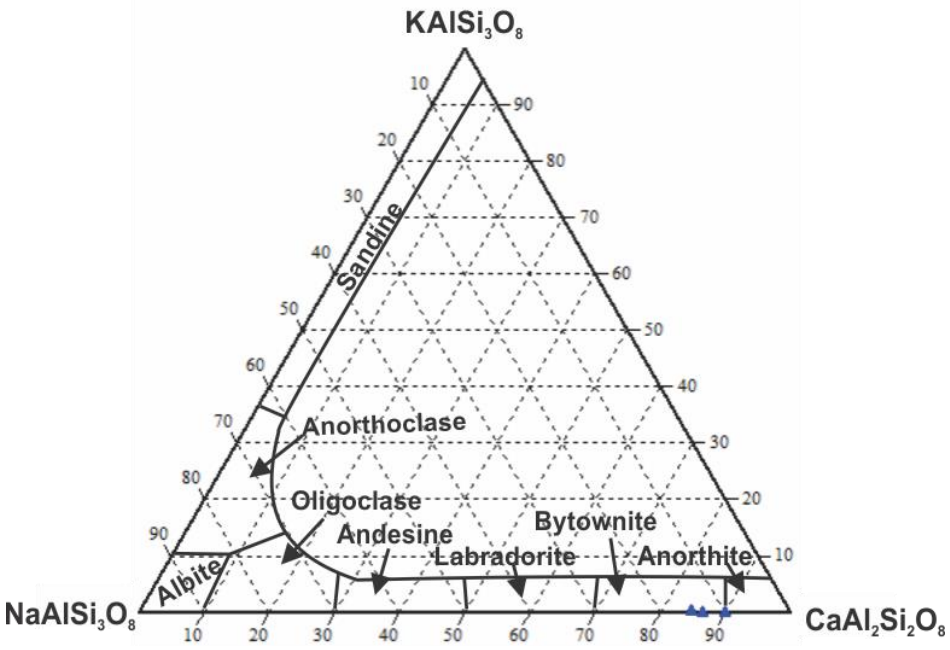

Fig 5.5.3. Ternary diagram of mol% content of the feldspars with respect to an, ab and ksp endmembers.

Orthopyroxene

The orthopyroxenes are classified as enstatite with a composition of 54-56% enstatite and 41-42% ferrosilite, and X_{Mg} of 0,566-0,579 (Table 5.5.1). Fig 5.5.2 shows pyroxene composition in a ternary diagram.

Feldspar

The feldspars in this sample is composed of ca 85-90% anorthite and 9-15% albite component. Fig 5.5.3 shows the composition of the feldspars and classifies them as bytownite and anorthite.

Amphibole

The amphiboles have a X_{Mg} of 0,591-0,720.

Biotite

The biotite in this sample has X_{Mg} of 0,610-0,621, with a Si content of 2,86-2,88 and Al content of 1,29-1,3 a.p.f.u. (Table 5.5.1).

5.6 NI-123 Migmatitic gneiss

This sample is composed of large garnet (13%), feldspars (40%) and quartz (40%) with smaller amount of biotite (5%) and muscovite (2%) (Fig 5.6.1). K-feldpsar is partially replaced by myrmekite. Two types of texture of biotite is observed: (1) fine grained that grows around fractured garnet crystals; (2) coarse-grained (300-500µm).

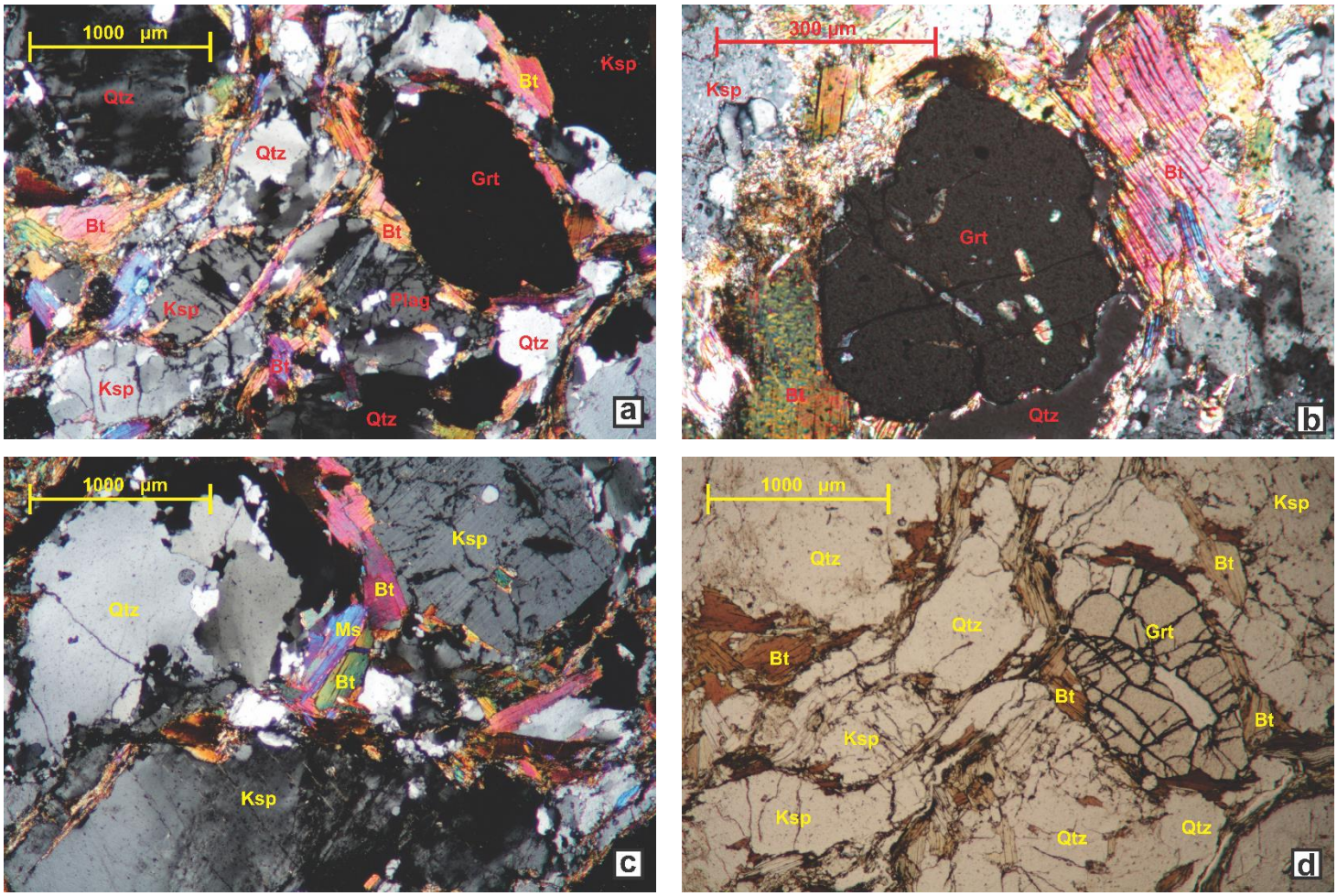

Fig 5.6.1. a) Large garnet, feldspars and quartz surrounded by smaller biotite, quartz and feldspars. b) Garnet surrounded by biotite, feldspar and quartz. Fine grained biotite grown around fractured garnet grains c) Large quartz and feldspars with smaller biotite and muscovite with some fine grained biotite. d) Fractured garnet surrounded by biotite.

Table 5.6.1. Representative electron microprobe analyses in wt%. recalculated to structural formulas with indicated number of oxygens. Grt: Garnet; Bt:Biotite; Plag: Plagioclase; Ksp: K-feldspar; Mu: Muscovite.

Sample:	**NI-123**											
Position												
Mineral	Grt	Grt	Grt	Ms	Ms	Ms	Bt	Bt	Bt	Ksp	Plag	Plag
Data set/point	111 / 1 .	112 / 1 .	118 / 1 .	115 / 1 .	117 / 1 .	128 / 1 .	114 / 1 .	129 / 1 .	114 / 1 .	131 / 1 .	132 / 1 .	133 / 1 .
SiO2	36,477	36,553	37,104	46,830	45,617	46,024	34,868	35,027	34,334	64,556	61,294	60,649
TiO2	0,013	0,000	0,000	1,360	1,277	0,912	3,525	2,713	3,176	0,017	0,000	0,003
Cr2O3	0,007	0,051	0,012	0,000	0,047	0,007	0,003	0,014	0,023	0,008	0,000	0,000
Al2O3	20,942	20,887	20,853	32,791	35,339	35,812	18,527	18,093	18,934	18,455	24,770	24,880
FeO	30,779	28,428	29,308	1,763	1,175	1,157	21,495	20,983	20,870	0,023	0,024	0,020
MnO	7,952	10,411	9,924	0,020	0,004	0,031	0,372	0,364	0,337	0,049	0,000	0,006
MgO	2,763	2,189	2,274	1,207	0,681	0,732	7,364	7,872	7,055	0,000	0,000	0,000
CaO	1,262	1,385	1,205	0,000	0,000	0,000	0,000	0,000	0,000	0,000	6,683	6,874
Na2O	0,003	0,043	0,013	0,219	0,451	0,502	0,083	0,060	0,119	1,145	7,799	7,599
K2O	0,000	0,028	0,000	10,952	10,740	10,705	9,980	9,761	9,953	15,281	0,306	0,358
Total	100,199	99,974	100,691	95,144	95,332	95,881	96,218	94,886	94,801	99,534	100,876	100,387
No.O	12,000	12,000	12,000	11,000	11,000	11,000	11,000	11,000	11,000	8,000	8,000	8,000
Si	2,944	2,964	2,989	3,147	3,048	3,050	2,749	2,787	2,742	2,987	2,709	2,695
Ti	0,001	0,000	0,000	0,069	0,064	0,045	0,209	0,162	0,191	0,001	0,000	0,000
Cr	0,000	0,003	0,001	0,000	0,003	0,000	0,000	0,001	0,001	0,000	0,000	0,000
Al	1,992	1,996	1,980	2,598	2,784	2,798	1,722	1,697	1,782	1,007	1,291	1,303
Fe3+	0,117	0,084	0,043	0,000	0,000	0,000	0,000	0,000	0,000	0,001	0,000	0,000
Fe2+	1,960	1,844	1,932	0,099	0,066	0,064	1,417	1,396	1,394	0,000	0,001	0,001
Mn	0,544	0,715	0,677	0,001	0,000	0,002	0,025	0,024	0,023	0,002	0,000	0,000
Mg	0,332	0,265	0,273	0,000	0,000	0,000	0,865	0,934	0,840	0,000	0,000	0,000
Ca	0,109	0,120	0,104	0,121	0,068	0,072	0,000	0,000	0,000	0,000	0,316	0,327
Na	0,001	0,007	0,002	0,000	0,000	0,000	0,013	0,009	0,018	0,103	0,668	0,655
K	0,000	0,003	0,000	0,029	0,058	0,064	1,004	0,991	1,014	0,902	0,017	0,020
Total	8,001	8,001	8,001	0,939	0,915	0,905	8,004	8,002	8,004	5,002	5,002	5,002
X_{Mg}	0,138	0,121	0,122	0,550	0,508	0,530	0,379	0,391	0,379			
Py	0,104	0,084	0,089						**An**	0,000	0,316	0,327
Alm	0,614	0,588	0,630						**Ab**	0,102	0,667	0,653
Grss	0,034	0,038	0,034						**Ksp**	0,899	0,017	0,020
Spss	0,170	0,228	0,221									

MINERAL COMPOSITION FOR NI-123

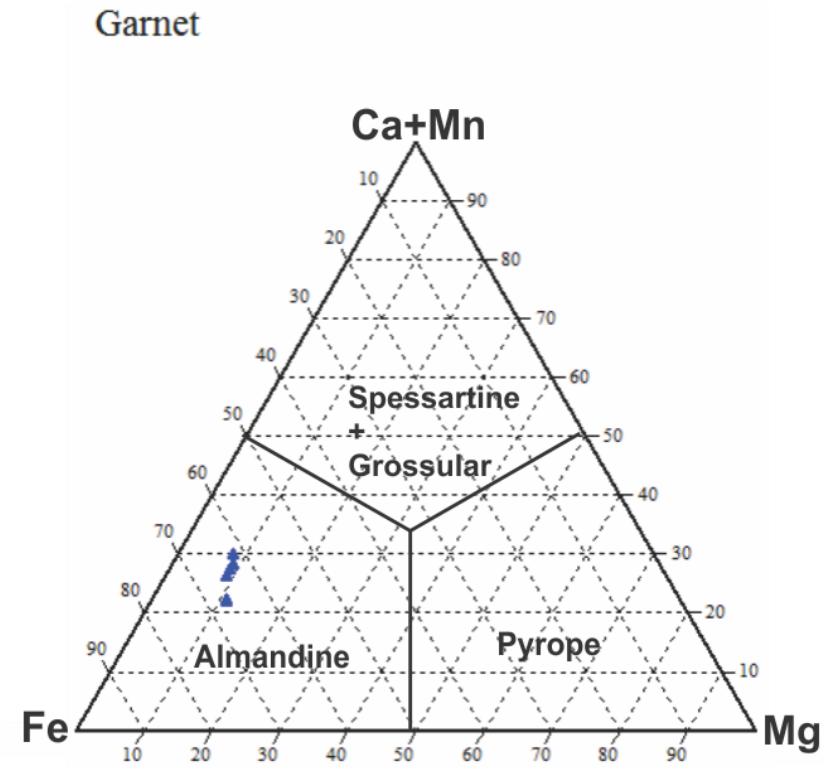

Fig 5.6.2. Ternary diagram of mol% of the endmembers almandine, pyrope and spessartine+grossular in garnet from the sample NI-123.

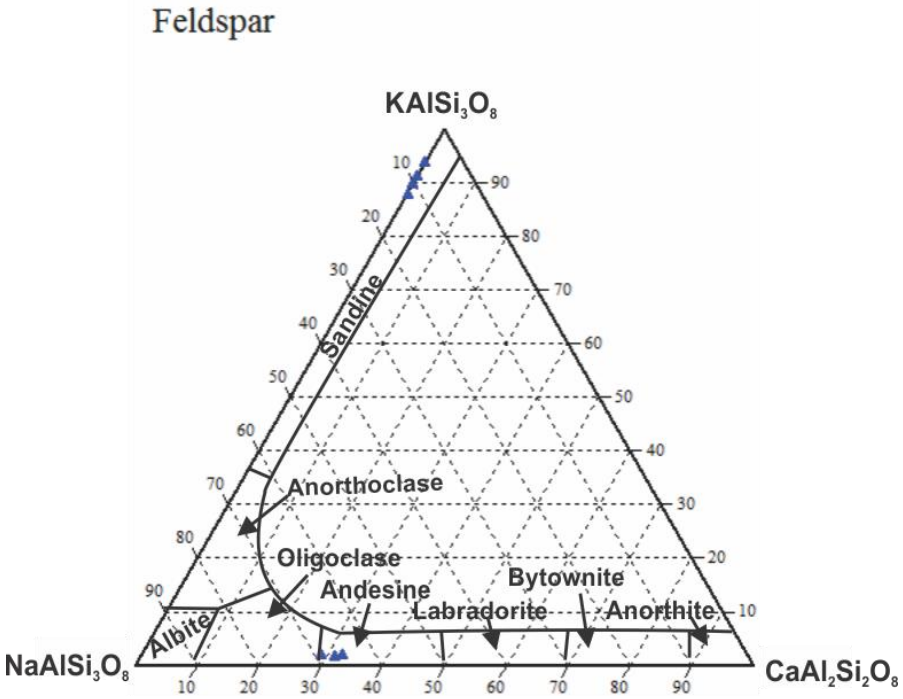

Fig 5.6.3. Ternary diagram of mol% content of the feldspars with respect to an, ab and ksp endmembers.

Garnet

The proportion of the garnet endmembers are $Alm_{57-64}Py_{8-11}Grss_{3,2-3,8}$ and $Spss_{17-24}$, and these are plotted in a ternary diagram (Fig 5.6.2). The garnets have a X_{Mg} of 0,118-0,145 (Table 5.6.1), and the analysis of rim and the core show only small difference in composition.

Feldspar

The plagioclases in this sample have endmember compositions of 29-33% anorthite and, 65-69% albite. In the K-feldspars the albite component is 6-12% and the K-feldspar component is 88-94%.(Table 5.6.1). Fig 5.6.3 shows the feldspars in this sample plotted in a ternary diagram and these feldspars are classified as andesine and sandine.

Biotite

X_{Mg} of the biotite in this samples is 0,376-0,401, with a Si and Al content of 2,74-2,79 and 1,70-1,78 a.p.f.u. respectively (Table 5.6.1).

5.7 NO-08 Migmatitc gneiss

This sample contains ca. 45% quartz, 43% feldspar, 10% biotite and 2% garnet (Fig 5.7.1). The crystals vary in size from 10 µm to >1mm, with garnet crystals only being around 100 µm-500 µm. The garnets are slightly fractured with biotite growing in the fractures, and some biotite is being replaced by chlorite.

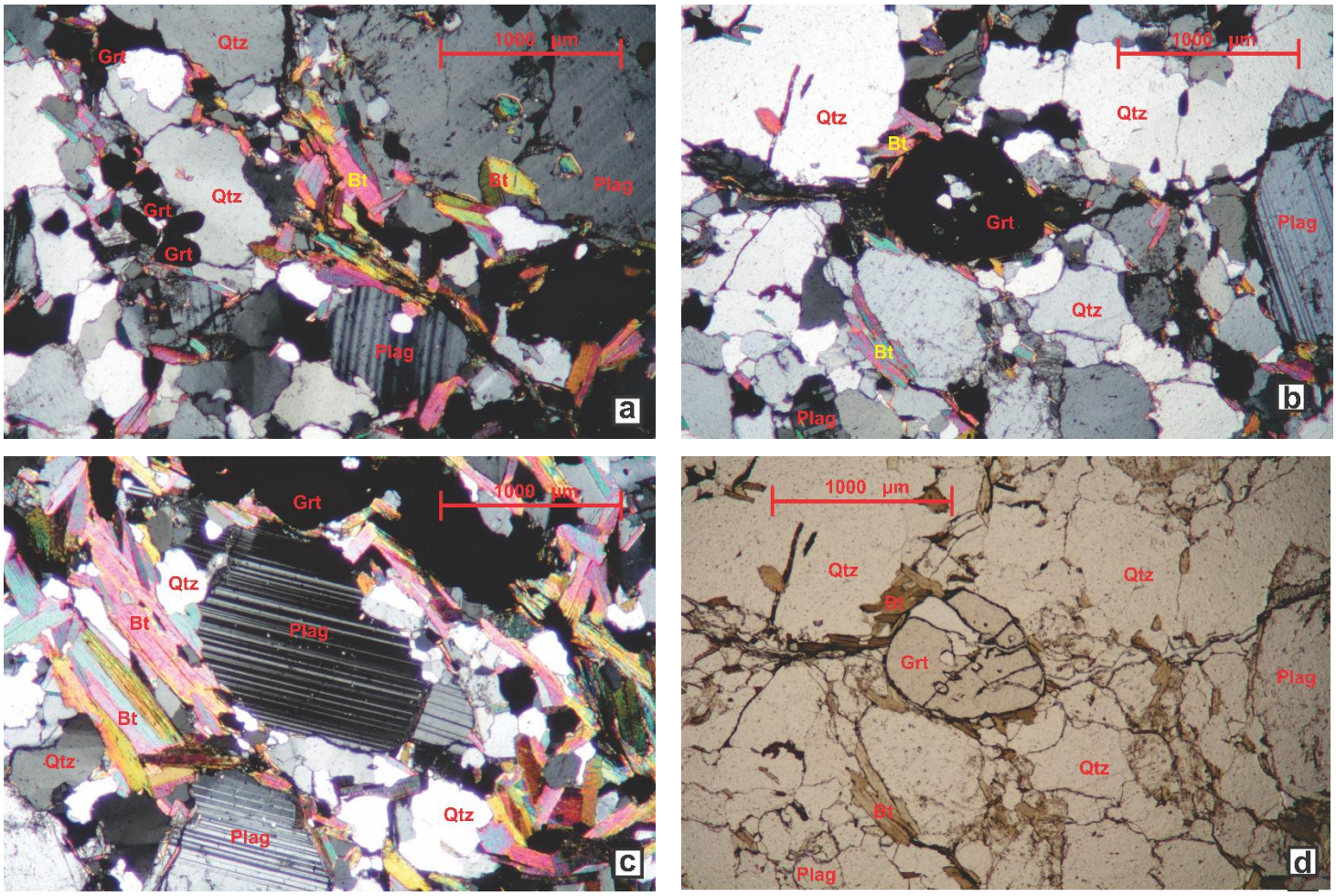

Fig 5.7.1. a) Large quartz and feldspars with smaller crystals of biotite and garnet. b) A larger garnet surrounded by quartz feldspars and biotite. c) Large biotite and feldspar and a small garnet crystal. d) Slightly fractured garnet with biotite growing around. Larger crystals of quartz and feldspar around.

Table 5.7.1. Representative electron microprobe analyses in wt%. recalculated to structural formulas with indicated number of oxygens. Grt: Garnet; Bt:Biotite; Plag: Plagioclase.

Sample:	**NO-08**											
Position												
Mineral	Grt	Grt	Grt	Grt	Bt	Bt	Bt	Bt	Plag	Plag	Plag	Plag
Data set/point	138 / 1 .	139 / 1 .	140 / 1 .	141 / 1 .	134 / 1 .	136 / 1 .	146 / 1 .	147 / 1 .	135 / 1 .	137 / 1 .	142 / 1 .	145 / 1 .
SiO2	37,256	37,508	37,436	37,407	35,506	35,610	35,149	36,219	60,155	60,304	59,696	60,998
TiO2	0,000	0,001	0,020	0,000	1,636	1,660	1,694	1,796	0,000	0,000	0,000	0,000
Cr2O3	0,000	0,032	0,001	0,000	0,049	0,000	0,043	0,000	0,000	0,028	0,000	0,003
Al2O3	21,001	21,008	20,840	21,021	19,505	19,294	19,144	19,639	25,162	25,018	24,894	24,576
FeO	33,858	33,227	33,255	33,491	19,064	19,521	19,662	18,871	0,113	0,048	0,000	0,016
MnO	4,451	4,186	4,146	4,646	0,079	0,088	0,034	0,041	0,000	0,011	0,033	0,014
MgO	2,784	3,009	2,919	2,444	9,903	9,634	9,718	9,779	0,000	0,000	0,000	0,000
CaO	1,473	1,496	1,496	1,488	0,000	0,000	0,000	0,000	7,179	6,922	6,886	6,291
Na2O	0,000	0,042	0,083	0,038	0,171	0,185	0,169	0,186	7,640	7,690	7,921	8,173
K2O	0,013	0,000	0,040	0,010	9,285	9,406	9,259	9,193	0,104	0,098	0,084	0,103
Total	100,835	100,508	100,236	100,543	95,197	95,398	94,871	95,723	100,353	100,120	99,513	100,174
No.O	12,000	12,000	12,000	12,000	11,000	11,000	11,000	11,000	8,000	8,000	8,000	8,000
Si	2,986	3,007	3,010	3,009	2,766	2,775	2,754	2,808	2,673	2,685	2,669	2,706
Ti	0,000	0,000	0,001	0,000	0,096	0,097	0,100	0,105	0,000	0,000	0,000	0,000
Cr	0,000	0,002	0,000	0,000	0,003	0,000	0,003	0,000	0,000	0,001	0,000	0,000
Al	1,984	1,985	1,975	1,993	1,791	1,772	1,768	1,795	1,318	1,313	1,312	1,285
Fe3+	0,045	0,006	0,020	0,000	0,000	0,000	0,000	0,000	0,000	0,000	0,000	0,001
Fe2+	2,224	2,222	2,216	2,253	1,242	1,272	1,288	1,223	0,004	0,002	0,000	0,000
Mn	0,302	0,284	0,282	0,317	0,005	0,006	0,002	0,003	0,000	0,000	0,001	0,001
Mg	0,333	0,360	0,350	0,293	1,150	1,119	1,135	1,130	0,000	0,000	0,000	0,000
Ca	0,126	0,129	0,129	0,128	0,000	0,000	0,000	0,000	0,342	0,330	0,330	0,299
Na	0,000	0,006	0,013	0,006	0,026	0,028	0,026	0,028	0,658	0,664	0,687	0,703
K	0,000	0,000	0,004	0,001	0,923	0,935	0,925	0,909	0,006	0,006	0,005	0,006
Total	8,001	8,000	8,000	8,001	8,000	8,005	8,001	8,001	5,000	5,001	5,002	5,000
$\mathbf{X_{Mg}}$	0,128	0,139	0,135	0,115	0,481	0,468	0,468	0,480				
Py	0,108	0,118	0,114	0,096				**An**	0,340	0,330	0,323	0,297
Alm	0,725	0,731	0,721	0,742				**Ab**	0,654	0,664	0,672	0,698
Grss	0,041	0,042	0,042	0,042				**Ksp**	0,006	0,006	0,005	0,006
Spss	0,099	0,094	0,092	0,104								

MINERAL COMPOSITION FOR NO-08

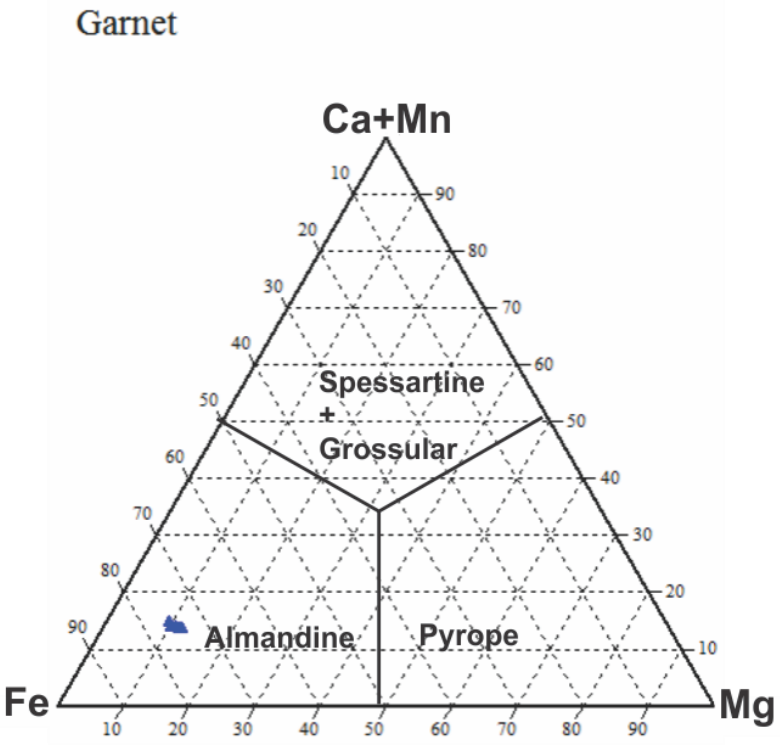

Fig 5.7.2. Ternary diagram of mol% of the endmembers almandine, pyrope and spessartine+grossular in garnet from the sample NO-08.

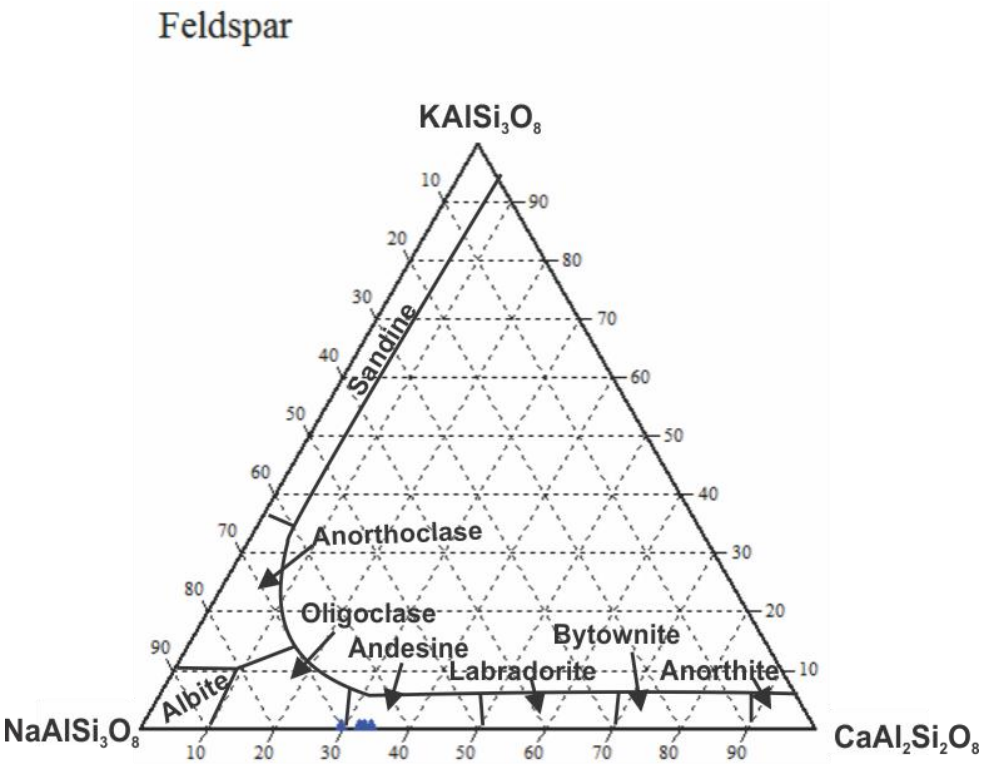

Fig 5.7.3. Ternary diagram of mol% content of the feldspars with respect to an, ab and ksp endmembers.

Garnet

The composition of the garnets is $Alm_{72-75}Py_{10-12}Grss_{3,7-4,2}$ and $Spss_{9-10,}$ with a X_{Mg} of 0,115-0,140 (Table 5.7.1). The analysis of rim and core show no difference in composition. The endmember composition in mol% is shown in the ternary diagram in Fig 5.7.2.

Feldspar

The feldspars have a composition of 30-34% anorthite and 65-70% albite (Table 5.7.1), classifying these feldspars as oligoclase and andesine. Fig 5.7.3 shows the feldspars plotted in a ternary diagram.

Biotite

Biotite in this sample has a X_{Mg} of 0,468-0,481, and a Si and Al content of 2,76-2,81 and 1,77-1,80 a.p.f.u. respectively (Table 5.7.1).

6 Spinel-bearing domains

Two of the samples UA-31B and UA-11 contains spinel-bearing domains that are clearly isolated from the matrix. Because of this, the whole rock composition would not be appropriate for modelling of the P-T conditions of these samples. Therefore, in order to constrain the equilibration conditions for these domains, an estimation of an effective bulk composition was made for these domains.

6.1 Introduction

The paper by Tajcmanova et al. (2006), discussed diffusion-controlled development of silica-undersaturated domains in felsic granulites. In their samples, they looked at plagioclase rims around metastable kyanite crystals. The plagioclase corona is a manifestation of diffusion-driven transfer of CaO and Na_2O from the surrounding matrix that resulted in isolation of kyanite grains from the quartz- and K-feldspar-bearing matrix. This results in Si-undersaturated conditions along the plagioclase-kyanite interface allowing spinels to grow during low-pressure metamorphism. When the rocks are fluid-saturated, the effective bulk composition is approximately the same as the whole-rock chemistry However, equilibration of mineral assemblages in fluid undersaturated rocks is often limited by diffusion, making the equilibration volume small. In such case, other methods of estimating the effective bulk composition is required.

6.2 Method

The method described by Stüwe et al. (1995) was used for the estimate of the bulk composition of the spinel-bearing domains in the samples UA-11 and UA-31B. To estimate the bulk composition of the minerals in the spinel-bearing zone a backscatter image was used. Mineral volume percent was estimated, and the bulk composition of each mineral was calculated and then added together to estimate bulk composition. It was assumed that the mineral volume was represented by a 2D section. Each mineral grain was digitized by hand to acquire as accurate a volume estimation as possible. To calculate the moles of each mineral (e.g. the number of moles of garnet) the estimated volume of the mineral in the sample was multiplied by its molar volume, which was obtained from the data set of Holland and Powell, (1998; 2004) and converted to cm^3/mol. In order to estimate the bulk composition of each mineral, each oxide component was calculated by multiplying the number of moles of the mineral by the number of moles of the individual components of the mineral measured by

microprobe analysis (e.g. 0,1045 mole of garnet * 0,6986 mole of Mg-element in garnet (from microprobe) = 0,073 moles of MgO oxide in garnet). The estimated bulk composition of each mineral was then summed in order to estimate a bulk rock composition.

7 Modelling of the metamorphic conditions

7.1 Introduction

All the studied samples, except the sample R10-18, contained garnet, which is a good mineral phase to use for geothermobarometric purposes, as it has a multi-component nature, plagioclase is also a good mineral to use for geothermobaromety. Other minerals present in the samples that are suitable for geothermobarometry is biotite, cordierite, spinel and orthopyroxene, as the exchange between the cations Mg^{2+} and Fe^{2+} is temperature dependent (Indares et al., 1985; Karabinos, 1985; Moazzen, 2004). Perple_X (Connolly, 2005; 2009), a thermodynamic modelling software was used to estimate the pressure and temperatures at which the mineral assemblages have formed. Solution models for the minerals representing solid solutions were used in the modelling together with Holland and Powell's (1998; 2004) internally consistent thermodynamic data set. In the Perple_X, the Werami and Pstable tools were used to extract the compositional values for the mineral phases and plot them as isopleths in the phase diagrams. Compositional isopleths representing the chemistry of the minerals are drawn in the calculated P-T sections. The assumption is that the isopleths for the mineral in equilibrium will cross in a small P-T range within the stability field of the observed mineral assemblage. The best estimation of the metamorphic conditions is then the area where the compositional isopleths cross.

7.2 UB-02 Felsic granulite

The mineral assemblage of this sample is: Pl-Bt-Qtz-Grt-Ksp-Sill, and Ms (only grows in fractures of garnet). The P-T section was calculated for the temperatures between 600-970°C and 1-10 kbar, in a system of Na_2O, MgO, Al_2O_3, SiO_2, K_2O, CaO, TiO_2, MnO, FeO and H_2O, and without saturated components. The LOI content was used for water content. The whole rock composition of weight percent was used and is indicated in Table 5.1.1. The solution models used are orthopyroxene (Holland and Powell, 1999), biotite (Tajcmanova et al., 2009), feldspar (Fuhrman et al., 1988), garnet (Holland and Powell, 1998), ilmenite (White et al., 2000), cordierite (Baumgartner, 2003), clinopyroxene (Holland and Powell, 1996), muscovite (Holland and Powell, 1998), spinel (Holland and Powell, 1998), melt (Holland and Powell, 2001).

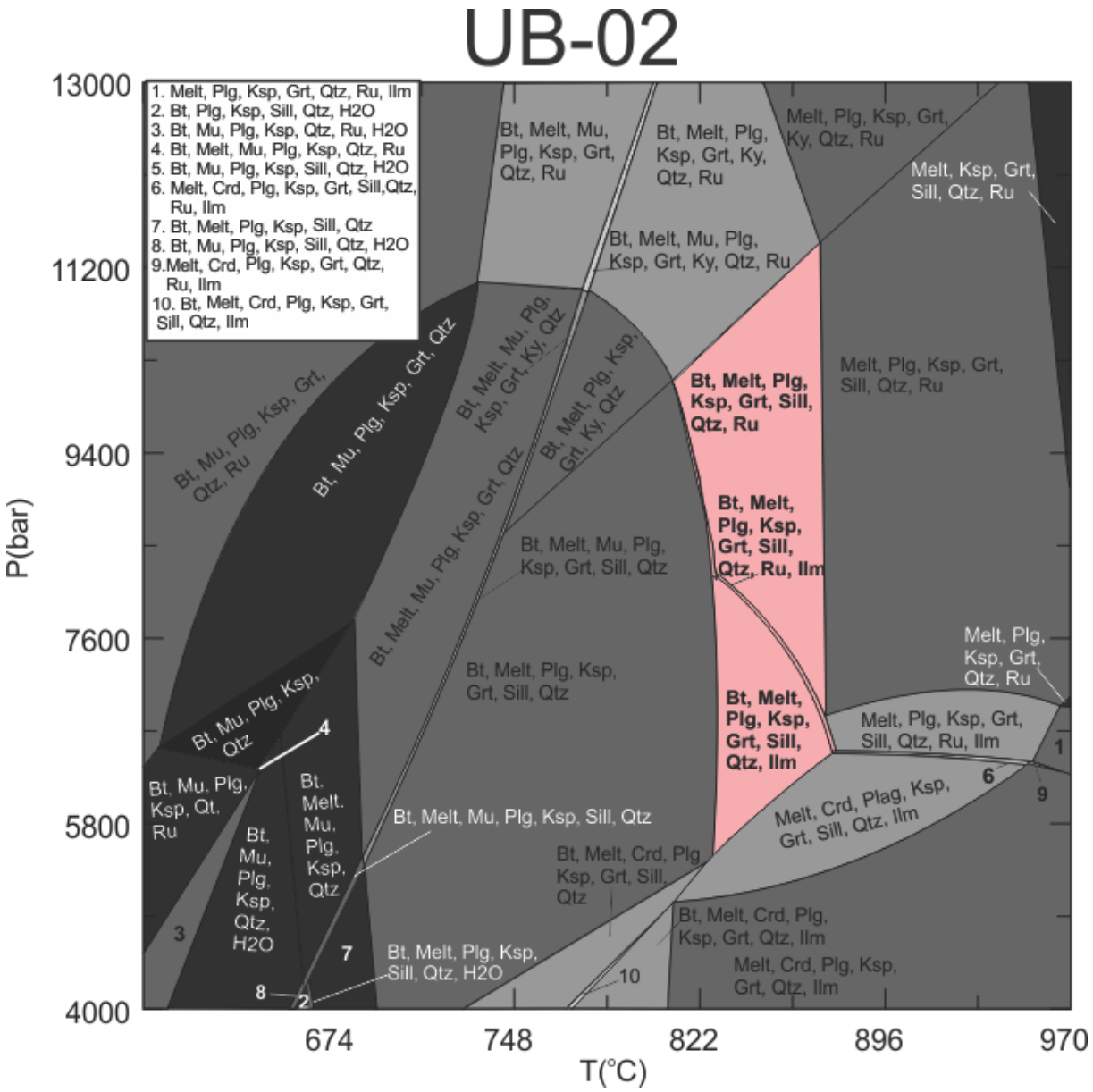

Fig 7.2.1. The P-T section calculated for the whole-rock chemistry of the UB-02 sample. The stability field marked in pink is the assemblage corresponding to the assemblage observed in the sample. Both ilmenite and rutile were observed in the samples, so both fields with ilmenite and rutile are marked. The fields are large and to further constrain the P-T conditions, compositional isopleths that represent the evolution of the minerals were plotted. Bt: Biotite; Ilm: Ilmenite; Crd: Cordierite; Plg: Plagioclase; Ksp: K-feldspar; Spl: Spinel; Qtz: Quartz; Ru: Rutile; Sill: Sillimanite; Grt: Garnet; Mu: Muscovite; Ky: Kyanite.

7.2.1 Modelling for UB-02

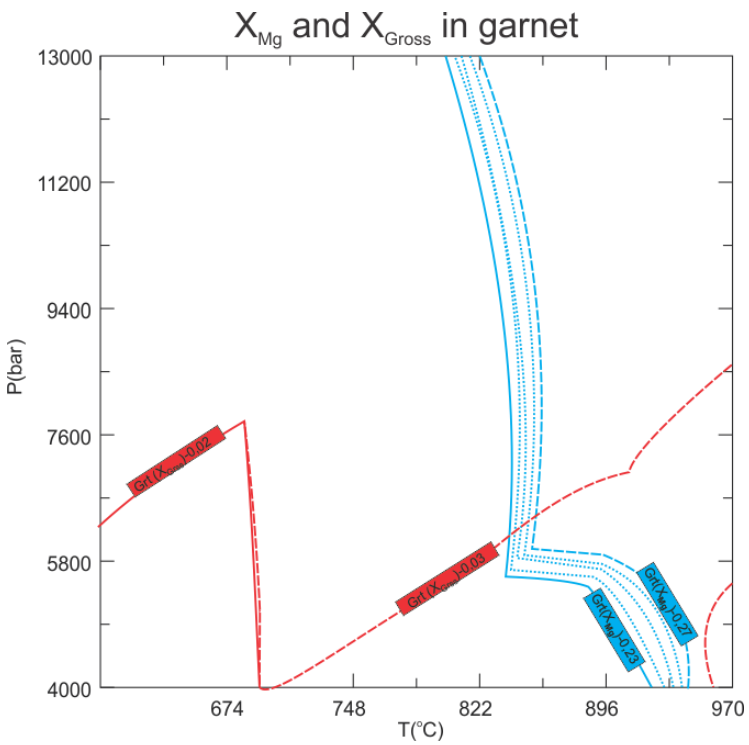

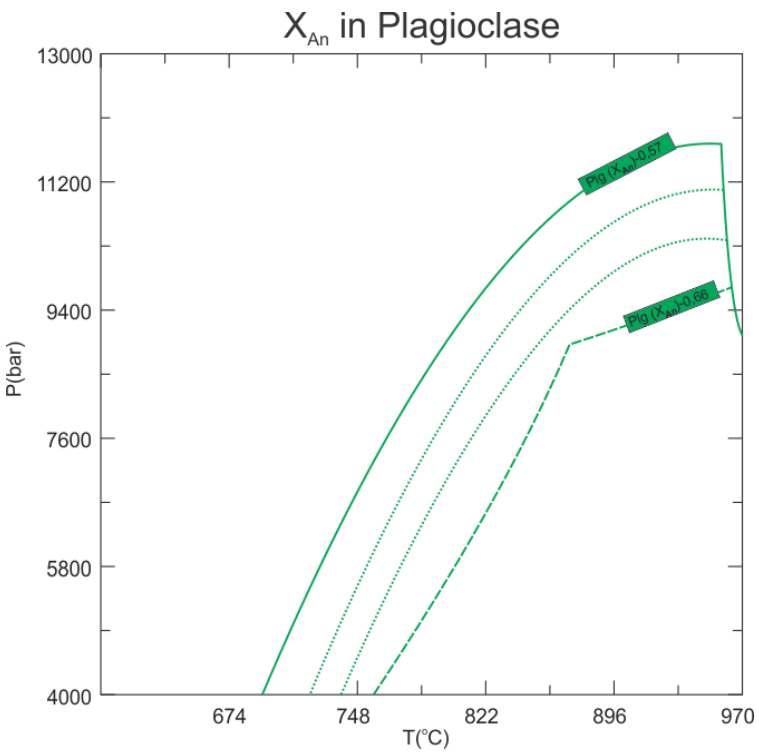

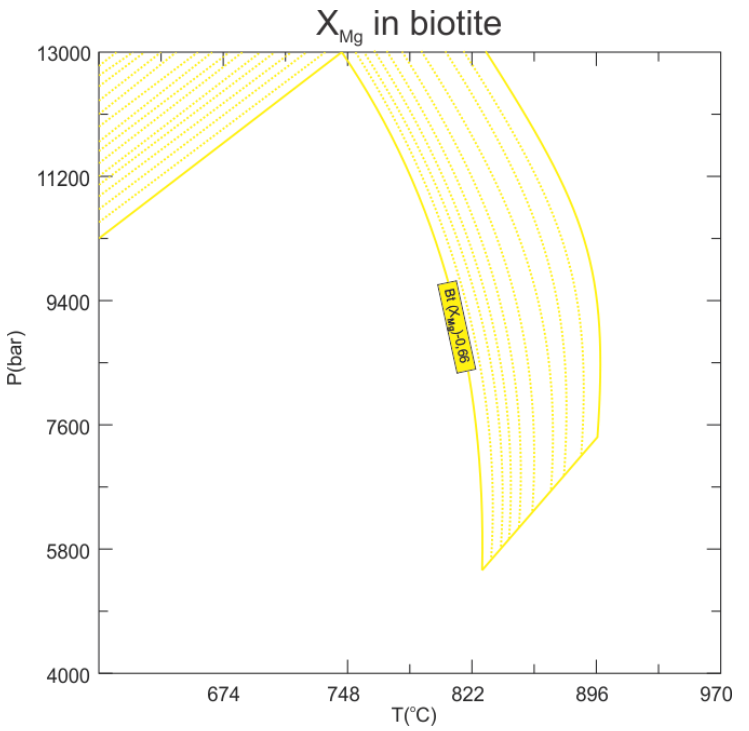

Fig 7.2.2. The various isopleths as derived from the calculated PT section plotted for ranges of mineral composition observed in the UB-02 sample. The steps are 0.01 for compositional isopleths.

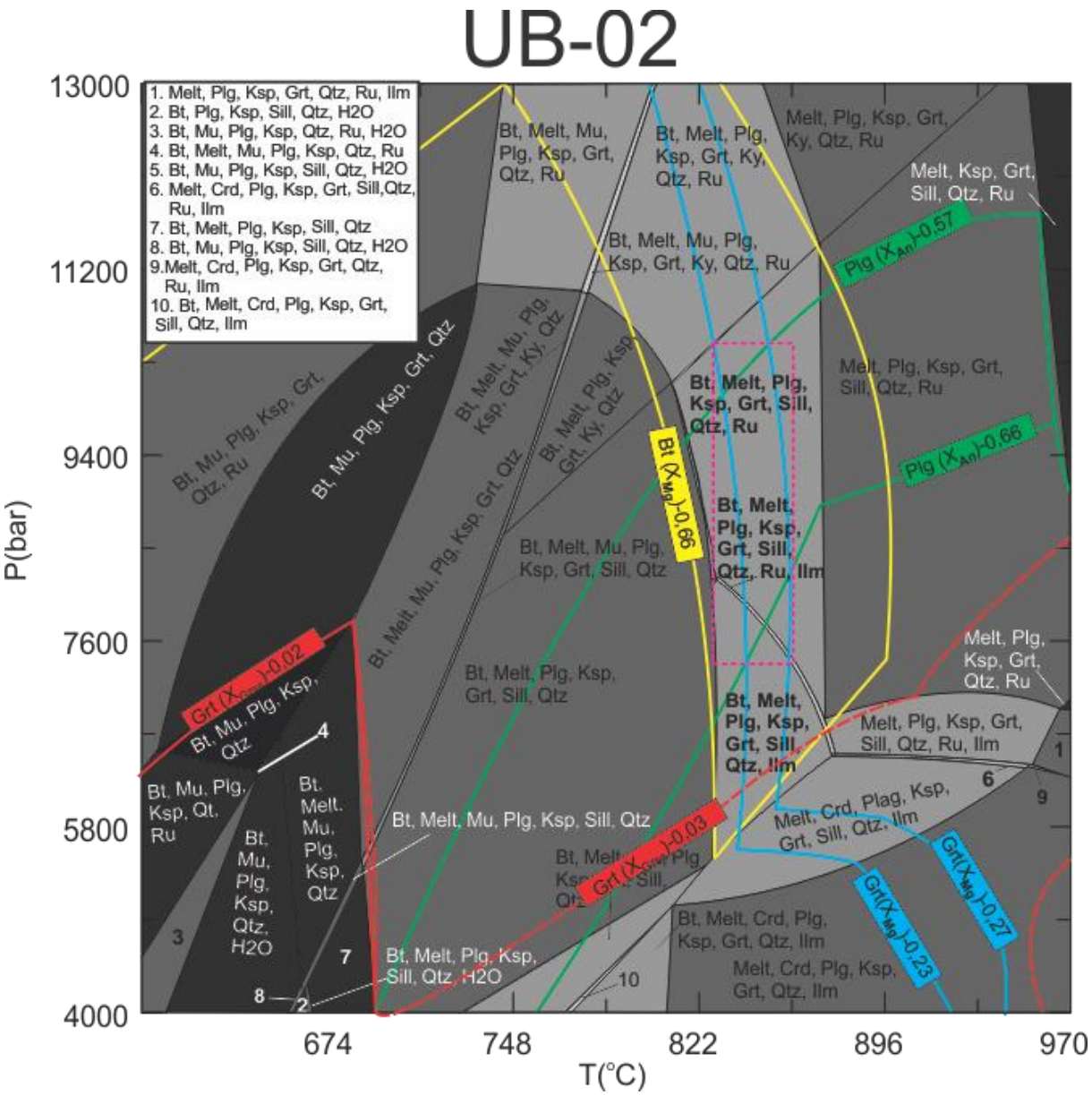

Fig 7.2.3. Compositional isopleths for the UB-02 minerals plotted on the P-T diagram. Bt: Biotite; Ilm: Ilmenite; Crd: Cordierite; Plg: Plagioclase; Ksp: K-feldspar; Spl: Spinel; Qtz: Quartz; Ru: Rutile; Sill: Sillimanite; Grt: Garnet; Mu: Muscovite; Ky: Kyanite.

7.2.2 Result

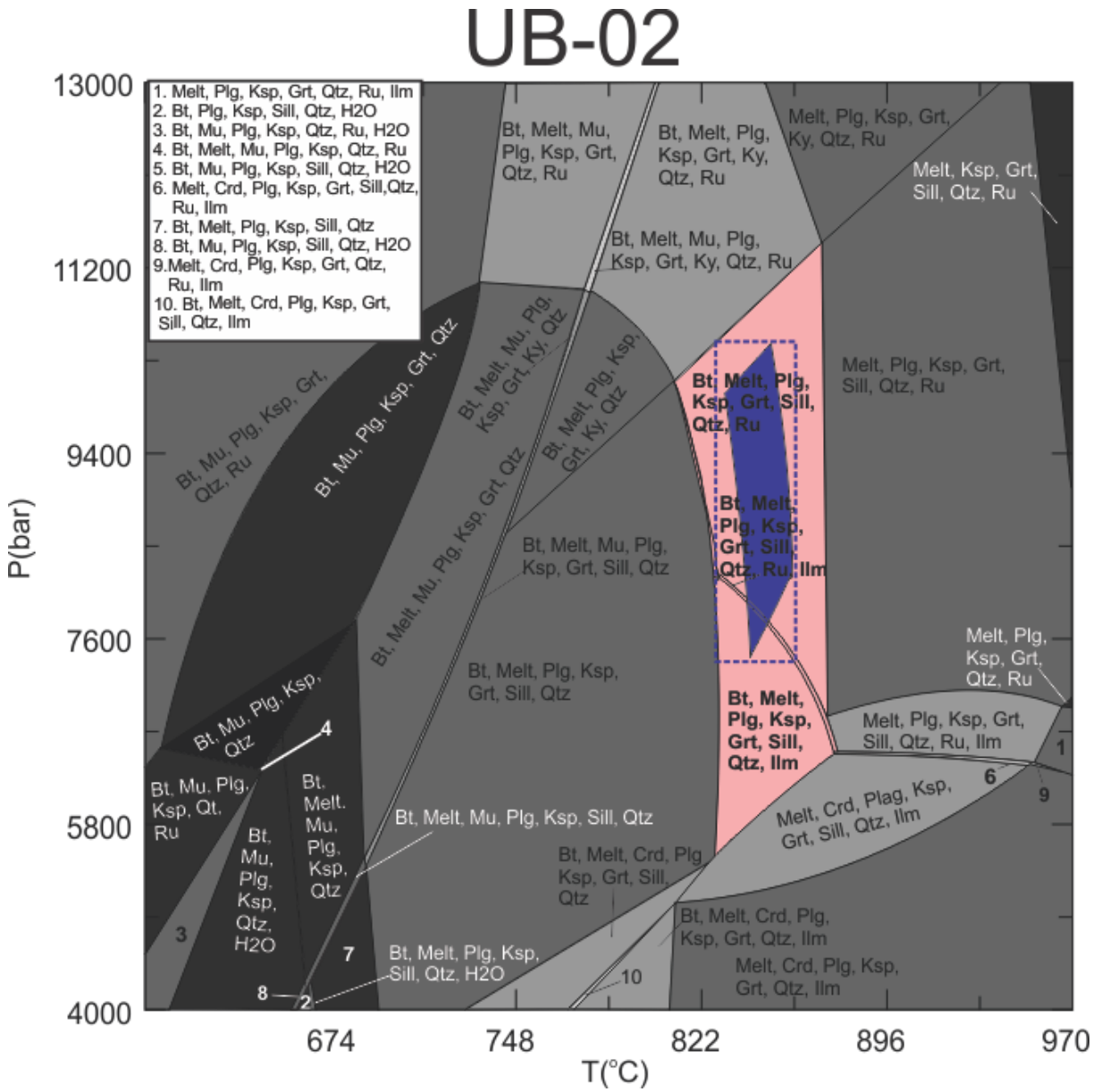

Fig 7.2.4. The P-T diagram with the P-T conditions (in blue) for UB-02 sample. Bt: Biotite; Ilm: Ilmenite; Crd: Cordierite; Plg: Plagioclase; Ksp: K-feldspar; Spl: Spinel; Qtz: Quartz; Ru: Rutile; Sill: Sillimanite; Grt: Garnet; Mu: Muscovite; Ky: Kyanite.

Comment on the results (Fig 7.2.4)

The mineral assemblage observed in the sample UB-02 contained only a small amount of rutile and even smaller amount of ilmenite. The assemblages that best fit the observed mineral assemblage are highlighted in pink, and suggest temperatures between c. 820-860°C and pressures of 5,5-11,5 kbar. The compositional isopleths constrain the equilibration of the sample to temperatures of c. 830-860°C and pressures of c. 7,5-10,5 kbar (blue box in Fig 7.2.4).

7.3 UA-11 Felsic granulite

As described earlier, this sample contains spinel enclosed within cordierite crystals. In order to characterize P-T conditions of the granulite formation, a P-T pseudosection was calculated for the bulk rock composition (Table 5.1.1). The estimated effective bulk composition was chosen to represent the spinel-bearing domain. The mineral assemblage of the sample UA-11 is: Pl-Bt-Qtz-Grt-Ksp-Sill-Spl-Crd-Ilm, while the mineral assemblage of the spinel-bearing domain is: Crd-Ksp-Sill-Ilm-Grt-Sp. The P-T sections was calculated for temperatures between 650-950°C and pressures of 1-10 kbar, in a system of Na_2O, MgO, Al_2O_3, SiO_2, K_2O, CaO, TiO_2, MnO, FeO and H_2O, and without any saturated components. The LOI content was used for water content. Table 5.1.1 shows the whole-rock composition and the effective bulk composition used. The solution models used are orthopyroxene (Holland and Powell, 1999), biotite (Tajcmanova et al., 2009), feldspar (Fuhrman et al., 1988) garnet (Holland and Powell, 1998), ilmenite (White et al., 2000), cordierite (Baumgartner, 2003), clinopyroxene (Holland and Powell, 1996), muscovite (Holland and Powell, 1998), spinel (Holland and Powell, 1998), melt (Holland and Powell, 2001).

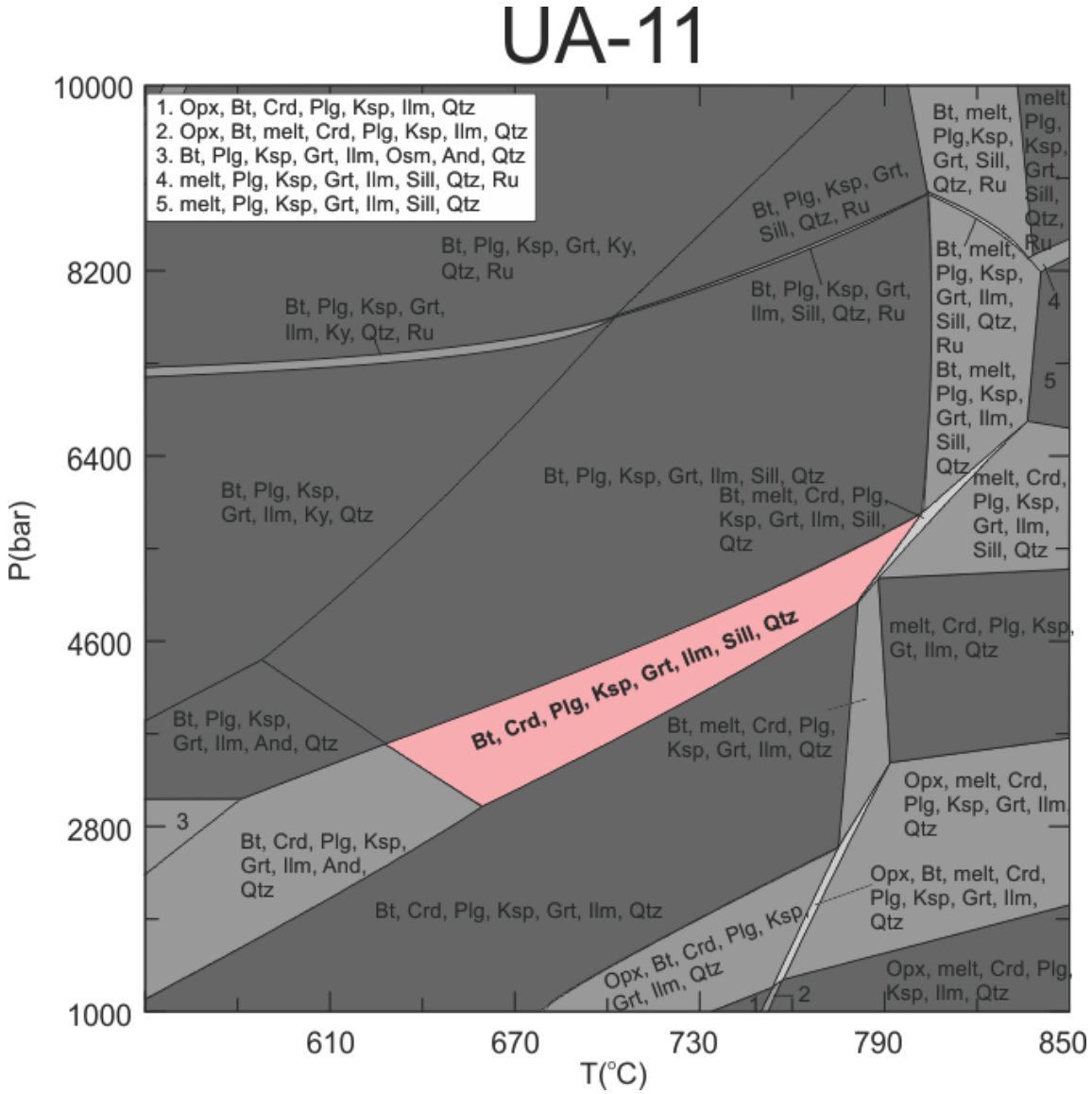

Fig 7.3.1. The P-T section calculated for the effective bulk composition of the UA-11 sample. The stability field marked in pink is the assemblage that best corresponds to the assemblage observed in the isolated spinel-bearing domains. Bt: Biotite; Ilm: Ilmenite; Crd: Cordierite; Plg: Plagioclase; Ksp: K-feldspar; Spl: Spinel; Qtz: Quartz; Ru: Rutile; Sill: Sillimanite; Grt: Garnet; Ky: Kyanite; Opx: Orthopyroxene; Osm: Osumilite; And: Andalusite.

7.3.1 Modelling for UA-11 whole-rock composition

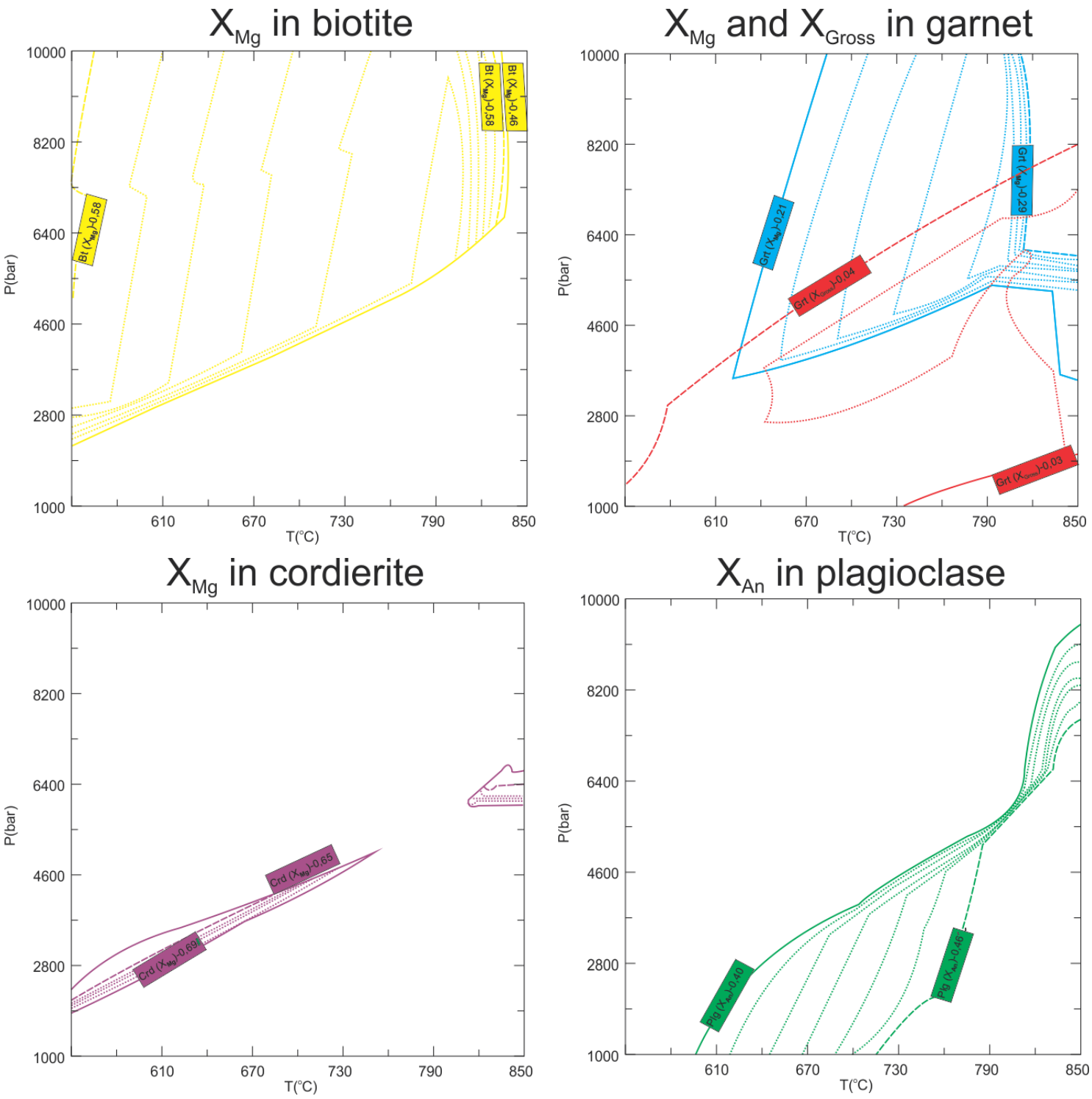

Fig 7.3.2. The various isopleths as derived from the calculated PT section plotted for ranges of mineral composition observed in the UA-11 sample. The steps are 0.01 for compositional isopleths.

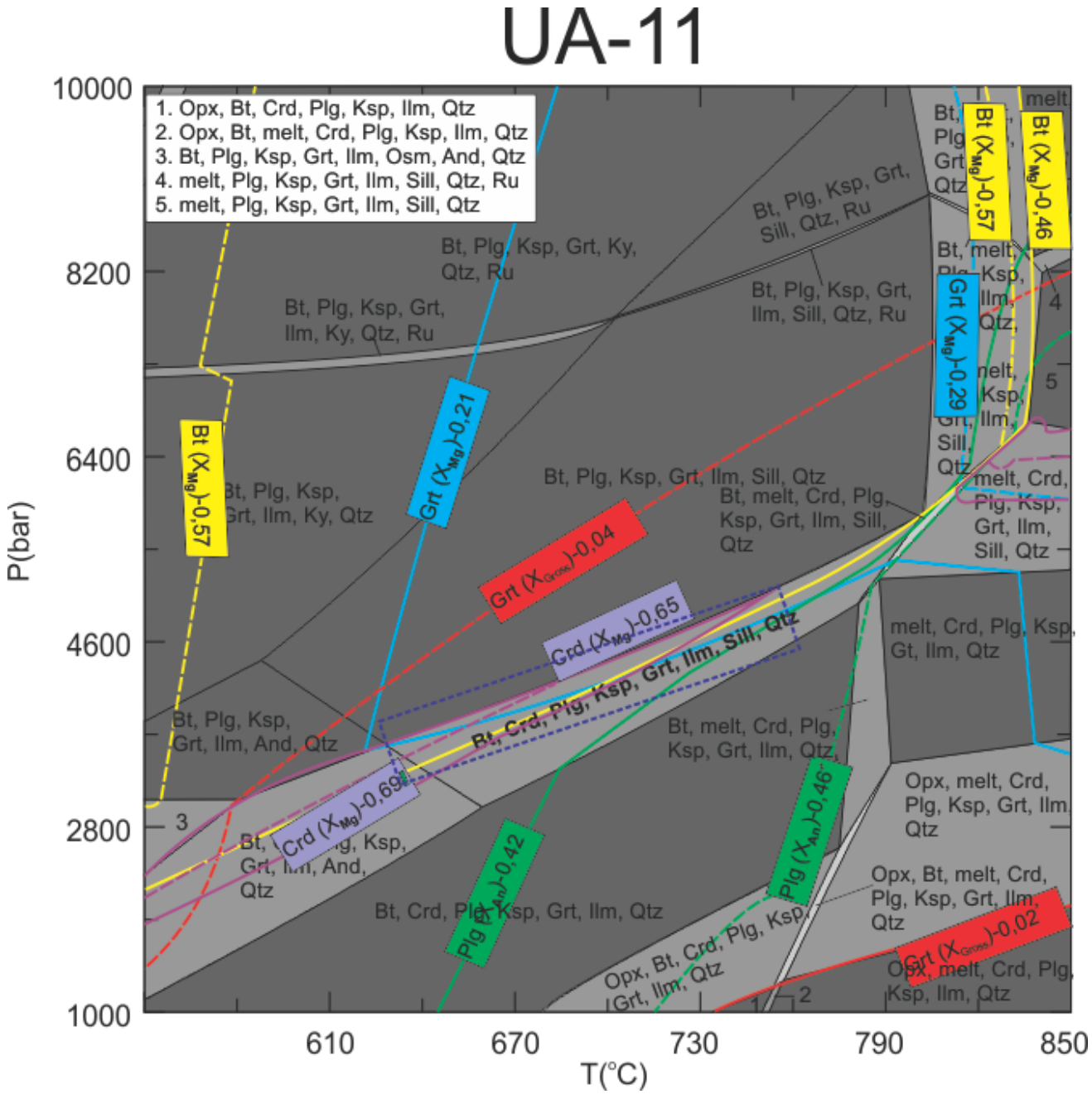

Fig 7.3.3. Compositional isopleths for the UA-11 minerals plotted on the P-T diagram. The light blue box show the best assemblage for the sample UA-11. Bt: Biotite; Ilm: Ilmenite; Crd: Cordierite; Plg: Plagioclase; Ksp: K-feldspar; Spl: Spinel; Qtz: Quartz; Ru: Rutile; Sill: Sillimanite; Grt: Garnet; Ky: Kyanite; Opx: Orthopyroxene; Osm: Osumilite; And: Andalusite.

7.3.2 Result whole-rock composition

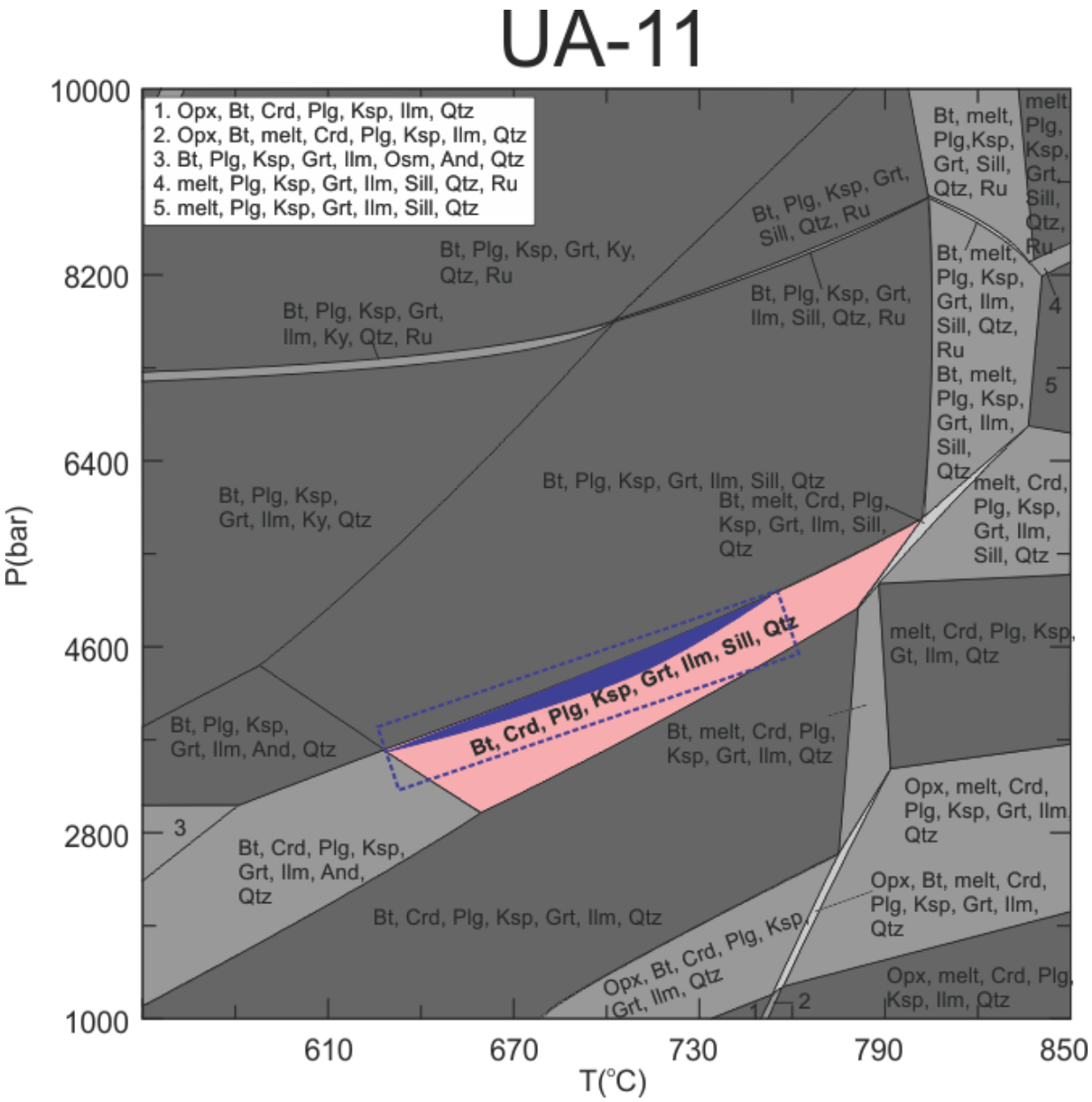

Fig 7.3.4. The P-T pseudosection with the estimated P-T conditions (in blue) for UA-11 whole-rock composition. Bt: Biotite; Ilm: Ilmenite; Crd: Cordierite; Plg: Plagioclase; Ksp: K-feldspar; Spl: Spinel; Qtz: Quartz; Ru: Rutile; Sill: Sillimanite; Grt: Garnet; Ky: Kyanite; Opx: Orthopyroxene; Osm: Osumilite; And: Andalusite.

Comment to the result (Fig 7.3.4)

The mineral assemblage shows temperatures of c. 620-810°C and pressure of 2,8-6,0 kbar,. With the isopleths plotted, the metamorphic conditions suggest temperatures between c. 620-760°C and pressure of c. 3,5-5,4 kbar. This stability field does not show spinel and thus makes it inadequate to use for thermobarometry for this sample.

EFFECTIVE BULK COMPOSITION

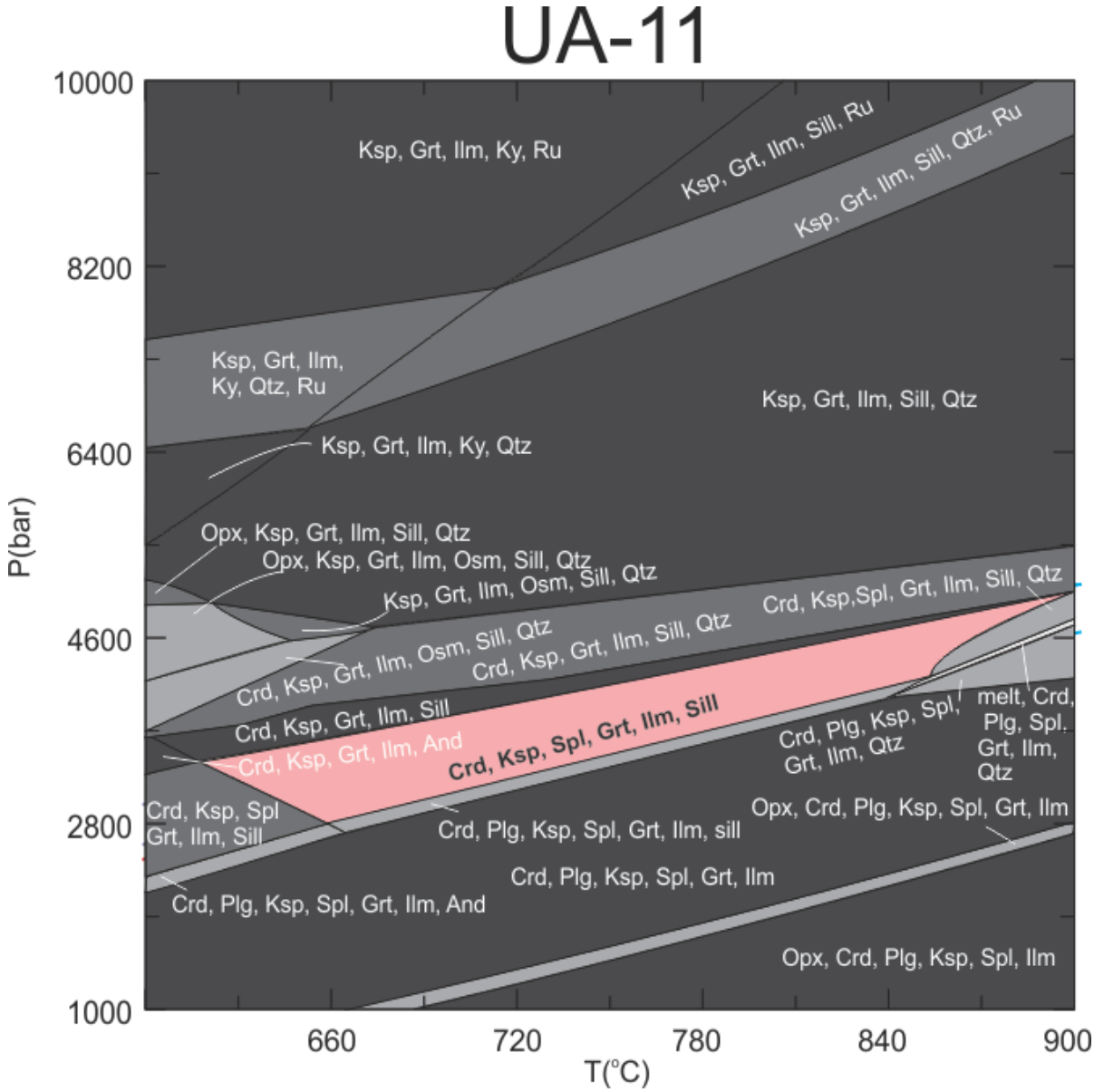

Fig 7.3.5. The P-T section calculated for the effective bulk composition of the UA-11 sample. The stability field marked in pink is the assemblage that best corresponds to the assemblage observed in the isolated spinel-bearing zone the sample. Bt: Biotite; Ilm: Ilmenite; Crd: Cordierite; Plg: Plagioclase; Ksp: K-feldspar; Spl: Spinel; Qtz: Quartz; Ru: Rutile; Sill: Sillimanite; Grt: Garnet; Ky: Kyanite; Opx: Orthopyroxene; Osm: Osumilite; And: Andalusite.

7.3.3 Modelling for UA-11 Effective bulk composition

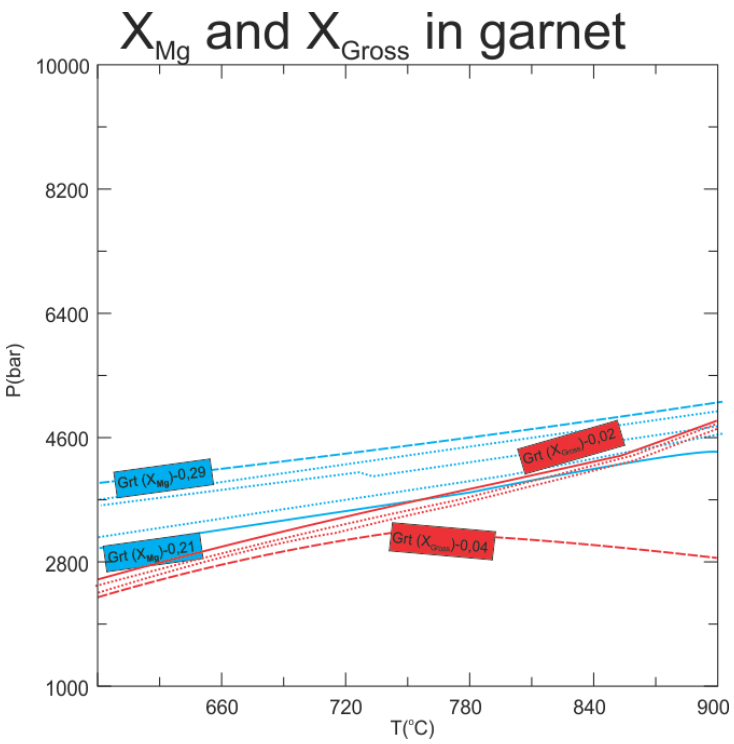

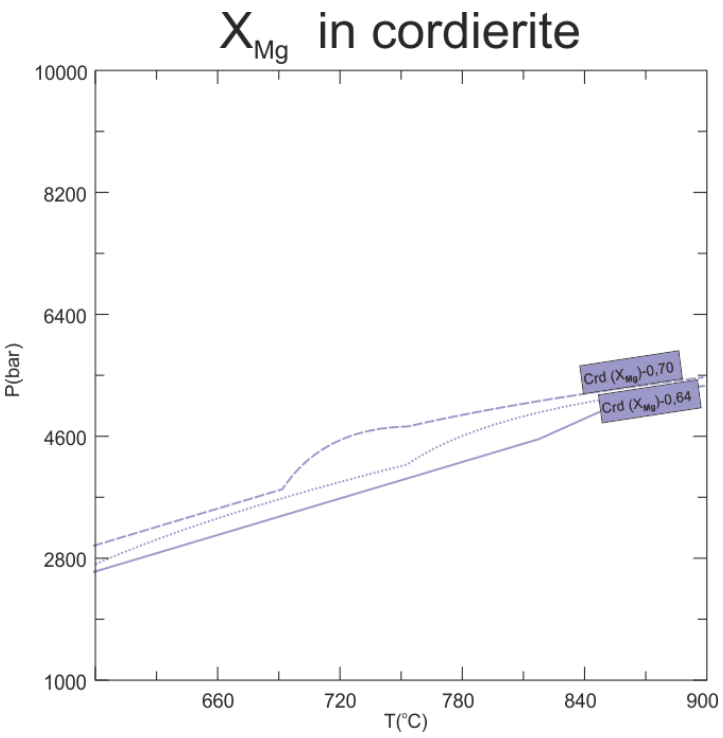

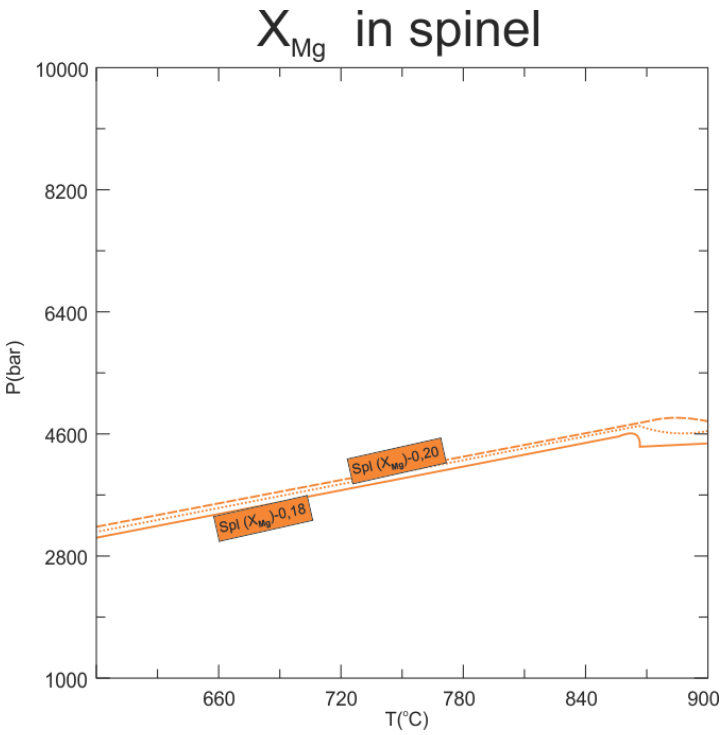

Fig 7.3.6. The various isopleths as derived from the calculated PT section plotted for ranges of mineral composition observed in the UA-11 sample. The steps are 0.01 for compositional isopleths.

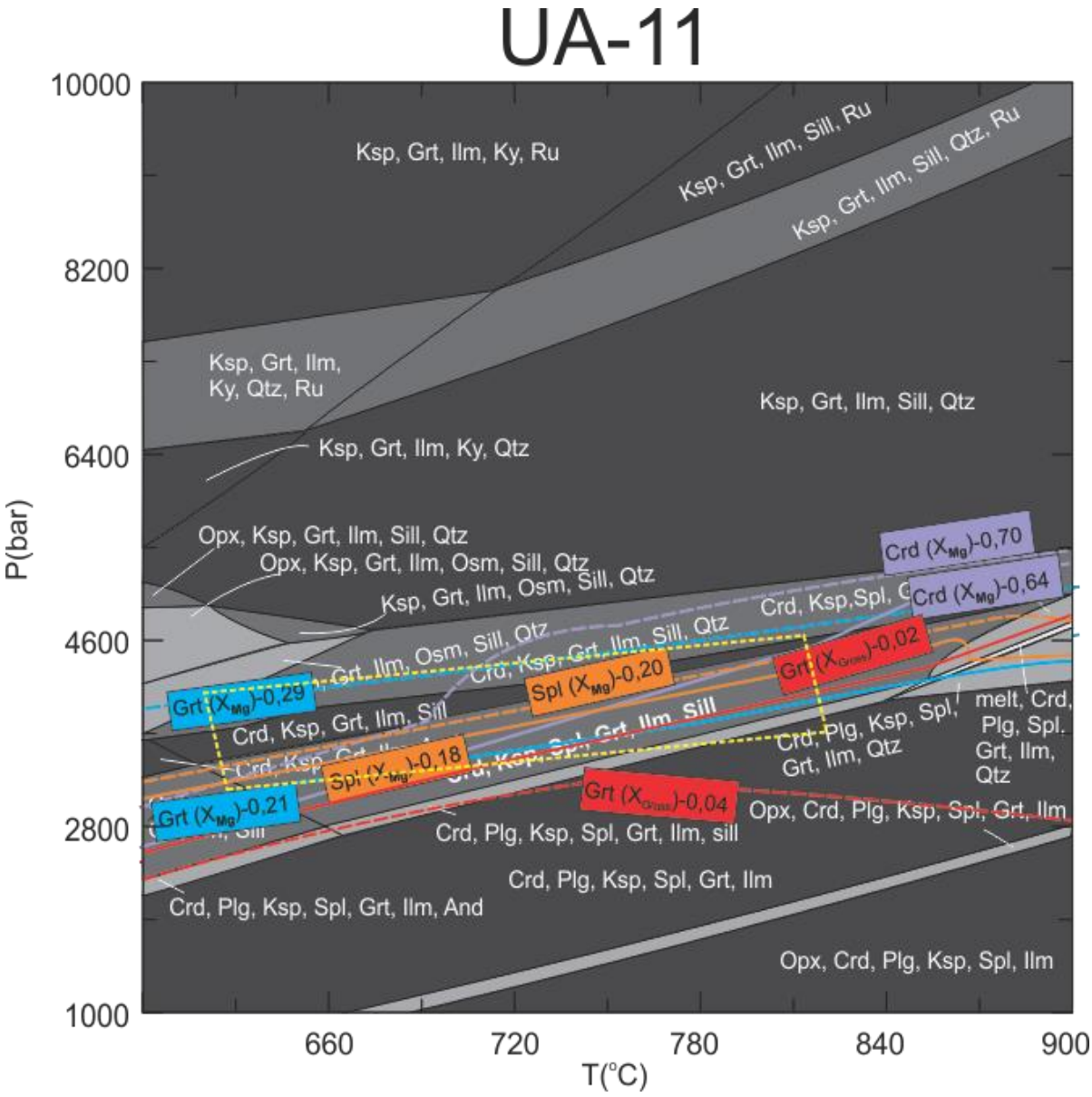

Fig 7.3.7. Compositional isopleths for the UA-11 minerals plotted on the P-T diagram. The green box show the best assemblage for the sample UA-11. Bt: Biotite; Ilm: Ilmenite; Crd: Cordierite; Plg: Plagioclase; Ksp: K-feldspar; Spl: Spinel; Qtz: Quartz; Ru: Rutile; Sill: Sillimanite; Grt: Garnet;; Ky: Kyanite; Opx: Orthopyroxene; Osm: Osumilite; And: Andalusite.

7.3.4 Result effective bulk composition

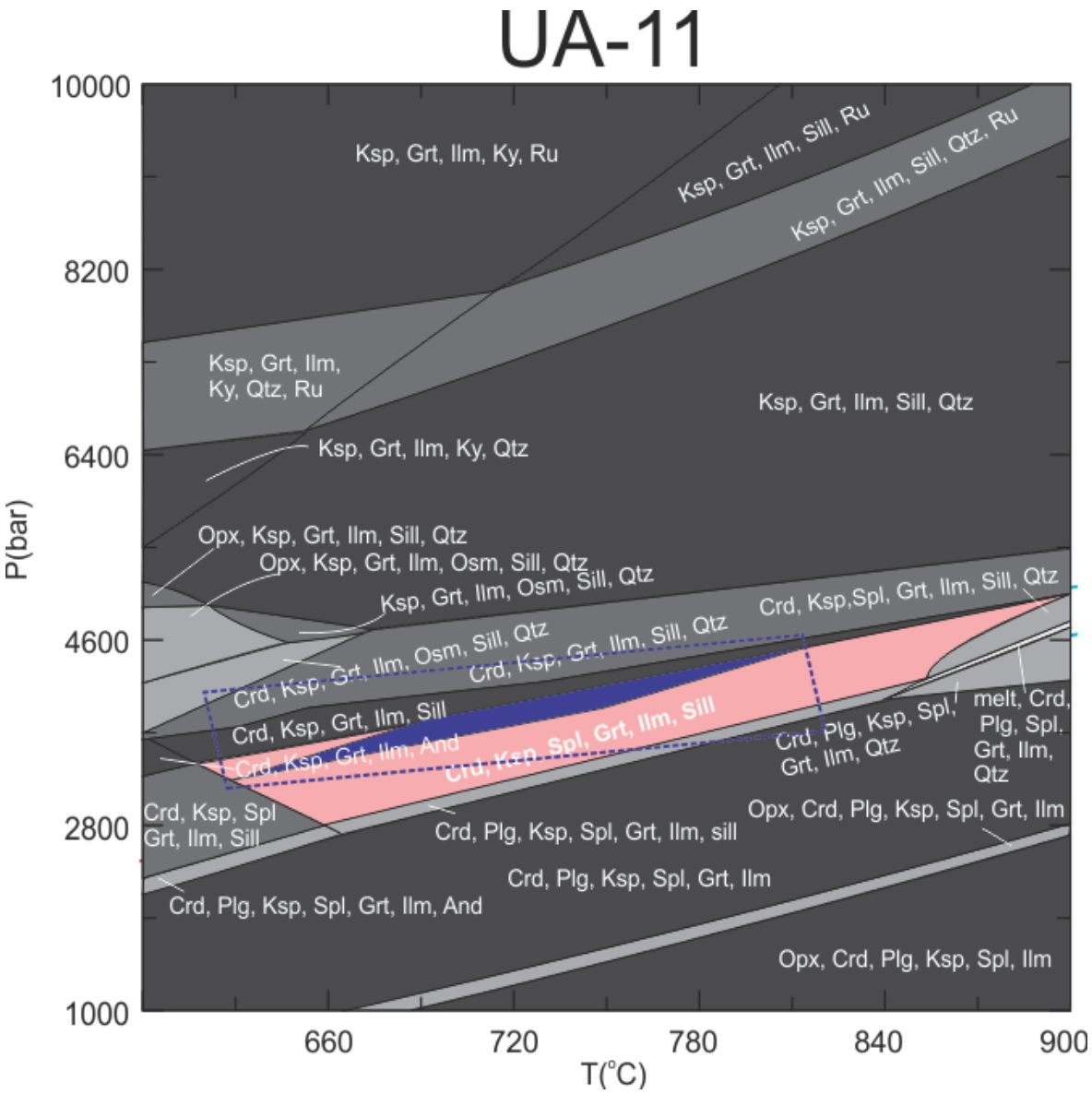

Fig 7.3.8. The P-T diagram with the P-T conditions (in blue) for UA-11 for the estimated effective bulk composition. T yellow box show the stability field constrined by the isopleths. Bt: Biotite; Ilm: Ilmenite; Crd: Cordierite; Plg: Plagioclase; Ksp: K-feldspar; Spl: Spinel; Qtz: Quartz; Ru: Rutile; Sill: Sillimanite; Grt: Garnet;; Ky: Kyanite; Opx: Orthopyroxene; Osm: Osumilite; And: Andalusite.

Comment to the result (Fig 7.3.8)

The stability field that best fits the observed assemblage in the spinel-bearing domains does not contain any biotite, plagioclase or quartz, but is fully consistent with the assemblage observed in the spinel-bearing zone. The field with the observed mineral assemblage suggests temperatures of equilibration between c. 600°C and 890°C and pressure of c. 3,0-4,5 kbar. The conditions of equilibration are restricted by the compositional isopleths to temperatures of c. 630-800°C and pressures of c. 2,8-4,2 kbar.

7.4 UA-31B Intermediate granulite

The mineral assemblage for the spinel-bearing domain in the sample UA-31B is: Bt-Plg-Crd-Ksp-Sill-Ilm-Grt-Sp. The P-T sections was calculated at temperatures between 650-1000°C and 1-10 kbar, in a system of Na_2O, MgO, Al_2O_3, SiO_2, K_2O, CaO, TiO_2, MnO, FeO and H_2O, and without any saturated components. The LOI content was used for water content. The effective bulk composition was used and is shown in Table 5.1.1. The solution models used are orthopyroxene (Holland and Powell, 1999), biotite (Tajcmanova et al., 2009), feldspar (Fuhrman et al., 1988) garnet (Holland and Powell, 1998), ilmenite (White et al., 2000), cordierite (Baumgartner, 2003), clinopyroxene (Holland and Powell, 1996), muscovite (Holland and Powell, 1998), spinel (Holland and Powell, 1998), melt (Holland and Powell, 2001), amphibole (Diener et al, 2011).

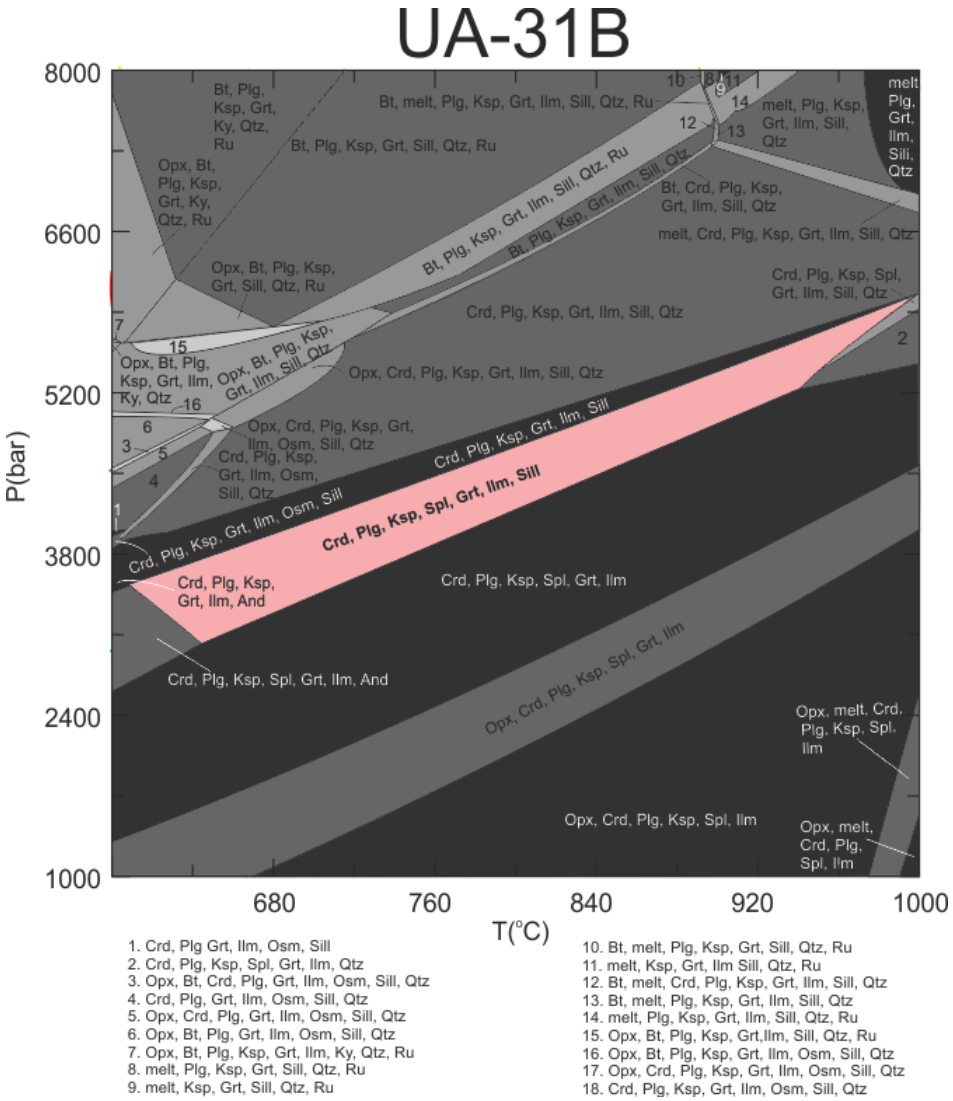

Fig 7.4.1. The P-T section calculated for the whole-rock chemistry of the UA-31B sample. The stability field marked in pink is the assemblage that best corresponds to the assemblage observed in the isolated spinel-bearing zone the sample. Bt: Biotite; Ilm: Ilmenite; Crd: Cordierite; Plg: Plagioclase; Ksp: K-feldspar; Spl: Spinel; Qtz: Quartz; Ru: Rutile; Sill: Sillimanite; Grt: Garnet; Mu: Muscovite; Ky: Kyanite; Opx: Orthopyroxene; Cpx: Clinopyroxene

7.4.1 Modelling for UA-31B

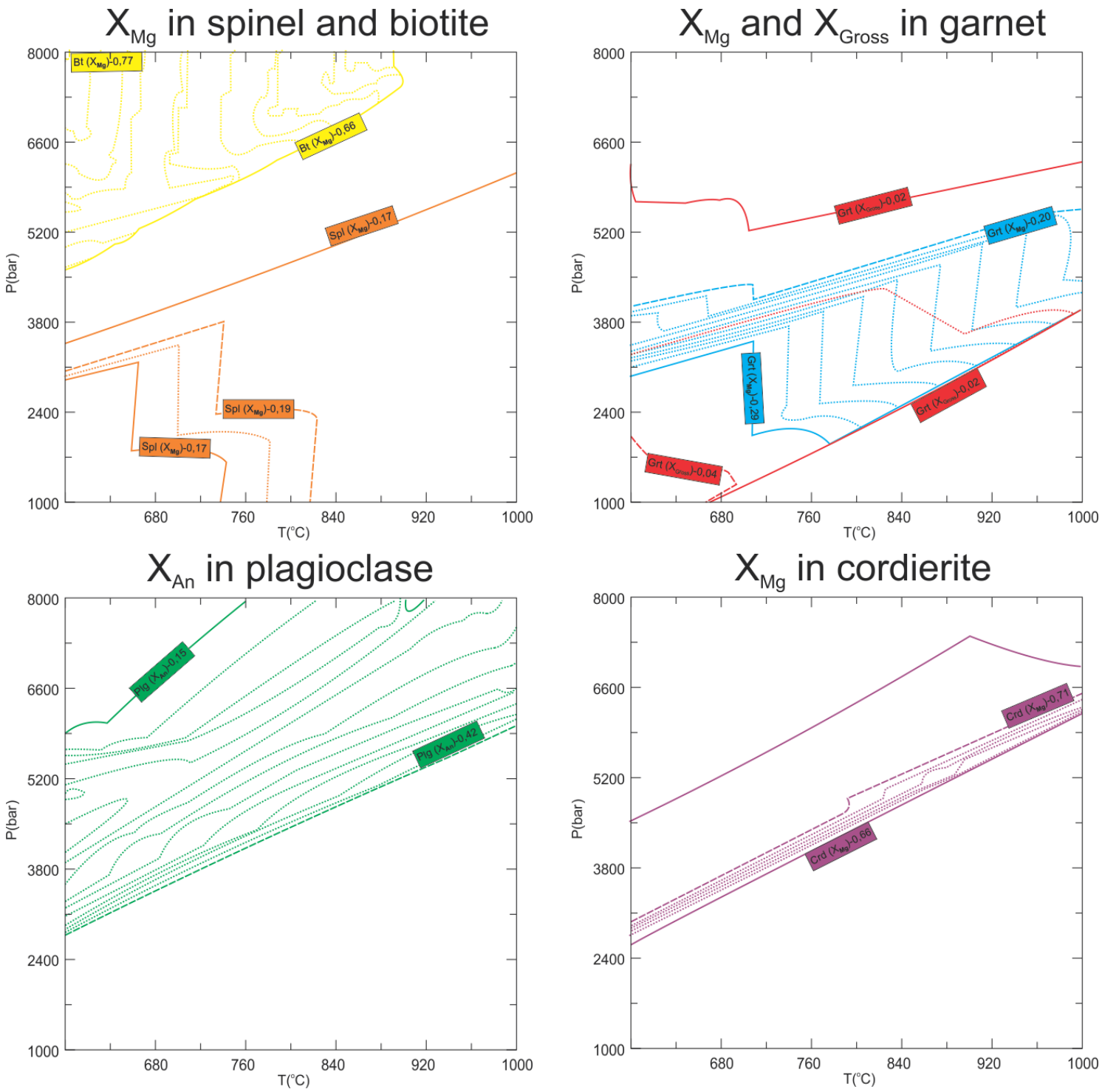

Fig 7.4.2. The various isopleths as derived from the calculated P-T section plotted for ranges of mineral composition observed in the UA-31B sample. The steps are 0.01 for compositional isopleths for all excluding the isopleths for plagioclase which is 0,02.

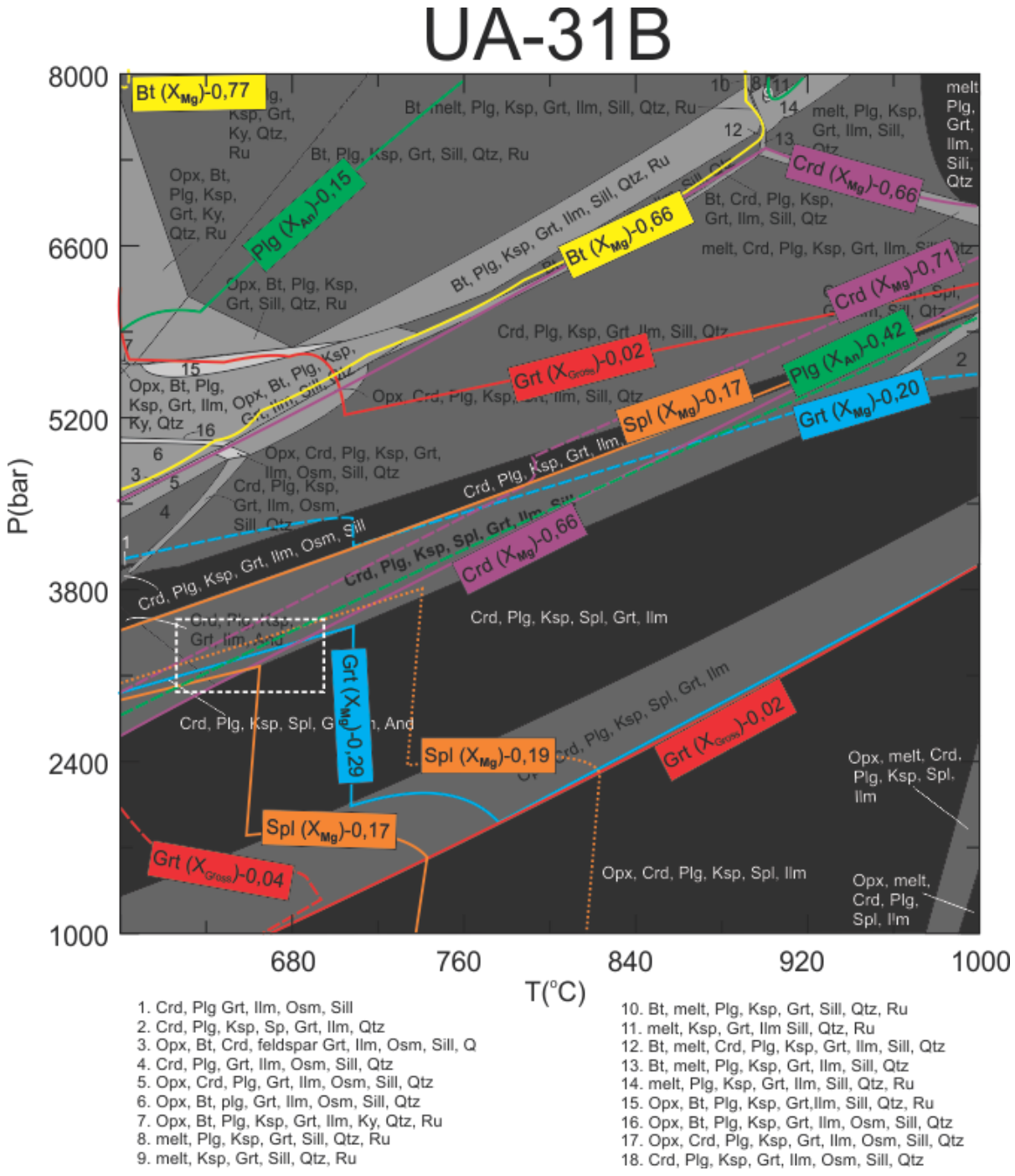

Fig 7.4.3. Compositional isopleths for the UA-31B minerals plotted on the P-T diagram. The white box show the best assemblage for the sample UA-31B. Bt: Biotite; Ilm: Ilmenite; Crd: Cordierite; Plg: Plagioclase; Ksp: K-feldspar; Spl: Spinel; Qtz: Quartz; Ru: Rutile; Sill: Sillimanite; Grt: Garnet; Mu: Muscovite; Ky: Kyanite; Opx: Orthopyroxene; Cpx: Clinopyroxene.

7.4.2 Result

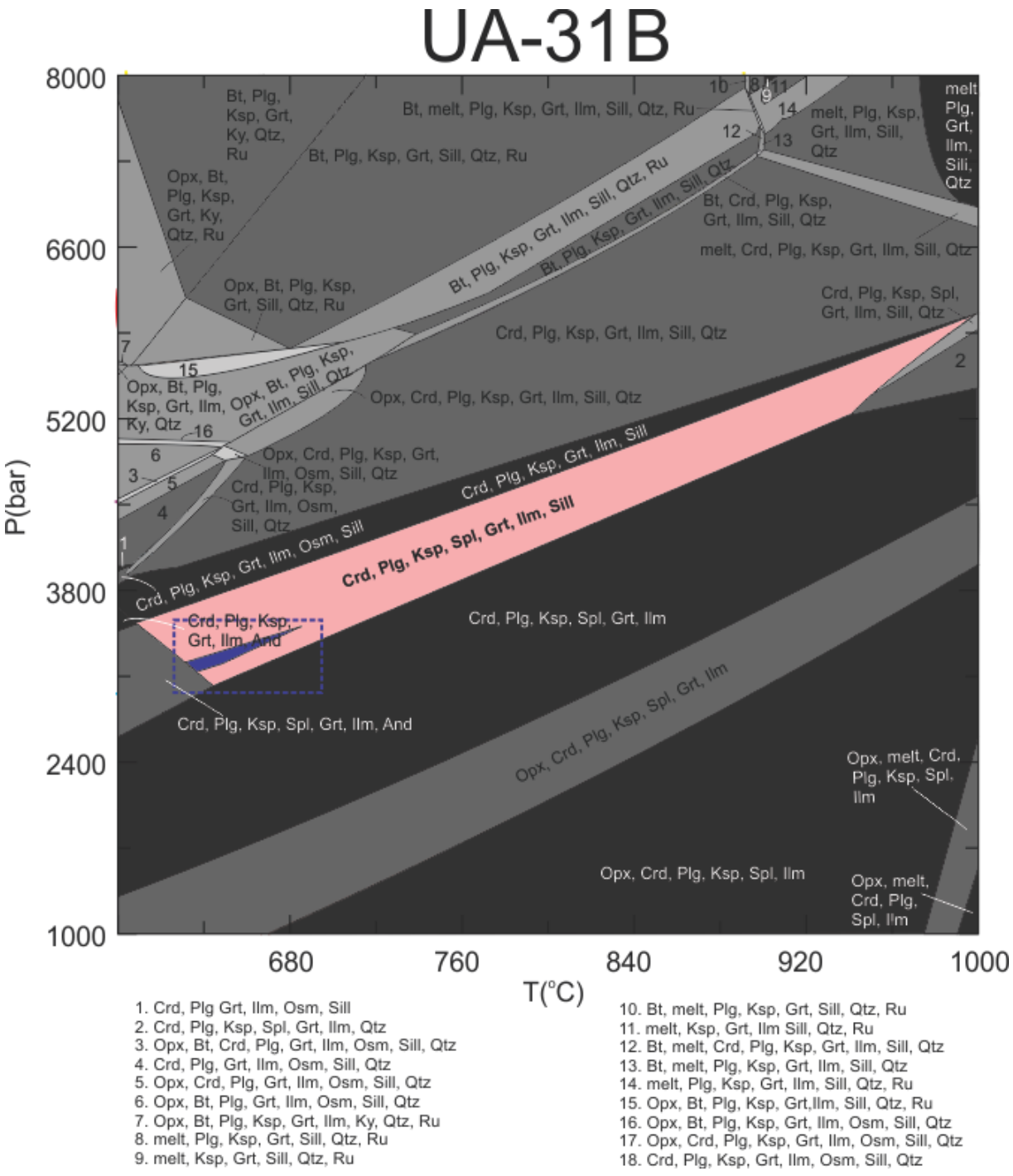

Fig 7.4.4. The P-T diagram with the P-T conditions (in blue) for UA-31B. Bt: Biotite; Ilm: Ilmenite; Crd: Cordierite; Plg: Plagioclase; Ksp: K-feldspar; Spl: Spinel; Qtz: Quartz; Ru: Rutile; Sill: Sillimanite; Grt: Garnet; Mu: Muscovite; Ky: Kyanite; Opx: Orthopyroxene; Cpx: Clinopyroxene

Comments to the result (Fig 7.4.4)

The mineral assemblage observed in the spinel-bearing domain corresponds to the stability field highlighted in pink in Fig. 7.5.4., except that biotite was observed in the domain. One reason for the absence biotite in the modelled stability field could be inaccuracy in the

solution models for biotite and cordierite. One other reason could be that the estimation for the effective bulk composition is not accurate enough. The field with the mineral assemblage is not temperature dependent, but is located between pressures of c. 3,0-6,0 kbar. The compositional isopleths (X_{Mg} in biotite, cordierite, spinel and garnet, X_{An} in plagioclase and X_{Gross} in garnet) constrain the field further to temperatures between c. 640-690°C and pressure of c. 3,0-3,5 kbar.

7.5 R10-18 Mafic granulite

The mineral assemblage for the R10-18 sample is: Pl-Bt-Qtz-Opx-Amp. The P-T sections was calculated at temperatures between 650-950°C and 1-10 kbar, in a system of Na_2O, MgO, Al_2O_3, SiO_2, K_2O, CaO, TiO_2, MnO, FeO and H_2O, and without saturated components. The LOI content was used for water content. The whole rock composition of weight percent was used and is indicated in Table 5.1.1. The solution models used are orthopyroxene (Holland and Powell, 1999), biotite (Holland and Powell, 1999), feldspar (Fuhrman et al., 1988) garnet (Holland and Powell, 1998), ilmenite (White et al., 2000), cordierite (Baumgartner, 2003), clinopyroxene (Holland and Powell, 1996), muscovite (Holland and Powell, 1998), spinel (Holland and Powell, 1998), melt (Holland and Powell, 2001), amphibole (Diener et al, 2011).

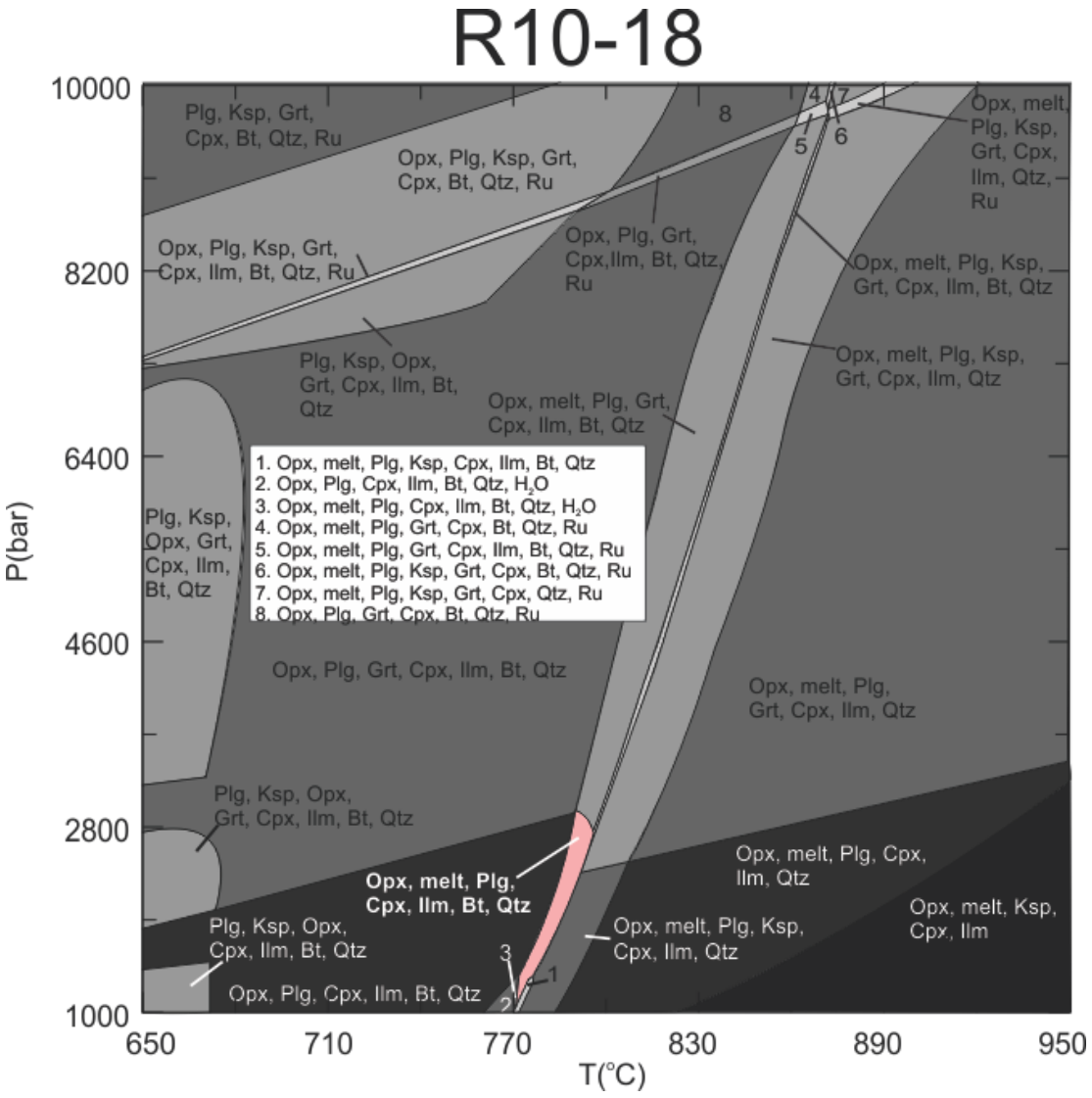

Fig 7.5.1. The P-T section calculated for the whole-rock chemistry of the R10-18 sample. The stability field marked in pink is the assemblage corresponding to the assemblage observed in the sample. Bt: Biotite; Ilm: Ilmenite; Crd: Cordierite; Plg: Plagioclase; Ksp: K-feldspar; Spl: Spinel; Qtz: Quartz; Ru: Rutile; Grt: Garnet; Opx: Orthopyroxene; Cpx: Clinopyroxene.

7.5.1 Modelling for R10-18

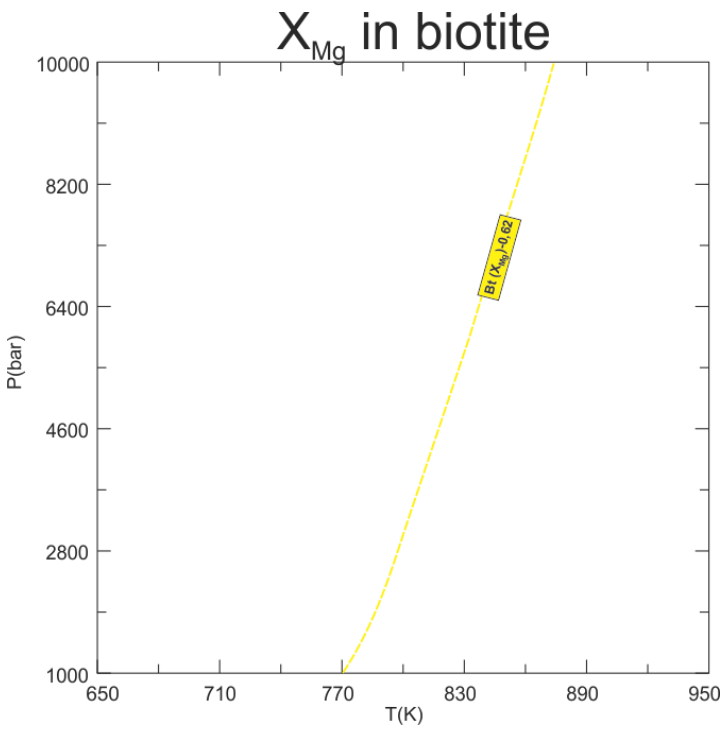

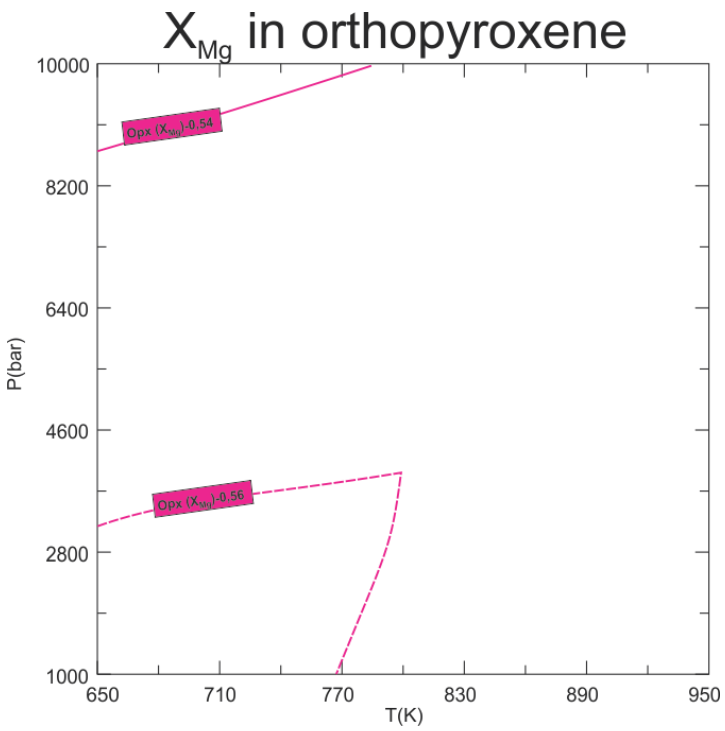

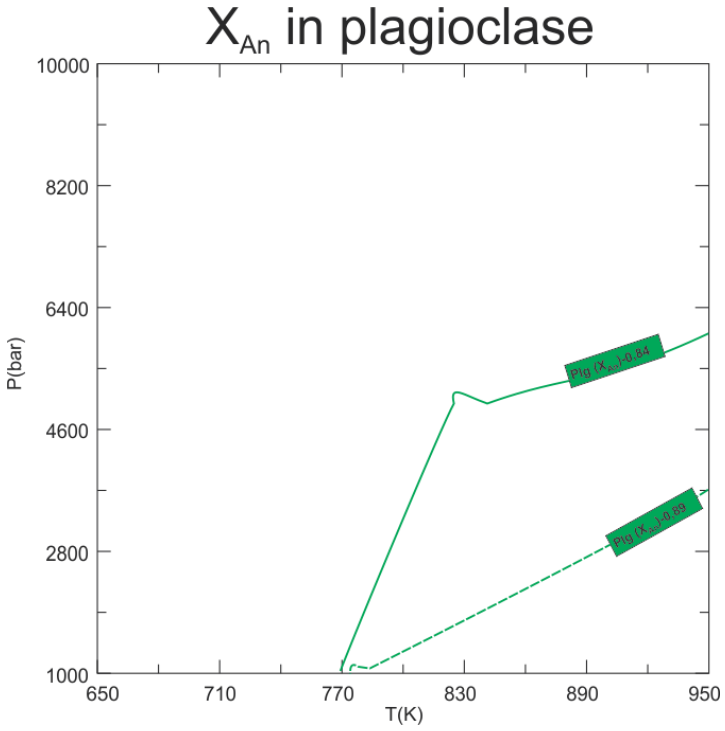

Fig 7.5.2. The various isopleths as derived from the calculated P-T section plotted for ranges of mineral compositions observed in the R10-18 sample. The steps are 0.01 for compositional isopleths.

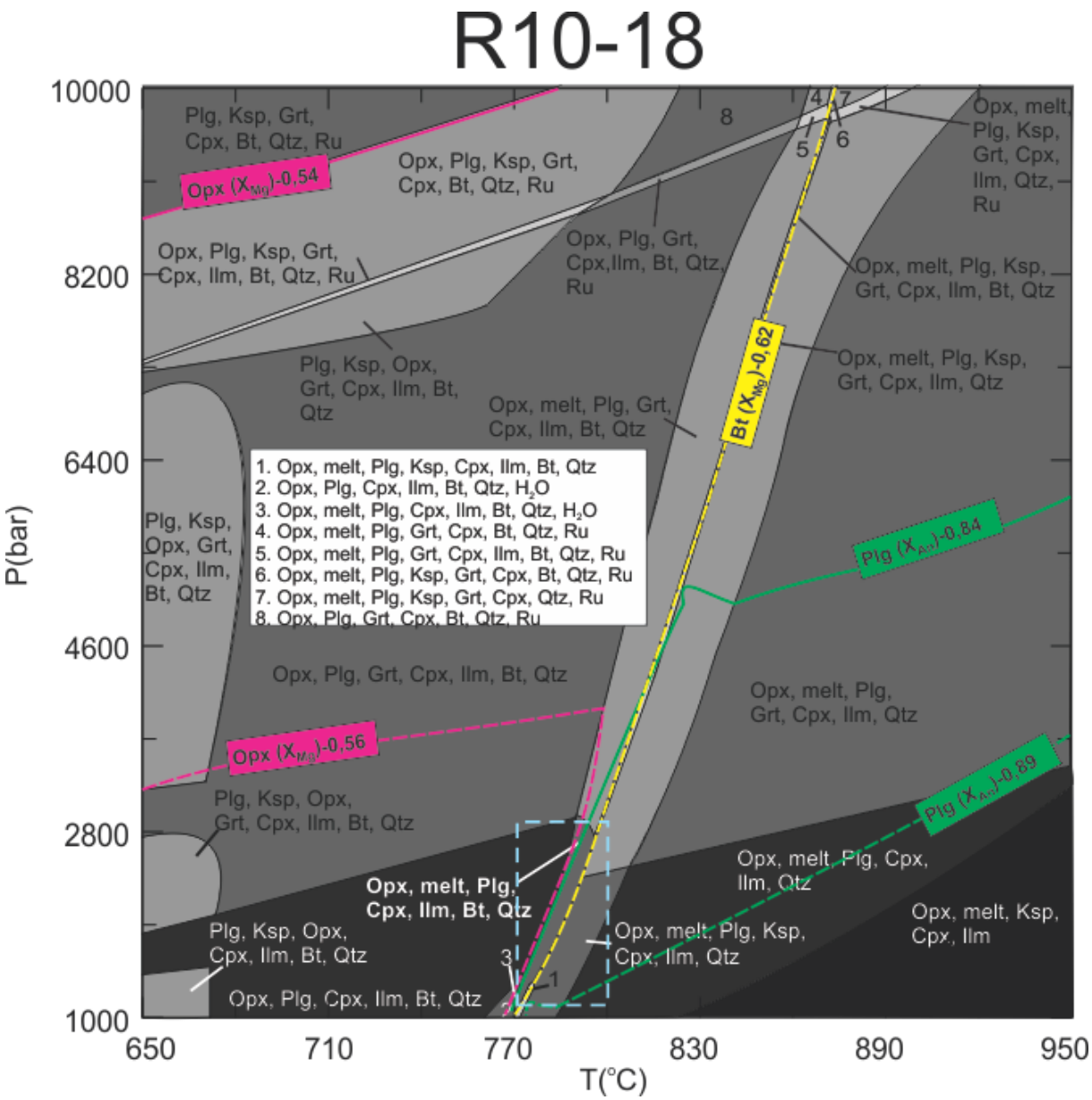

Fig 7.5.3. Compositional isopleths for the R10-18 minerals plotted on the P-T diagram. Light blue box show area where the isopleths cross Bt: Biotite; Ilm: Ilmenite; Crd: Cordierite; Plg: Plagioclase; Ksp: K-feldspar; Spl: Spinel; Qtz: Quartz; Ru: Rutile; Grt: Garnet; Opx: Orthopyroxene; Cpx: Clinopyroxene.

7.5.2 Result

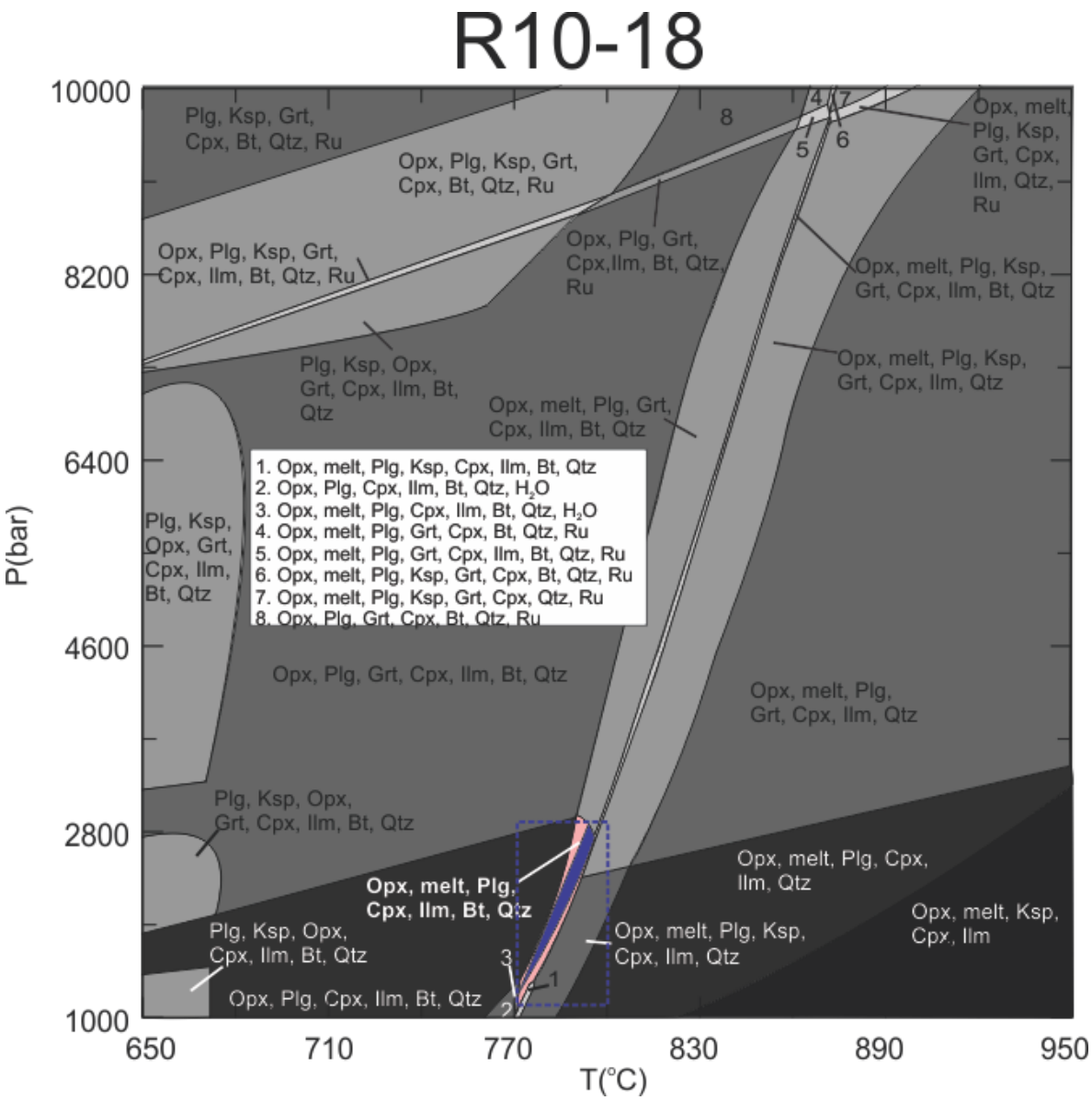

Fig 7.5.4. The P-T diagram with the P-T conditions (in blue) for the R10-18 sample.. Bt: Biotite; Ilm: Ilmenite; Crd: Cordierite; Plg: Plagioclase; Ksp: K-feldspar; Spl: Spinel; Qtz: Quartz; Ru: Rutile; Grt: Garnet; Opx: Orthopyroxene; Cpx: Clinopyroxene.

Comments on the results Fig 7.5.4

The stability filed that best covers the mineral assemblage of the sample R10-18 can be found between the temperatures of c. 770-800°C and pressures between c. 1,0-3,0 kbar. The compositional isopleths of orthopyroxene, biotite and plagioclase constrains the field further and show that the stability field can be found at temperature of c. 780-790°C and pressure of c. 1,4-2,0 kbar. The stability field for garnet is also a constrain for the pressure, as no garnet was observed in the sample and garnet is present in all the fields above pressures of c. 2,8 kbar.

Clinopyroxene was not observed in the thin section, but it is present in the mineral stability field where the isopleths cross. A reason for this could be that the whole-rock composition is slightly incorrect, or the rock is not as homogenous as originally thought and the thin section was made in an area of the sample where no clinopyroxene was present. The modelled volume of clinopyroxene is only around 2%. When plotting the variable CaO content into a T-X diagram (Fig 7.5.5), the boundary between cpx-bearing and cpx-free assemblages suggest a difference in CaO content of c. 0,7 wt%.

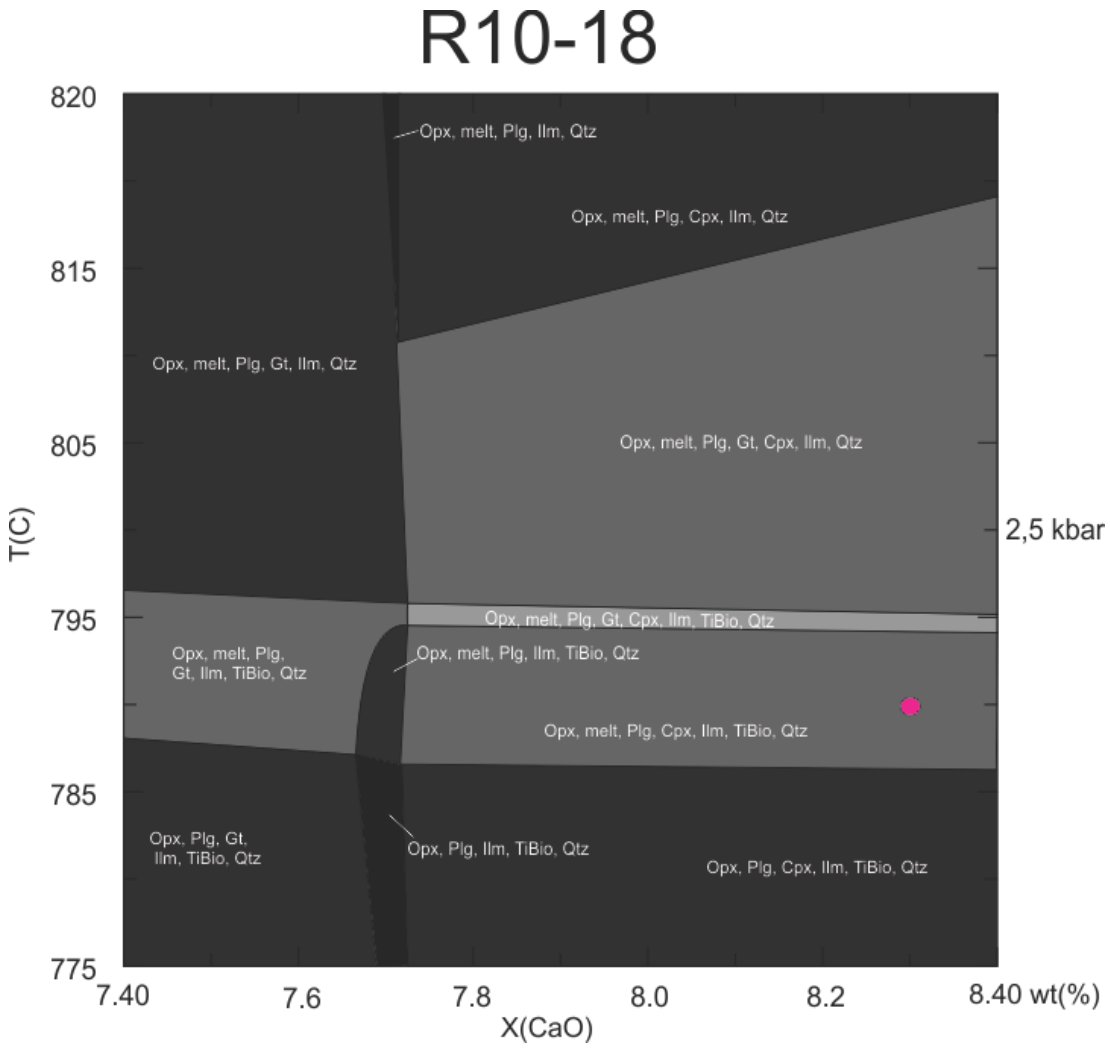

Fig 7.5.5. T-X_{CaO} diagram calculated for the system composition corresponding to the whole-rock composition of the sample R10-18. The diagram presents only the variation of CaO. TiBio: Biotite; Ilm: Ilmenite; Crd: Cordierite; Plg: Plagioclase; Ksp: K-feldspar; Spl: Spinel; Qtz: Quartz; Ru: Rutile; Grt: Garnet; Opx: Orthopyroxene; Cpx: Clinopyroxene.

Even though amphibole is observed in the thin section, it is not shown in the mineral assemblage in the pseudosection. One reason could be that the amphibole solution model is not accurate enough.

7.6 NI-123 Migmatitic gneiss

The mineral assemblage for this sample is: Pl-Bt-Qtz-Grt-Ksp-Ms. The P-T section was calculated for temperatures between 500-700°C and pressures of 1-8 kbar, in a system of Na_2O, MgO, Al_2O_3, SiO_2, K_2O, CaO, TiO_2, MnO, FeO and H_2O, and without any saturated components. The LOI content was used for water content. The whole rock composition in weight percent was used and is indicated in Table 5.1.1. The solution models used are: orthopyroxene (Holland and Powell, 1999), biotite (Tajcmanova et al., 2009), feldspar (Fuhrman et al., 1988) garnet (Holland and Powell, 1998), ilmenite (White et al., 2000), cordierite (Baumgartner, 2003), clinopyroxene (Holland and Powell, 1996), muscovite (Holland and Powell, 1998), spinel (Holland and Powell, 1998), melt (Holland and Powell, 2001).

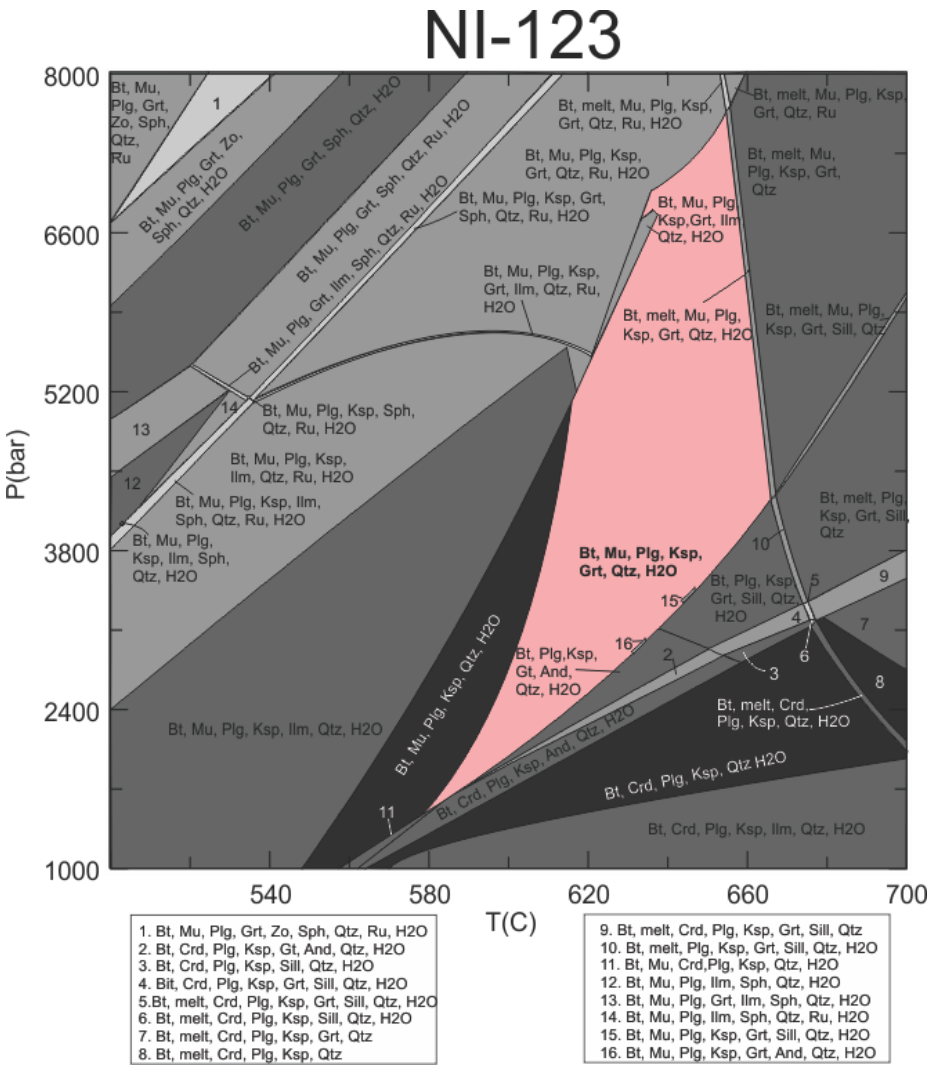

Fig 7.6.1. The P-T section calculated for the whole-rock chemistry of the NI-123 sample. The stability field marked in pink is the assemblage corresponding to the assemblage observed in the sample NI-123. Bt: Biotite; Ilm: Ilmenite; Crd: Cordierite; Plg: Plagioclase; Ksp: K-feldspar; Qtz: Quartz; Ru: Rutile; Sill: Sillimanite; Grt: Garnet; And: Andesite; Mu: Muscovite; Sph: Sphene; Zo: Zoisite.

7.6.1 Modelling for NI-123

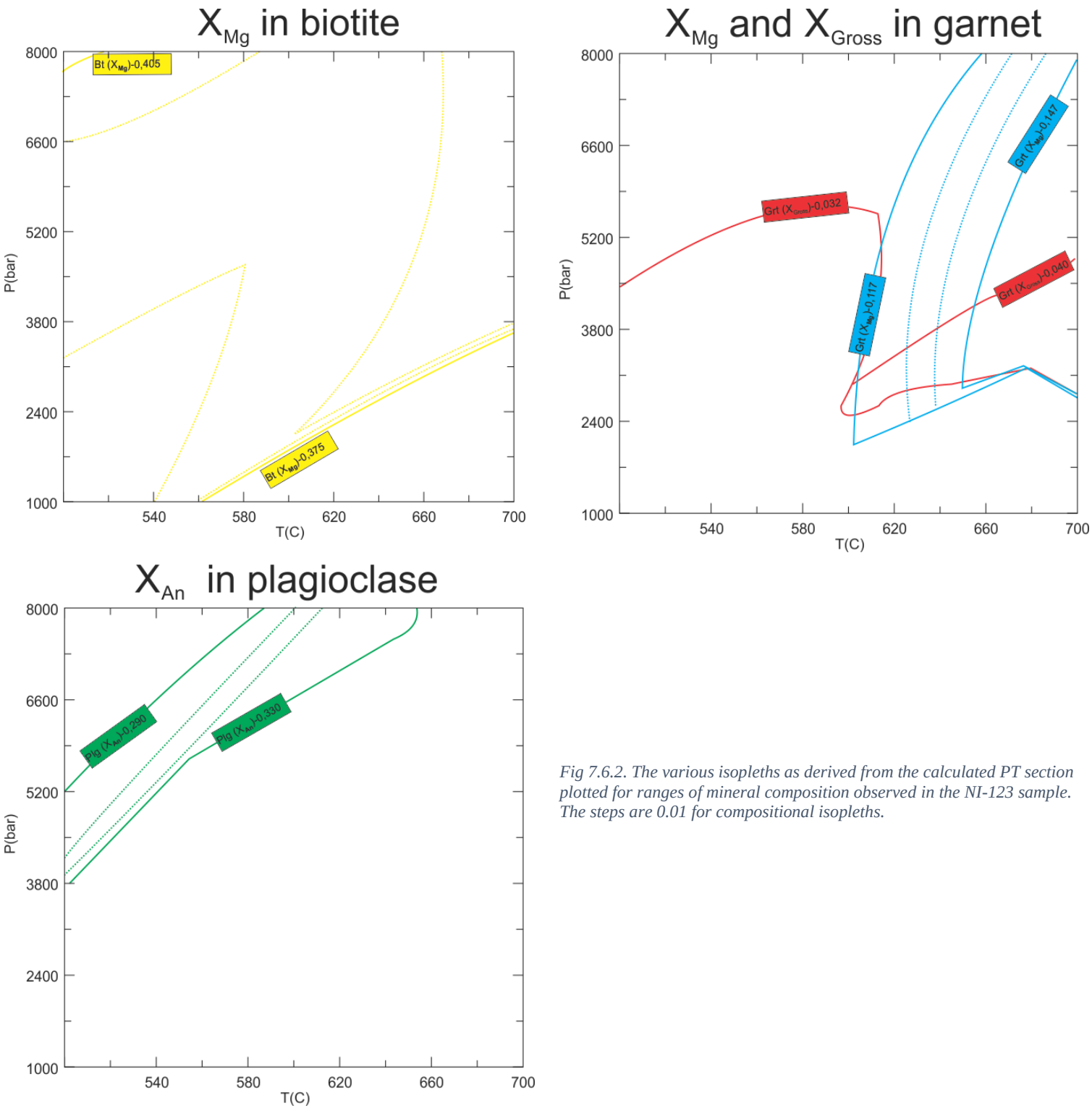

Fig 7.6.2. The various isopleths as derived from the calculated PT section plotted for ranges of mineral composition observed in the NI-123 sample. The steps are 0.01 for compositional isopleths.

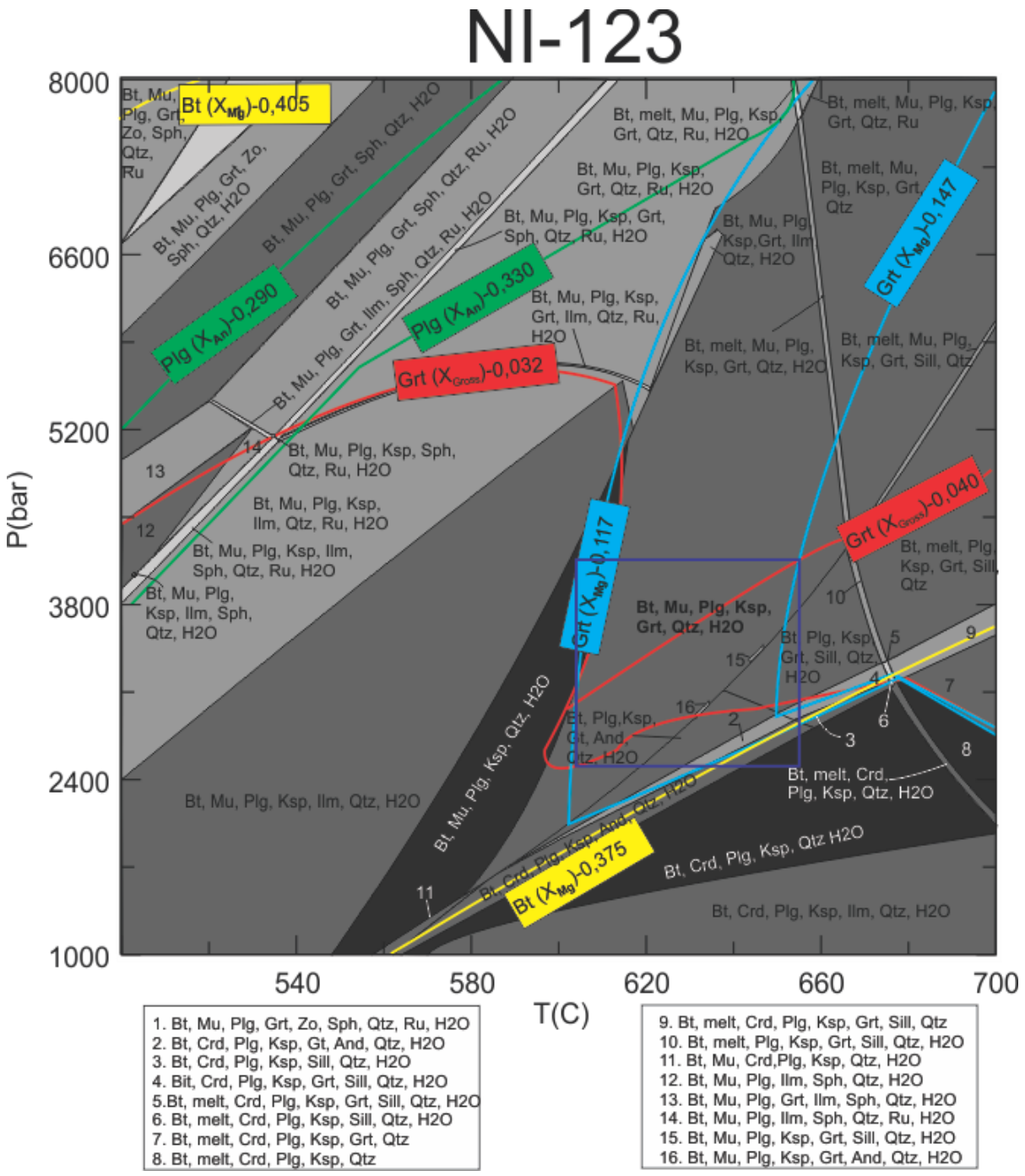

Fig 7.6.3. Compositional isopleths for the NI-123 minerals plotted on the P-T diagram. Bt: Biotite; Ilm: Ilmenite; Crd: Cordierite; Plg: Plagioclase; Ksp: K-feldspar; Qtz: Quartz; Ru: Rutile; Sill: Sillimanite; Grt: Garnet; And: Andalusite; Mu: Muscovite; Sph: Sphene; Zo: Zoisite.

7.6.2 Result

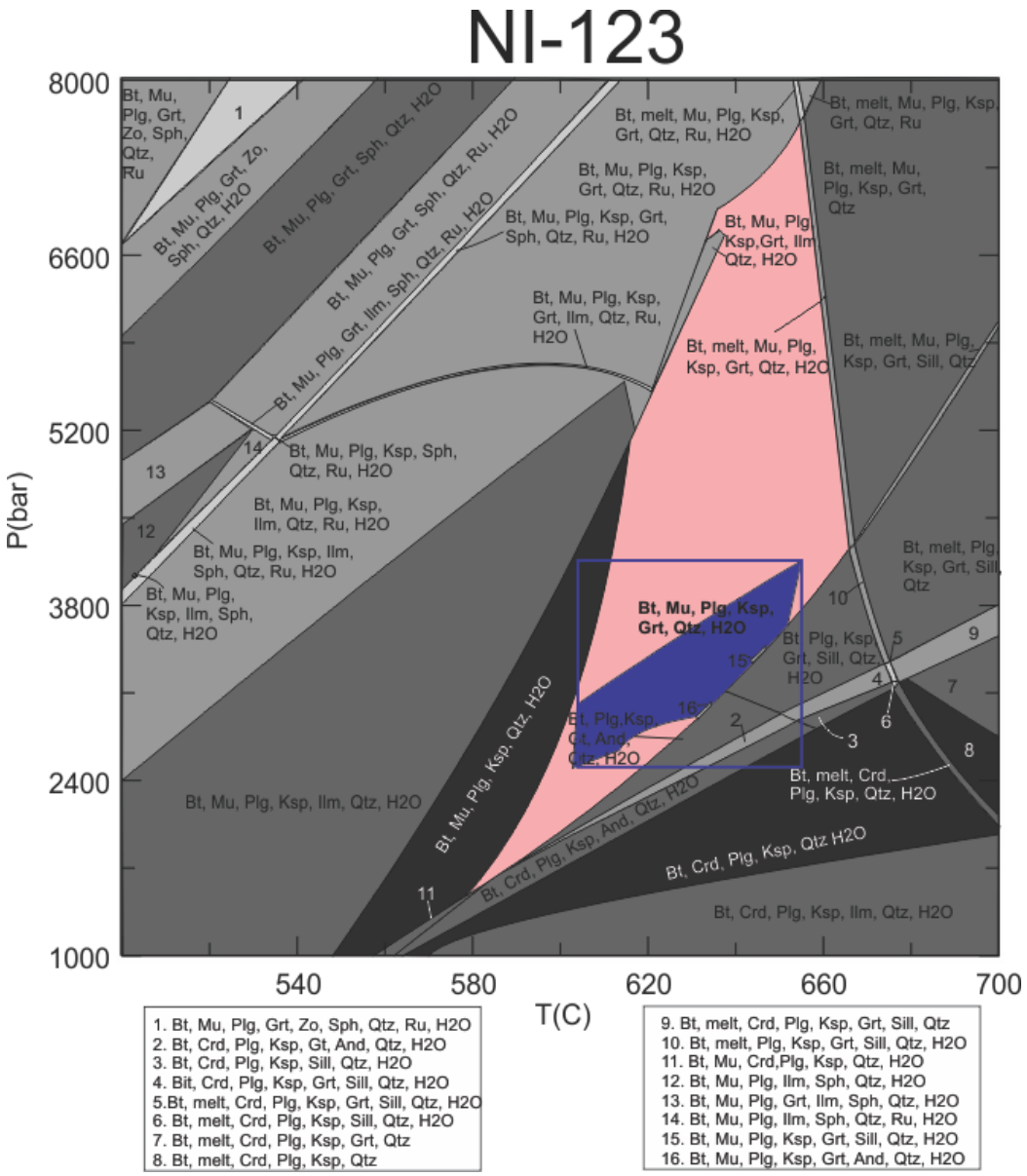

Fig 7.6.4. The P-T diagram with the P-T conditions (in blue) for the NI-123 sample. Bt: Biotite; Ilm: Ilmenite; Crd: Cordierite; Plg: Plagioclase; Ksp: K-feldspar; Qtz: Quartz; Ru: Rutile; Sill: Sillimanite; Grt: Garnet; And: Andalusite; Mu: Muscovite; Sph: Sphene; Zo: Zoisite.

Comments on the result (Fig 7.6.4)

The stability field of the NI-123 assemblage is located in between temperatures of c. 580 and 660°C; the pressure could not be estimated. To further constrain the condition of equilibration of the sample, compositional isopleths were used (X_{Mg}, X_{Gross} and X_{An}). These constrained the conditions of stabilization of the sample at temperatures of c. 600-640°C and pressures of c. 2,5-4,0 kbar. The X_{An} isopleth for the plagioclase apparently does not cross with the other isopleths, but in reality the plagioclase with An_{33} (observed in the sample) is stable in the whole lower part of the calculated P-T section.

7.7 NO-08 Migmatitic gneiss

The mineral assemblage for this sample is: Pl-Bt-Qtz-Grt-Ksp-Ms±Chl (little amount of chlorite is replacing biotite). The P-T section was calculated at temperatures between 500-700°C and 1-8 kbar, in a system of Na_2O, MgO, Al_2O_3, SiO_2, K_2O, CaO, TiO_2, MnO, FeO and H_2O, and without any saturated components. The LOI content was used for water content. The whole rock composition in weight percent of the components was used and is indicated in Table 5.1.1. The solution models used are: orthopyroxene (Holland and Powell, 1999), biotite (Tajcmanova et al., 2009), feldspar (Fuhrman et al., 1988) garnet (Holland and Powell, 1998), ilmenite (White et al., 2000), cordierite (Baumgartner, 2003), clinopyroxene (Holland and Powell, 1996), muscovite (Holland and Powell, 1998), spinel (Holland and Powell, 1998), melt (Holland and Powell, 2001), amphibole (Diener et al, 2011), chlorite (Holland and Powell, 1998).

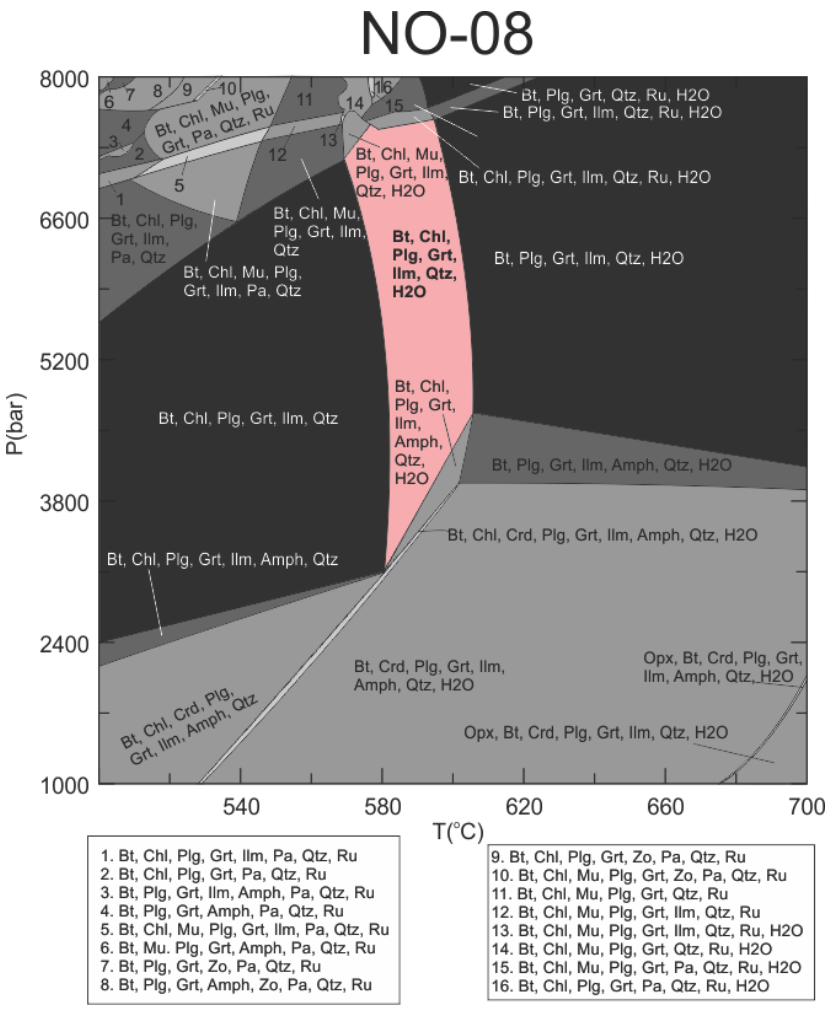

Fig 7.7.1. The P-T section calculated for the whole-rock chemistry of the NO-08 sample. The stability field marked in pink is the assemblage corresponding to the assemblage observed in the sample N0-08. Bt: Biotite; Ilm: Ilmenite; Crd: Cordierite; Plg: Plagioclase; Ksp: K-feldspar; Qtz: Quartz; Ru: Rutile; Sill: Sillimanite; Grt: Garnet; And: Andesite; Mu: Muscovite; Sph: Sphene; Zo: Zoisite; Opx: Orthopyroxene; Amph: Amphibole; Pa: Paragonite; Zo: Zoisite.

7.7.1 Modelling for NI-123

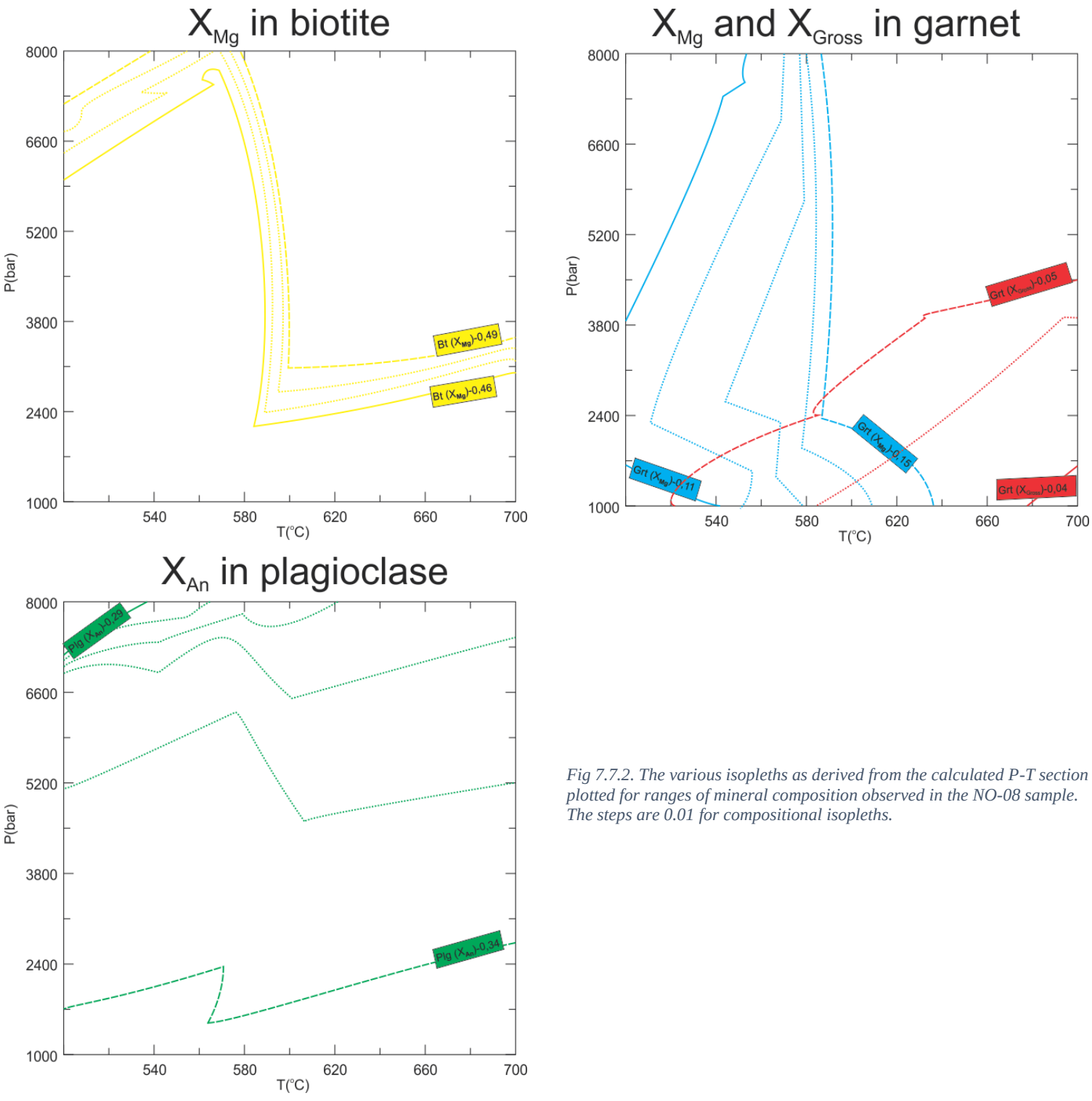

Fig 7.7.2. The various isopleths as derived from the calculated P-T section plotted for ranges of mineral composition observed in the NO-08 sample. The steps are 0.01 for compositional isopleths.

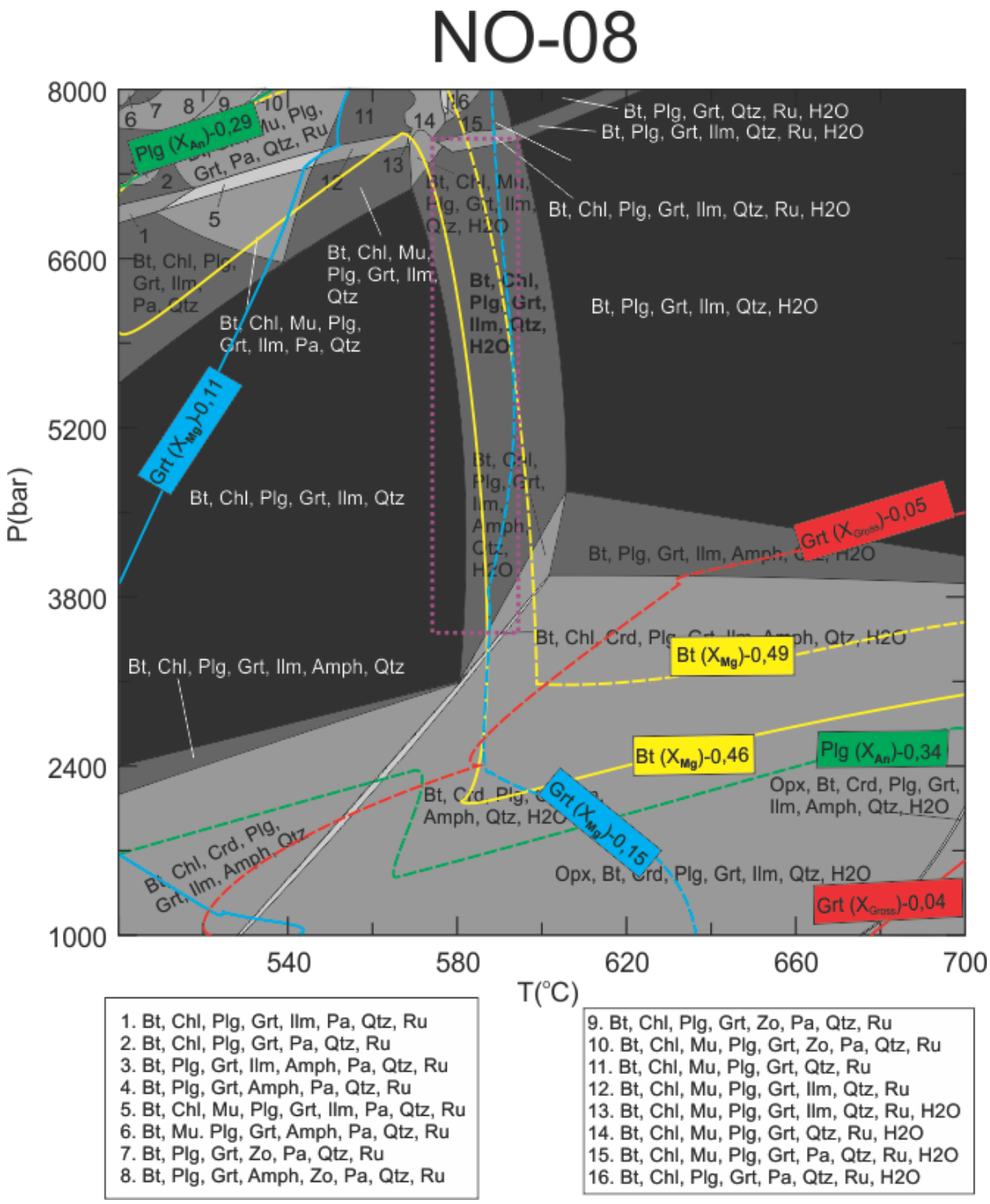

Fig 7.7.3. Compositional isopleths for the NO-08 minerals plotted on the P-T diagram. Bt: Biotite; Ilm: Ilmenite; Crd: Cordierite; Plg: Plagioclase; Ksp: K-feldspar; Qtz: Quartz; Ru: Rutile; Sill: Sillimanite; Grt: Garnet; And: Andesite; Mu: Muscovite; Sph: Sphene; Zo: Zoisite; Opx: Orthopyroxene; Amph: Amphibole; Pa: Paragonite; Zo: Zoisite.

7.7.2 Result

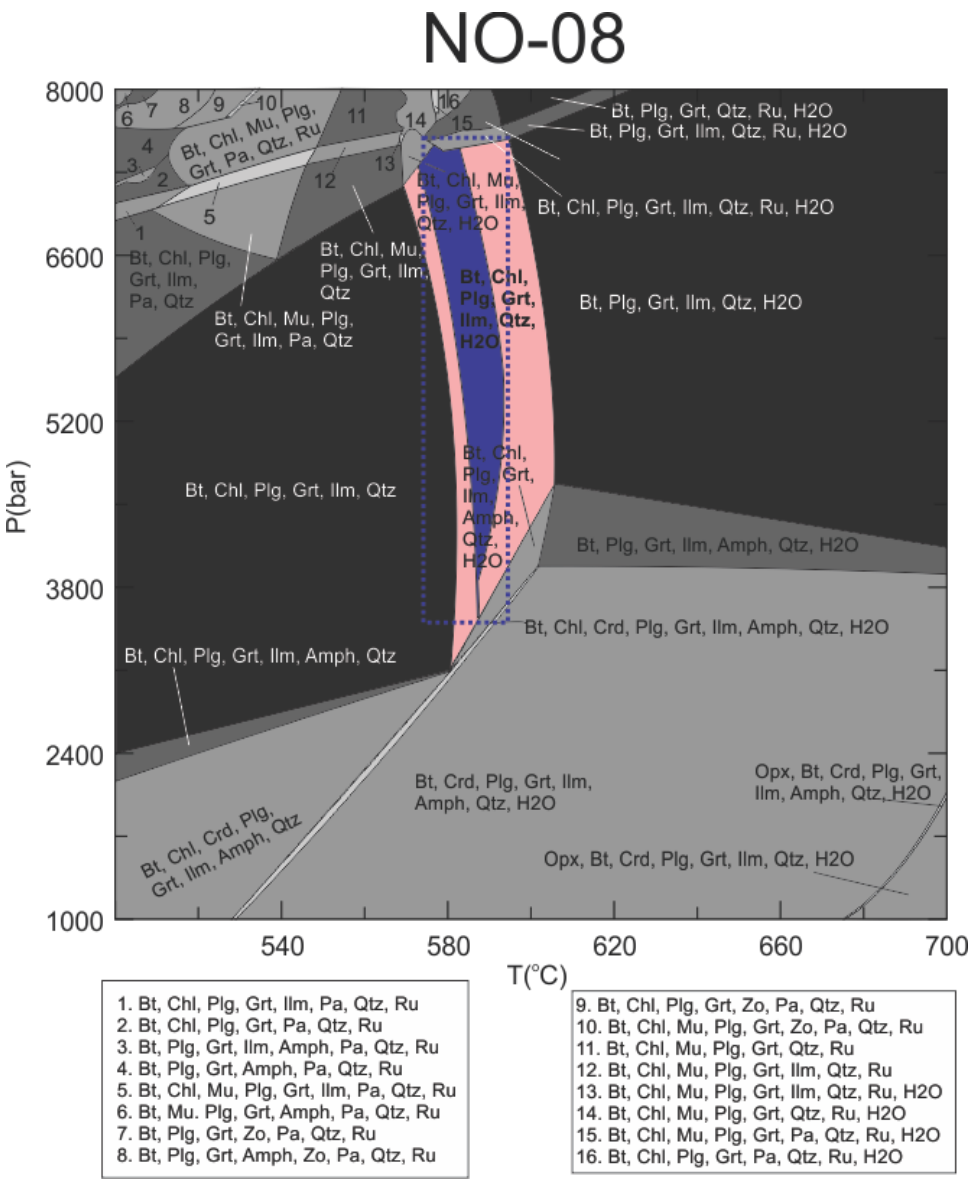

Fig 7.7.4. The P-T diagram with the P-T conditions (in blue) for the N-08 sample. Bt: Biotite; Ilm: Ilmenite; Crd: Cordierite; Plg: Plagioclase; Ksp: K-feldspar; Qtz: Quartz; Ru: Rutile; Grt: Garnet; And: Andesite; Mu: Muscovite; Sph: Sphene; Opx: Orthopyroxene; Amph: Amphibole; Pa: Paragonite.

Comments to the result Fig 7.7.4

The stability field of the mineral assemblage of the sample NO-08 can be found at temperatures between ca. 580 and 605°C and pressures of c. 3,1-7,5 kbar. With the compositional isopleths, the field was constrained to similar temperatures of c. 580-600°C. The pressure could not be constrained much further, only to c. 3,5-7,5 kbar. The isopleth for the X_{Gross} does not overlap the field for the observed mineral assemblage; this could be the same problem as with the isopleth X_{Gross} for the sample UB-02. The reason can be that the whole-rock composition is slightly inaccurate.

8 Discussion

8.1 UB-02 Felsic granulite

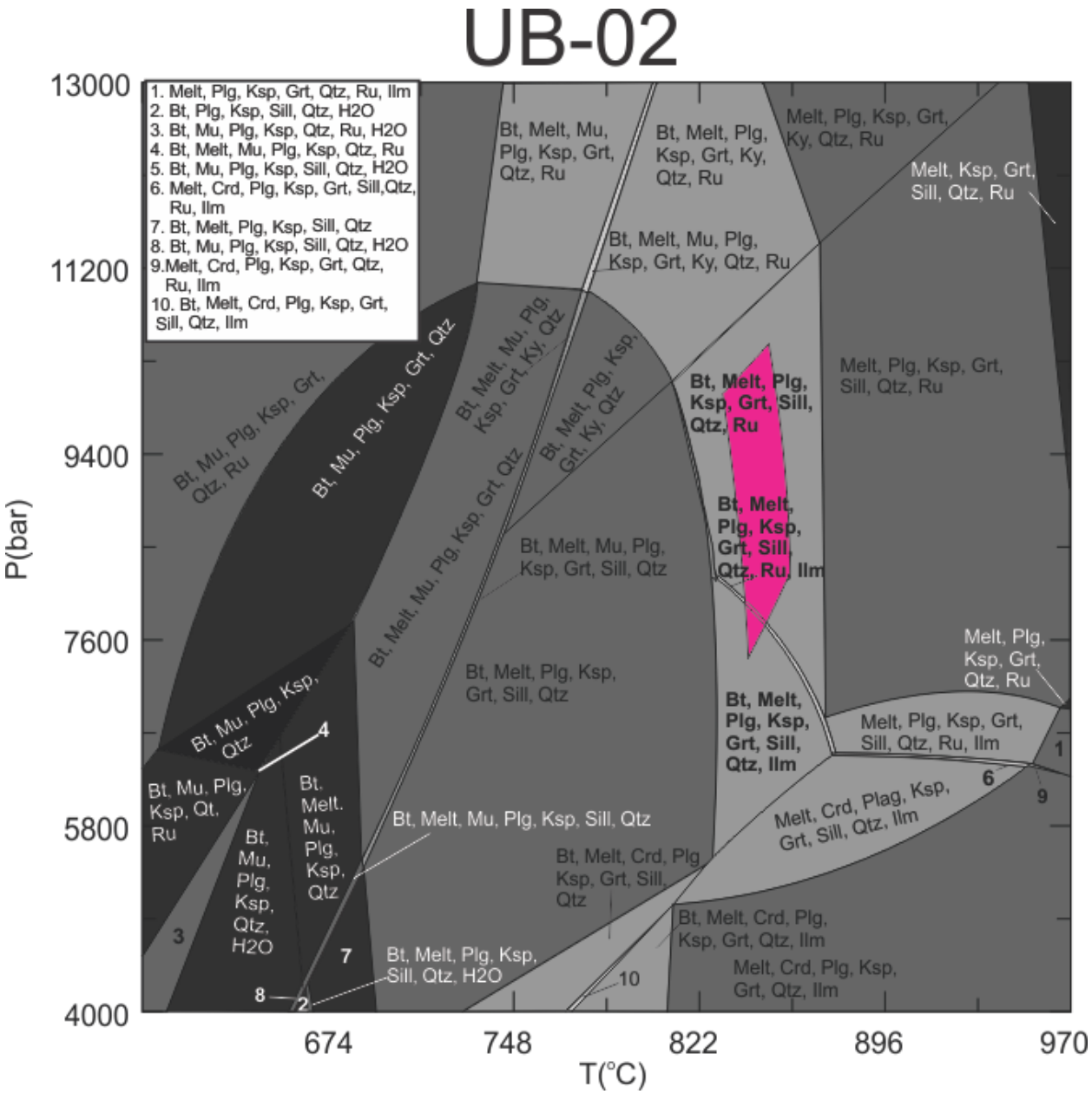

Fig 8.1.1. P-T section for UB-02. Bt: Biotite; Ilm: Ilmenite; Crd: Cordierite; Plg: Plagioclase; Ksp: K-feldspar; Spl: Spinel; Qtz: Quartz; Ru: Rutile; Sill: Sillimanite; Grt: Garnet; Mu: Muscovite; Ky: Kyanite.

The P-T diagram (Fig 8.1.1) shows the stable assemblage and P-T estimate for sample UB-02. The compositional isopleths of X_{Mg} in garnet and biotite and the X_{An} in plagioclase, constrain the field and show that the modelled assemblage for UB-02 lies within P-T conditions corresponding to the granulite facies at temperatures 830-840°C and pressures 7,5-10,5 kbar.

The stability fields of mineral phases such as kyanite and biotite, can also constrain the P-T conditions. Since kyanite was not observed in the sample, it constrains the upper limit for

peak pressure. The Al_2SiO_5-polymorphs are pressure and temperature sensitive, since sillimanite is present in the sample, and is only stable at high temperatures (ca. >500°C), the sample can be constrained to higher temperatures.

The garnet in the sample UB-2 has an almandine-pyrope composition with a low content of the grossular and spessartine components. The grossular content of the modelled garnet in the stability field of this sample has a higher calcium content than observed in the sample. A reason for this could be that the calcium content in the bulk rock analysis obtained from the sample may not be representative of the part of rock from which the thin section was made. The calcium in garnet decreases with decreasing pressure of equilibration and low content of grossular component thus indicates low-pressure regime for this bulk composition. Garnets in the sample are chemically homogeneous suggesting equilibration at high temperatures.

The fine-grained biotite grows in fractures and around the garnet, and seems to be consuming the garnet grains. This is an indication that water must have been reintroduced into the rock in order for biotite to crystallize as a late phase during retrogression. Since there is only a small amount of this type of biotite, and no other evidence for retrogression reactions, it suggests that the peak assemblage in this rock is well preserved.

The rock contains an abundance of quartz and feldspar and very little other minerals, and could be characterized as a quartz-feldspathic rock. It could originally have been a granitoid or a rhyolite. When converting estimated metamorphic pressure conditions to depth, the results suggest that the rock equilibrated at depths of c. 25-36 km and temperatures of 830-860°C. This suggests a thermal gradient of 24-32 ^{o}C/km.

8.2 UA-11 Felsic granulite

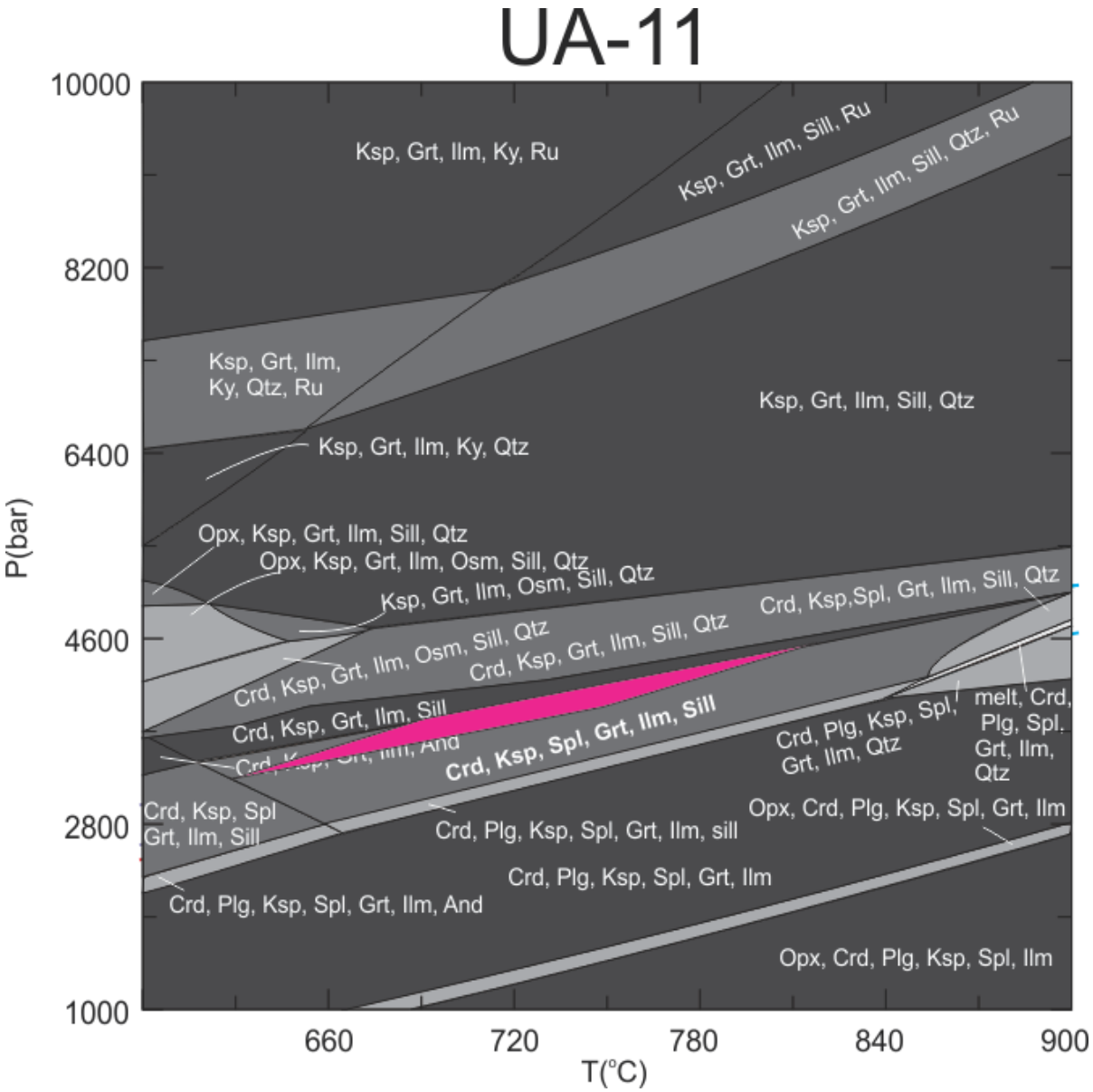

Fig 8.2.1. P-T section for the effective bulk composition for UA-11. Bt: Biotite; Ilm: Ilmenite; Crd: Cordierite; Plg: Plagioclase; Ksp: K-feldspar; Spl: Spinel; Qtz: Quartz; Ru: Rutile; Sill: Sillimanite; Grt: Garnet;; Ky: Kyanite; Opx: Orthopyroxene; Osm: Osumilite; And: Andalusite.

The P-T diagram was calculated from a bulk rock composition from the spinel-bearing domains in the thin section (Fig 8.2.1). The P-T section for the estimated bulk composition is consistent with the assemblage observed in the spinel-bearing domains of the thin section. The estimated P-T conditions for these zones are c. 630-810°C and c. 3,0-4,5 kbar. The pressure conditions of equilibration of the sample are well constrained by the compositional isopleths, but the temperature range is too wide to make a good estimate of metamorphic temperature.

The reason for the development of spinel-bearing domains could be that the decrease in pressure has allowed a large amount of cordierite to crystallize so quickly that it has enclosed some of the other minerals. The spinel-bearing domains are enclosed in cordierite, isolated from the quartz-bearing matrix, so that it is possible the cordierite effectively behaved as a barrier to diffusion of elements, such as silica, into the spinel-bearing zones. During metamorphism minerals from the matrix react with the cordierite in the barrier, leaving the enclosed domains poor in Si and therefore able to crystallize spinel.

As with the garnets in the sample UB-02, the garnets in this sample are have a homogeneous almandine-pyrope composition with low grossular and spessartine contents, suggesting they have re-equilibrated at low-pressure. The isopleths for the modelled grossular content show only a minor discrepancy compared to the measured contents, predicting a higher calcium value for the stable assemblage than measured from the sample. When converting the estimated pressure conditions to depth, the estimates of the metamorphic conditions suggest the equilibration of the sample in c. 10-18 km at temperatures of c. 630-810°C. Such values suggest a high geothermal gradient of 74 ºC/km.

8.3 UA-31B Intermediate granulite

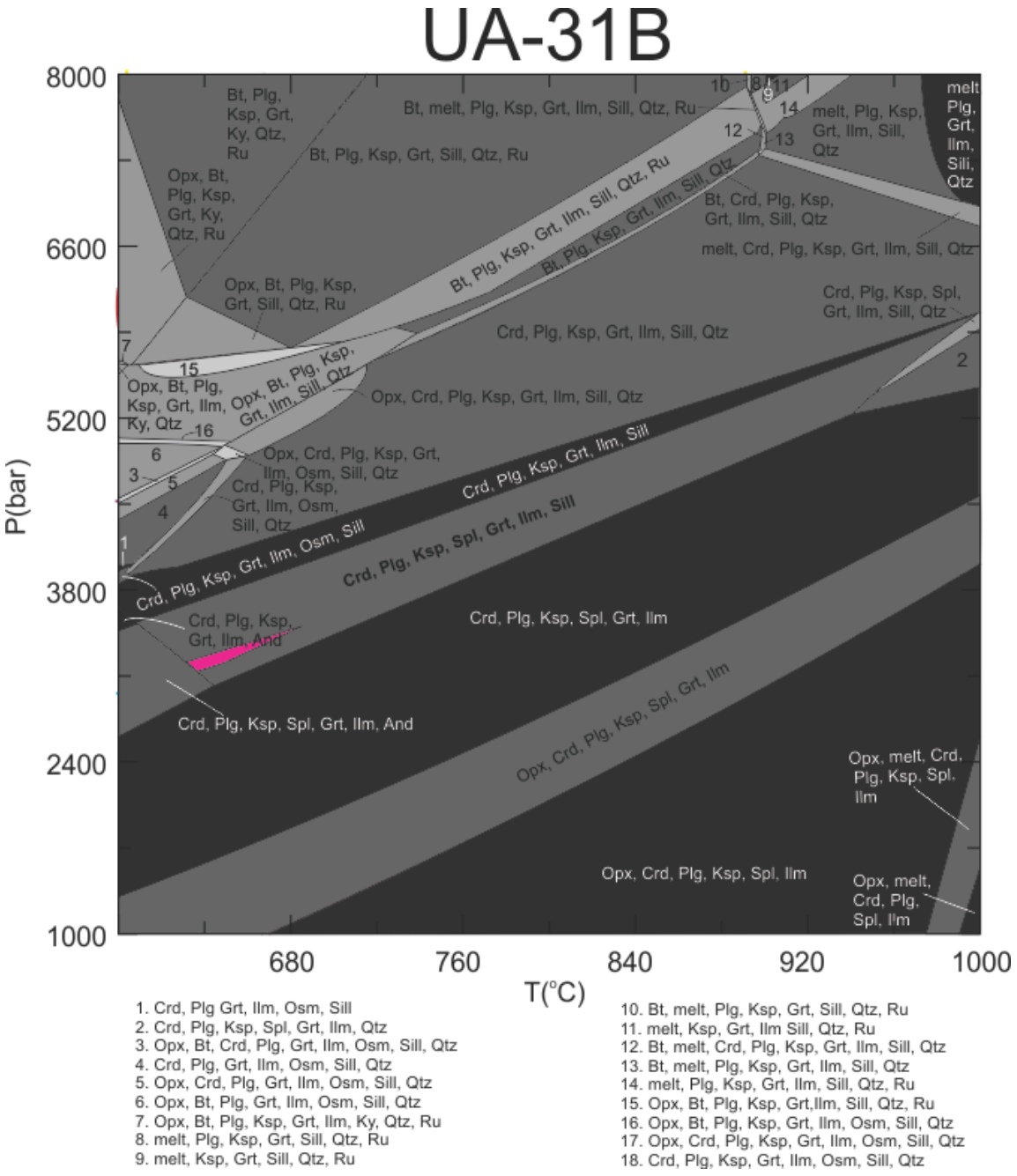

Fig 8.3.1. P-T section for UA-31B corresponding to the estimated effective bulk composition shown in pink. Bt: Biotite; Ilm: Ilmenite; Crd: Cordierite; Plg: Plagioclase; Ksp: K-feldspar; Spl: Spinel; Qtz: Quartz; Ru: Rutile; Sill: Sillimanite; Grt: Garnet; Mu: Muscovite; Ky: Kyanite; Opx: Orthopyroxene; Cpx: Clinopyroxene

The P-T diagram in Fig 8.3.1 shows the stability field for the UA-31B. This sample has several minerals suitable for thermobarometry, including cordierite, spinel, biotite, plagioclase and garnet. The temperature and pressure was constrained with the compositional isopleths to c. 640-690°C and c. 3,0-3,5 kbar. When converting pressure to depth, the result is 11-12 km with temperature of c. 640-690°C. The thermal gradient for this sample suggest c. 53-63 °C/km.

8.4 R10-18 Mafic granulite

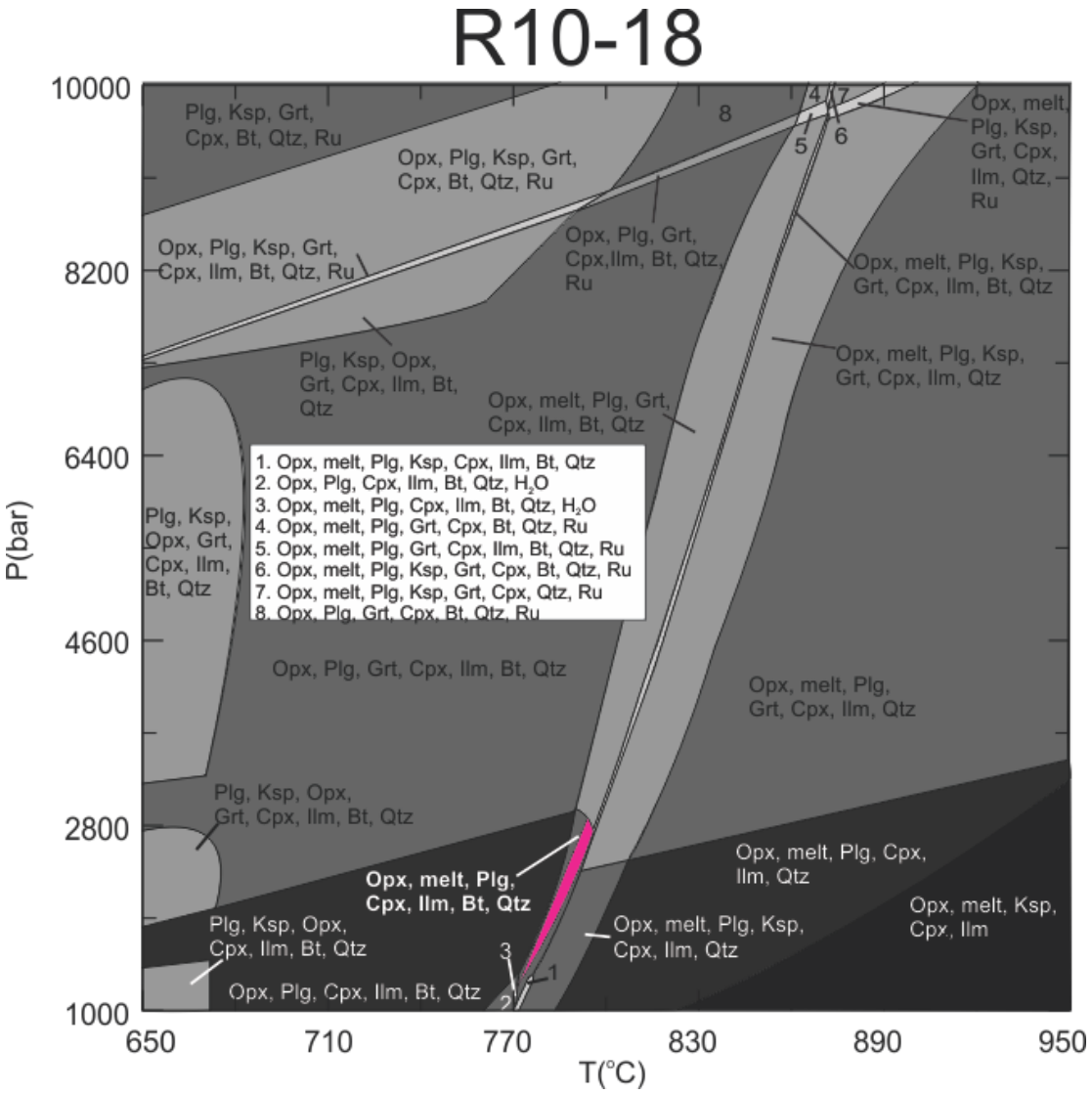

Fig 8.4.1. P-T section for R10-18. Bt: Biotite; Ilm: Ilmenite; Crd: Cordierite; Plg: Plagioclase; Ksp: K-feldspar; Spl: Spinel; Qtz: Quartz; Ru: Rutile; Grt: Garnet; Opx: Orthopyroxene; Cpx: Clinopyroxene.

The P-T diagram (Fig 8.4.1) shows the stability field where the R10-18 assemblage is located at temperatures of c. 780-790°C and pressure of c.1,0-3,0 kbar. The pressure converted to depth is 4-10 km. The stability field where the observed mineral assemblage is found suggests very low pressures of equilibration. Microsctuctures in some areas of the sample seem to be magmatic with large crystals of plagioclase and quartz, while in other places the microstructure suggests metamorphic recrystallization (Fig 5.5.1). It is not clear if this sample is a part of the metamorphic complex, in which case lower pressures of equilibration compared to the samples UB-11 and UB-31B would be expected and the very low-pressure conditions of equilibration reflect the intrusive origin of the sample. This rock may have intruded during the late stages of metamorphism of the Punta del Este Terrane when the unit

was already exhumed close to the surface at ca. 3-10 km. As the sample shows partial recrystallization, the rock must have undergone some deformation/recrystallization, perhaps during cooling. This might indicate that the timing of the metamorphism is not the same as for the other samples in that unit. The rock could have been emplaced in the Punta del Este Terrane after its exhumation but at a shallower level than the spinel-bearing rocks.

8.5 NI-123 Migmatitic gneiss

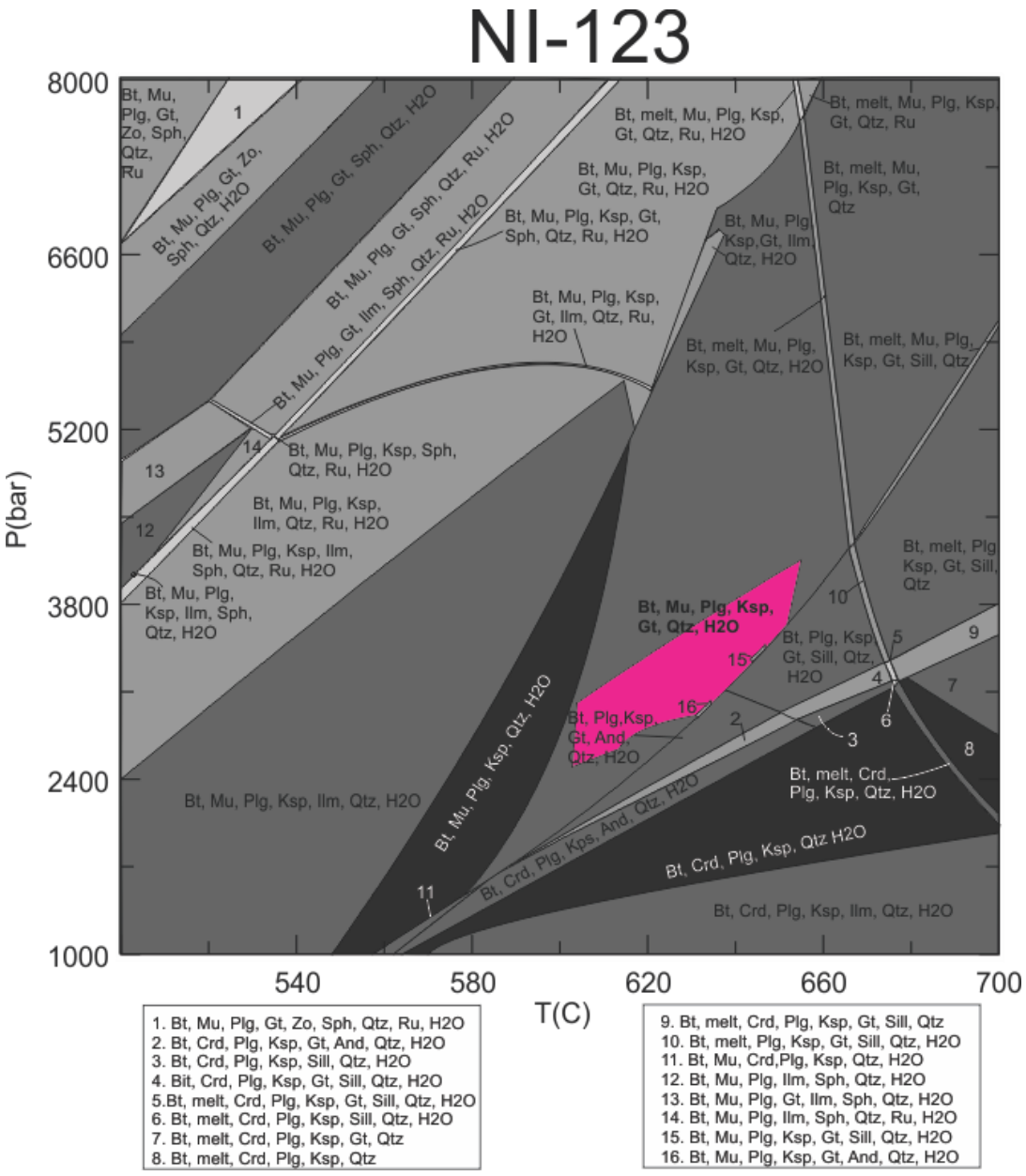

Fig 8.5.1. P-T section for NI-123. Bt: Biotite; Ilm: Ilmenite; Crd: Cordierite; Plg: Plagioclase; Ksp: K-feldspar; Qtz: Quartz; Ru: Rutile; Sill: Sillimanite; Grt: Garnet; And: Andalusite; Mu: Muscovite; Sph: Sphene; Zo: Zoisite.

The stability field for the NI-123 sample is shown in pink in the P-T diagram in Fig 8.5.1. The stability field for the NI-123 mineral assemblage is not well constrained with regards to pressure. The compositional isopleths constrained the P-T conditions of equilibration well and show that the modelled assemblage of NI-123 lies within P-T conditions of c. 600-640°C and c. 2,5-4,0 kbar, corresponding to the low pressure amphibolite facies. The depth is calculated to be 8-14 km. This suggest a thermal gradient of c. 74°C/km. The phase field with the stable mineral assemblage of this sample does not show melt. There could be two reasons for this: (1) There could be a problem with the pseudosection, that the water content that was used could cause the melt-in line to be predicted at a higher temperature than it should actually be. Essentially more water means lower meltingtemperature. Water saturated melting is the lowest temperature melting that is possible. This is probably not what the reason is in this case, as this sample has a high-ish LOI and there is free water in the phase fields just below melting. This suggests that the melting in the P-T diagram was water saturated, and therefore could not get any lower temperature. (2) The most likely problem could be that the melt releases water when it crystallizing. This water can react with the minerals in a type of retrogression reaction, with the forming of new mineral (biotite, muscovite or amphibole). These new minerals have compositions that plot right below the melt stability line, because they crystallize at temperatures just below the stability of melt. The P-T estimate does not display the highest temperature that the rock got to where the melting happened, but is actually showing the new growth of minerals that occurred when the rock crystallized, and the water that was released from the melt caused new mineral reactions to occur. As this rock is a migmatite, the P-T estimate reflects a lower temperature than the peak temperature and the thermal gradient could be higher.

8.6 NO-08 Migmatitic gneiss

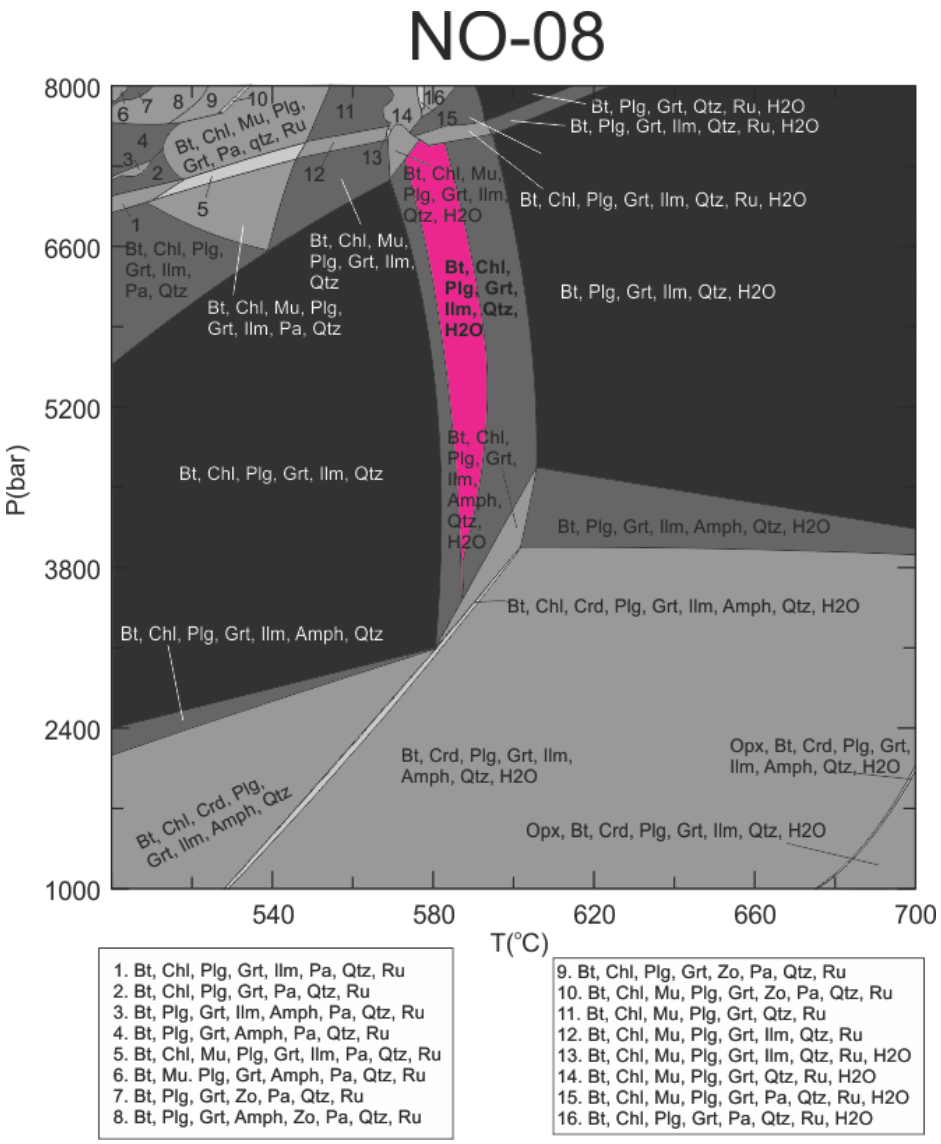

Fig 8.6.1. P-T section for NO-08. Bt: Biotite; Ilm: Ilmenite; Crd: Cordierite; Plg: Plagioclase; Ksp: K-feldspar; Qtz: Quartz; Ru: Rutile; Grt: Garnet; And: Andesite; Mu: Muscovite; Opx: Orthopyroxene; Amph: Amphibole; Pa: Paragonite.

The P-T estimate observed in the sample NO-08 is located at temperature c. 580-600° C and pressure between c. 3,5 and 7,5 kbar (Fig 8.6.1). The garnet isopleth for X_{Gross} does not exactly overlap with the stability field of the observed mineral assemblage, but the discrepancy is very small. The pressure is not well constrained and when converted to depth, the range is large c. 12-25 km. As with the sample NI-123, this sample does not show melt at the estimated P-T conditions. Since this rock contains leucosome, but the melt presence is not reflected by the modelled P-T estimate, it is likely that this rock represents a mineral assemblage formed during crystallization of melt, whereby water released from the melt contributed to crystallization of new minerals below the solidus. Therefore, this P-T estimate may represent a lower temperature than peak metamorphism of the sample.

8.7 A comparison of the samples

The UA-31B sample is complimentary to the sample UA-11. They have the same mineral assemblage, except UA-31B contains less biotite and more spinel and sillimanite. They both show garnets with the same chemistry, and larger variation in the X_{Mg} in the garnets. This could be caused by the fact that the analyses of the garnets were done in both the spinel-bearing domains and in the quartz-rich matrix, which have different bulk compostions relative to each other. The UA-11 has a wide temperature range and the estimated temperature conditions for the sample UA-31B overlap with the lower temperature limit of the conditions estimated for the sample UA-11. The pressure conditions estimated for these samples are approximately the same and show the values of 3,0-4,5 kbar.

The UB-02 sample shows the highest pressure and temperature conditions compared to the other samples collected in the Punta del Este Terrane. When compared with the conditions of the samples UA-11 and UA-31B, the sample UB-2 may not have completely re-equilibrated during the exhumation and could thus preserve the maximum pressures and temperature conditions of metamorphism of the Punta del Este Terrain.

UA-31B and UA-11 are more aluminum rich than UB-02. The UB-02 sample could reflect the P-T conditions (c. 830-840°C and 7,5-10,5 kbar) at the peak of the metamorphism, and the spinel-bearing samples may reflect the level to which the unit was exhumed and cooled. This means that the metamorphism (650-630 Ma) could have started at a depth of 25-36 km corresponding to the P-T conditions of the UB-02 sample and that this sample was not re-equilibrated during exhumation. In the case of the spinel-bearing samples, they could have started out with the same conditions as the UB-02, but during the exhumation they were re-equilibrated to the pressures recorded in the present samples (3,0-4,5 kbar corresponding to depths of 8-14km). The UA-11 and UA-31B do not contain any relics of the older and deeper metamorphism, and appear to have been completely re-equilibrated.

The semi-pelitic migmatites and mafic granulite samples of Gross et al. (2009) showed the same decrease in pressure as recorded in the samples in this thesis. They also described spinel-bearing domains with sillimanite enclosed in cordierite, and attributed it to indicate decompression. The semi-pelitic migmatites and mafic granulites they described preserved the high-P thermal peak minerals and their compositions with only a small modification during decompression, and the pelitic migmatites described did not preserve any of the high-P thermal peak. Gross et al. (2009) discussed three possible reasons for this: (1) A contrast in

rheology. As pelites are generally less competent than metabasites, plastic deformation can reduce grain sizes, which would decrease the intergranular diffusion lengths. This could introduce defects, which could enhance intercrystalline diffusion rate and the increase of grain-boundary surface area would increase the intercrysalline diffusion rate. (2) A localized presence of fluids could promote intergranular diffusion, leading to catalyzation of metamorphic reactions. The introduction of fluids could then stimulate re-equilibration. (3) A localized presence of melt could provide an effective diffusion pathway that would be faster in a partially molten rock, compared to a solid one. They concluded that the first was unlikely, as none of the lithology has shown any indication of deformation. The two latter could both have contributed, but are too difficult to resolve as they are strongly interconnected through the presence and abundance of melt.

The Namibian samples NI-123 and NO-08 were collected from the same unit. The distance is large between where the samples were taken, but the P-T conditions match closely. These samples show temperatures a little lower than the Uruguayan samples, and show the approximately same pressures as the UA-11 and UA-31B. The Namibian sample also show evidence of retrogression and could have started metamorphism at a lower lever in the crust. They do not show the peak metamorphic P-T conditions that would have a higer thermal gradient.

Geothermal gradients tell us about what kind of environment a metamorphism has happened in or the combination of P-T conditions in different tectonic environments. When displayed on a P vs. T plot showing different thermal gradients we see that the UA-31B, UA-11, NI-123 and NO-08 overlap slightly at the lower temperatures of the Uruguayan samples and at the higher temperatures of the Namibian samples. This overlap could indicate that the Uruguayan samples were exhumed to the same level as the Namibian samples when they cooled. The UB-02 samples almost lines up with the thermal gradient of the NO-08, but not with the NI-123. This is because the pressure range of the NO-08 is too wide, and it is not sufficient to say that their thermal gradients are the same. As discussed above, the retrogression in the Namibian samples could have lowered the thermal gradients of these samples and this could be a reason that they do not line up. The UB-02 sample follow a thermal gradient of c. 24-32 C°/km, while the UA-31B follow a c. 74 C°/km thermal gradient. The NI-123 follow a thermal gradient of c. 74 C°/km. the NO-08 has a very wide pressure range, and could follow a thermal gradient anywhere from 24-74 C°/km.

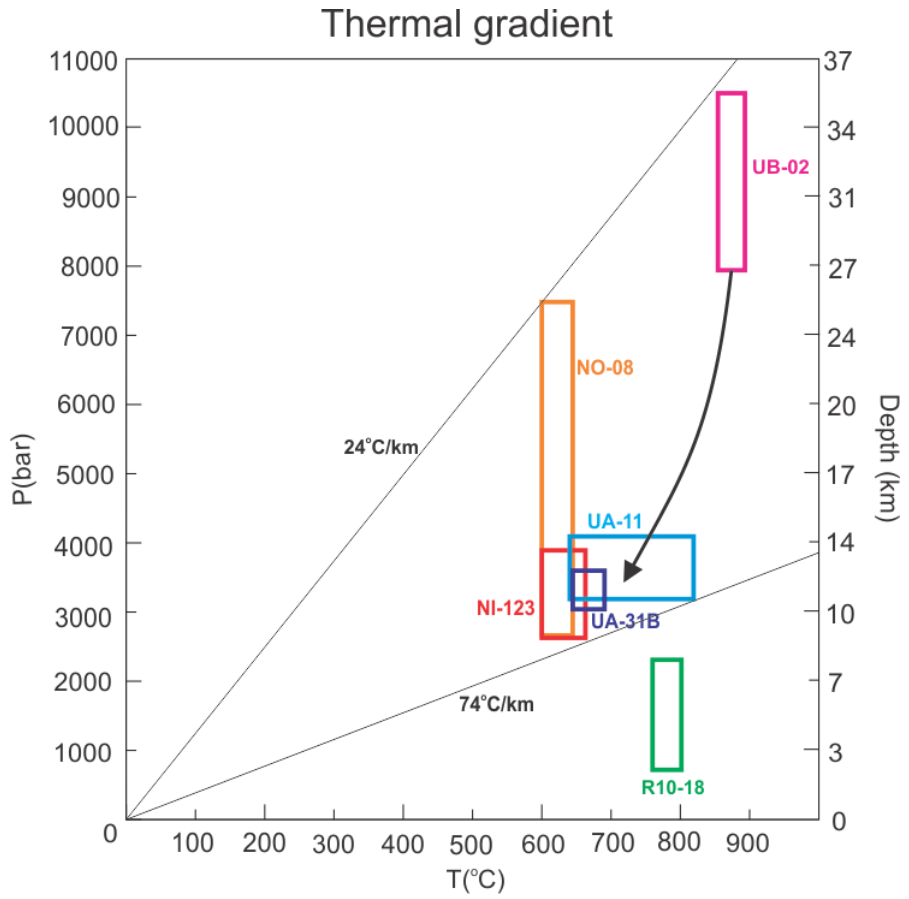

Fig 8.7.1. A comparison of the pressure and temperature conditions for the Uruguayan and Namibian samples. The arrow show the possible decompression pathway for the UA-11 and UA-31B.

The aim of this thesis was to analyze samples and to establish and compare their metamorphic conditions. Fig. 8.7.1. suggests that the peak metamorphism from Uruguay and Namibia may not follow the same thermal gradient, and that peak metamorphism for the Uruguayan samples was closer to 24 C°/km while peak metamorphism for the Namibian samples could have followed a thermal gradient closer to 74 C°/km. Given that the timing of metamorphism in the Namibian and the Uruguayan samples is approximately the same, c. 650-630 Ma (Konopásek et al., 2008; Lenz et al., 2011), the large difference in their peak metamorphic conditions indicate that the samples from Uruguay could have had a middle- to lower part in the crust at the peak of the metamorphism, and could have been exhumed to a higher level when cooled. The samples from Namibia could have originated from the upper part of the crust at peak metamorphism. Fig 8.7.2 is a simplified sketch that interprets how the samples went from their original positions to their current relative crustal position. The interpretation suggests that the Punta del Este Terrane began at a lower crustal position below what is now the Coastal Terrane of the Kaoko Belt. During the deformational event of the Brasiliano/Pan-

African orogeny the Punta del Este Terrane was thrust over the Rio de la Plata Craton, and the Coastal Terrane of the Kaoko Belt was thrust over the Central Kaoko Zone. The present day erosional level has exposed the samples from the different positions in the crust.

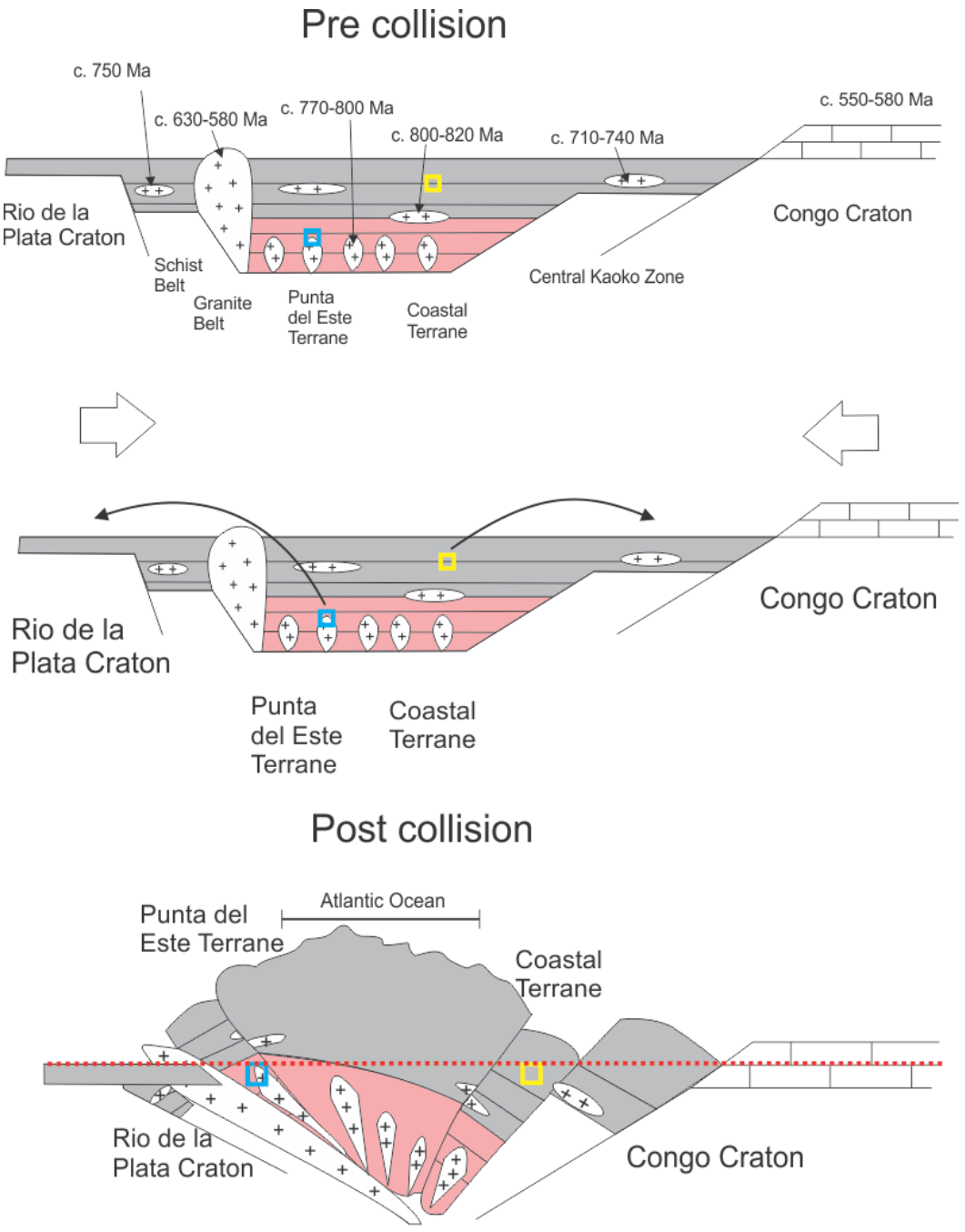

Fig 8.7.2. Simplyfied sketch of pre and post collision of the Brasiliano/Pan-african orogeny. The blue box represents the position of the samples from Uruguay, and the yellow box represents the position of the Namibian samples. The red dotted line in the lower most figure illustrated the present day erosion level. The Punta del Este Terrane was thrusted ontop of the Rio de la Plata Craton, while the Coastal Terrane of the Kaoko Belt was thrusted over the Central Kaoko Zone.

9 Conclusion

The conclusion of this thesis is that there is a possibility that the samples collected from the Punta del Este Terrane in Uruguay had a middle- to lower-crustal position in the same unit where the samples collected in the Coastal Terrane of the Kaoko Belt in Namibia could have had an upper-crustal position at the peak of the metamorphism at c. 650-630 Ma.

Bibliography

Basei, M. A. S., Campos Neto, M. C., Castro, N. A., Nutman, A. P., Wemmer, K., Yamamoto, M. T., Hueck, M., Osako, L., Siga, O., & Passarelli, C. R. (2011).T Tectonic evolution of the Brusque Group, Dom Feliciano belt, Santa Catarina, Southern Brazil. *Journal of South American Earth Sciences, 32*(4), 324-350.d doi:10.1016/j.jsames.2011.03.016

Basei, M. A. S., Peel, E., Sánchez Bettucci, L., Preciozzi, F., & Nutman, A. P. (2010). The basement of the Punta del Este Terrane (Uruguay): an African Mesoproterozoic fragment at the eastern border of the South American Río de La Plata craton. *International Journal of Earth Sciences, 100*(2-3), 289-304. doi:10.1007/s00531-010-0623-1

Basei, M. A. S., Siga Jr, O., Masqelin, H., Harara, O. M., Reis Neto, J. M., & Preciozzi, F. (2000). *The Don Feliciano Belt (Brazil-Uruguay) and its Foreland (Rio de la Plata Craton): framework, tectonic evolution and correlations with similar terranes of southwestern Africa.* Paper presented at the Tectonic Evolution of South America, 31st International Geological Congress, Rio de Janeiro,Brazil., Rio de Janeiro, Brazil.

Connolly JAD (2005) *Computation of phase equilibria by linear programming: A tool for geodynamic modeling and its application to subduction zone decarbonation*. Earth and Planetary Science Letters 236:524-541.

Connolly JAD (2009) *The geodynamic equation of state: what and how.* Geochemistry, Geophysics, Geosystems 10:Q10014 DOI:10.1029/2009GC002540.

De Waele, B., Johnson, S. P., & Pisarevsky, S. A. (2008). Palaeoproterozoic to Neoproterozoic growth and evolution of the eastern Congo Craton: Its role in the Rodinia puzzle. *Precambrian Research, 160*(1-2), 127-141. doi:10.1016/j.precamres.2007.04.020

Dür, S. B. and D. P. Dingeldey (1996). "The Kaoko belt (Namibia): Part of a late Neoproterozoic continental-scale strike-slip system." Geology **24**: 503-506.

Goscombe, B., M. Hand, D. Gray and J. Mawby (2003a). "*The Metamophic Architecture of a Transpressional Orogen the Kaoko Belt, Namibia*." Journal of Petrology **44**(4): 679-711.

Goscombe, B., Gray, D., & Hand, M. (2005b). Extrusional Tectonics in the Core of a Transpressional Orogen; the Kaoko Belt, Namibia. *Journal of Petrology, 46*(6), 1203-1241. doi:10.1093/petrology/egi014

Goscombe, B., & Gray, D. R. (2007). The Coastal Terrane of the Kaoko Belt, Namibia: Outboard arc-terrane and tectonic significance. *Precambrian Research, 155*(1-2), 139-158. doi:10.1016/j.precamres.2007.01.008

Goscombe, B. D., & Gray, D. R. (2008). Structure and strain variation at mid-crustal levels in a transpressional orogen: A review of Kaoko Belt structure and the character of West Gondwana amalgamation and dispersal. *Gondwana Research, 13*(1), 45-85. doi:10.1016/j.gr.2007.07.002

Gross, A. O. M. S., Droop, G. T. R., Porcher, C. C., & Fernandes, L. A. D. (2009). Petrology and thermobarometry of mafic granulites and migmatites from the Chafalote Metamorphic Suite: New insights into the Neoproterozoic P–T evolution of the Uruguayan—Sul-Rio-Grandense shield. *Precambrian Research, 170*(3-4), 157-174. doi:10.1016/j.precamres.2009.01.011

Holland TJB,Powell R (1998) *An internally consistent thermodynamic data set for phases of petrological interest.* Journal of Metamorphic Geology 16:309-43.

Indares, A., & Martignole, J. (1985). Biotite-garnet geothermometry in granulite-facies rocks: evaluation of equilibrium criteria. *Can. Mineral., 23*, 187-193.

Jung, S., Brandt, S., Nebel, O., Hellebrand, E., Seth, B., & Jung, C. (2014). The P–T–t paths of high-grade gneisses, Kaoko Belt, Namibia: Constraints from mineral data, U–Pb allanite and monazite and Sm–Nd/Lu–Hf garnet ages and garnet ion probe data. *Gondwana Research, 25*(2), 775-796. doi:10.1016/j.gr.2013.05.017

Karabinos, P. (1985). Garnet and staurolite producing reactions in a chlorite-chloritoid schist. *Contributions to Mineralogy and Petrology, 90*(2-3), 262-275.

Konopásek, J., Kosler, J., Tajčmanová, L., Ulrich, S., & Kitt, S. L. (2008). Neoproterzoic igneous complex emplaced along major tectonic boundary in the Kaoko Belt (NW Namibia): ion probe and LA-ICP-MS dating of magmatic and metamorphic zircons. *Journal of the Geological Society, London, 165*, 153-165.

Konopásek, J., Kröner, S., Kitt, S. L., Passchier, C. W., & Kröner, A. (2005). Oblique collision and evolution of large-scale transcurrent shear zones in the Kaoko belt, NW Namibia. *Precambrian Research, 136*(2), 139-157. doi:10.1016/j.precamres.2004.10.005

Konopásek, J., Sláma, J., & Kosler, J. (2016). Linking the basement geology along the Africa-South America coasts in the South Atlantic.

Kröner, S. U. G. (2005). *Geochronological and Structural Evolution of the Western and Central Kaoko Belt in NW Namibia.* (Doktor der Naturwissenschaft), Johannes Gutenberg-Universität, Mainz.

Lenz, C., Fernandes, L. A. D., McNaughton, N. J., Porcher, C. C., & Masquelin, H. (2011). U–Pb SHRIMP ages for the Cerro Bori Orthogneisses, Dom Feliciano Belt in Uruguay: Evidences of a ∼800Ma magmatic and ∼650Ma metamorphic event. *Precambrian Research, 185*(3-4), 149-163. doi:10.1016/j.precamres.2011.01.007

Masquelin, H., D'Avila Fernandes, L. A., Lenz, C., Porcher, C. C., & McNaughton, N. J. (2012). The Cerro Olivo Complex: a pre-collisional Neoproterozoic magmatic arc in Eastern Uruguay. *International Geology Review, 54*(10), 1161-1183. doi:10.1080/00206814.2011.626597

Meert, J. G., & Van Der Voo, R. (1997). The assembly of Gondwana 800-550 Ma. *Journal of Geodynamics, 23*(3), 223-235.

Miller, R.McG., (1983). *The Pan-African Damara Orogen of South West Africa/Namibia*. In: Miller, R.M.G. (Ed.), Evolution of the Damara Orogen of South West Africa/Namibia, vol. 11, pp. 431–515, Spec. Publ. Geol. Soc. S. Afr.

Moazzen, M. (2004). Chlorite–chloritoid–garnet equilibria and geothermometry in the Sanandaj–Sirjan metamorphic belt, southern Iran. *Iran J Sci Technol, 28*, 1-14.

Oyhantcabal, P., Siegesmund, S., Wemmer, K., Presnyakov, S., & Layer, P. (2009). Geochronological constraints on the evolution of the southern Dom Feliciano Belt (Uruguay). *Journal of the Geological Society, 166*(6), 1075-1084. doi:10.1144/0016-76492008-122

Porada, H. (1979). The Damara-Riberia orogen of the Pan-African-Brasiliano cycle in Namibia (southwest Africa) and Brazil as interpreted in terms of continental collision. *Tectonophysics, 57*, 237-265.

Preciozzi, F., Peel, E., Muzio, R., Ledesma, J. J., & Guerequiz, R. (2001). *Dom Feliciano Belt and Punta del Este Terrane: geochronological features.* Paper presented at the III South American Symposium on Isotope Geology (Abstract), Pucón, Chile.

Woodcock, N. H., & Strachan, R. A. (2009). *Geological history of Britain and Ireland*: John Wiley & Sons.

Appendix

Microprobe results

UB-02

Sample:	**UB-02**								
Mineral	Bt	Bt	Bt	Bt	Bt	Bt	Bt	Bt	Bt
Data set/point	70 / 1 .	78 / 1 .	79 / 1 .	80 / 1 .	81 / 1 .	82 / 1 .	83 / 1 .	84 / 1 .	85 / 1 .
SiO2	37,658	37,495	37,896	36,683	37,684	38,025	38,206	37,303	37,539
TiO2	3,091	5,290	4,807	3,729	3,918	3,313	2,964	5,455	4,857
Cr2O3	0,000	0,000	0,017	0,000	0,000	0,002	0,000	0,008	0,002
Al2O3	15,095	15,502	15,635	15,188	15,727	15,557	15,459	15,150	15,415
FeO	13,738	15,559	13,130	15,469	13,322	13,497	13,048	13,531	15,271
MnO	0,000	0,015	0,036	0,038	0,025	0,000	0,004	0,029	0,033
MgO	13,865	11,621	12,588	12,016	13,579	13,793	14,443	11,334	11,972
CaO	0,068	0,012	0,000	0,096	0,058	0,050	0,067	0,102	0,000
Na2O	0,120	0,109	0,110	0,145	0,090	0,052	0,102	0,170	0,064
K2O	8,992	9,900	9,802	9,200	9,388	9,456	9,416	8,936	10,057
Total	92,625	95,502	94,020	92,563	93,792	93,744	93,710	92,018	95,210
No.O	11,000	11,000	11,000	11,000	11,000	11,000	11,000	11,000	11,000
Si	2,962	2,914	2,960	2,924	2,933	2,956	2,957	3,004	2,918
Ti	0,183	0,309	0,282	0,223	0,229	0,194	0,172	0,330	0,284
Cr	0,000	0,000	0,001	0,000	0,000	0,000	0,000	0,001	0,000
Al	1,400	1,420	1,440	1,427	1,443	1,426	1,410	1,438	1,413
Fe3+	0,000	0,000	0,000	0,000	0,000	0,000	0,000	0,000	0,000
Fe2+	0,904	1,011	0,858	1,031	0,867	0,877	0,844	0,911	0,993
Mn	0,000	0,001	0,002	0,003	0,002	0,000	0,000	0,002	0,002
Mg	1,626	1,346	1,465	1,428	1,576	1,598	1,666	1,360	1,387
Ca	0,006	0,001	0,000	0,008	0,005	0,004	0,006	0,009	0,000
Na	0,018	0,016	0,017	0,022	0,014	0,008	0,015	0,027	0,010
K	0,902	0,981	0,977	0,935	0,932	0,938	0,929	0,918	0,997
Total	8,000	8,000	8,002	8,002	8,001	8,001	8,000	8,000	8,004
X_{Mg}	0,643	0,571	0,631	0,581	0,645	0,646	0,664	0,599	0,583

Sample:	**UB-02**				
Position	Core	Rim	Rim		Core
Mineral	Grt	Grt	Grt	Grt	Grt
Data set/point	66 / 1 .	67 / 1 .	72 / 1 .	73 / 1 .	74 / 1 .
SiO2	38,036	37,964	37,896	37,466	37,624
TiO2	0,053	0,028	0,042	0,009	0,029
Cr2O3	0,000	0,024	0,002	0,052	0,051
Al2O3	21,418	21,427	21,540	21,310	21,376
FeO	32,791	32,165	32,833	33,304	33,493
MnO	0,630	0,575	0,680	0,638	0,690
MgO	6,537	6,552	5,661	5,803	5,968
CaO	0,907	0,958	0,995	0,978	0,897
Na2O	0,005	0,041	0,000	0,007	0,017
K2O	0,000	0,000	0,005	0,006	0,006
Total	100,376	99,733	99,653	99,574	100,151
No.O	12,000	12,000	12,000	12,000	12,000
Si	2,984	2,992	3,006	2,975	2,969
Ti	0,003	0,002	0,002	0,001	0,002
Cr	0,000	0,001	0,000	0,003	0,003
Al	1,980	1,991	2,014	1,995	1,988
Fe3+	0,046	0,026	0,000	0,052	0,070
Fe2+	2,104	2,093	2,178	2,160	2,141
Mn	0,042	0,038	0,046	0,043	0,046
Mg	0,764	0,770	0,669	0,687	0,702
Ca	0,076	0,081	0,085	0,083	0,076
Na	0,001	0,006	0,000	0,001	0,003
K	0,000	0,000	0,000	0,001	0,001
Total	8,000	8,000	8,000	8,000	8,000
$\mathbf{X_{Mg}}$	0,262	0,266	0,235	0,237	0,241
Py	0,248	0,253	0,221	0,222	0,225
Alm	0,684	0,687	0,718	0,700	0,686
Grss	0,025	0,027	0,028	0,027	0,024
Spss	0,014	0,013	0,015	0,014	0,015

Sample:	**UB-02**					
Mineral	Plag	Ksp	Ksp	Plag	Plag	Ksp
Data set/point	68 / 1 .	69 / 1 .	71 / 1 .	75 / 1 .	76 / 1 .	77 / 1 .
SiO2	59,119	64,116	64,236	58,620	58,710	63,032
TiO2	0,002	0,052	0,045	0,045	0,020	0,047
Cr2O3	0,015	0,000	0,000	0,023	0,000	0,023
Al2O3	25,274	18,630	18,740	25,778	25,380	18,428
FeO	0,044	0,047	0,048	0,037	0,037	0,040
MnO	0,010	0,000	0,000	0,021	0,000	0,000
MgO	0,000	0,006	0,006	0,000	0,000	0,003
CaO	7,617	0,185	0,229	7,612	7,735	0,104
Na2O	7,481	1,308	2,473	7,371	7,361	1,148
K2O	0,324	15,209	13,386	0,181	0,146	15,391
Total	99,885	99,553	99,162	99,686	99,389	98,217
No.O	8,000	8,000	8,000	8,000	8,000	8,000
Si	2,638	2,961	2,960	2,622	2,636	2,951
Ti	0,000	0,002	0,002	0,002	0,001	0,002
Cr	0,001	0,000	0,000	0,001	0,000	0,001
Al	1,329	1,014	1,018	1,359	1,343	1,017
Fe3+	0,002	0,002	0,002	0,001	0,001	0,002
Fe2+	0,000	0,000	0,000	0,000	0,000	0,000
Mn	0,000	0,000	0,000	0,001	0,000	0,000
Mg	0,000	0,000	0,000	0,000	0,000	0,000
Ca	0,364	0,009	0,011	0,365	0,372	0,005
Na	0,647	0,117	0,221	0,639	0,641	0,104
K	0,018	0,896	0,787	0,010	0,008	0,919
Total	5,000	5,000	5,000	5,000	5,002	5,001
An	0,354	0,009	0,011	0,360	0,364	0,005
Ab	0,628	0,115	0,217	0,630	0,627	0,101
Ksp	0,018	0,877	0,772	0,010	0,008	0,894

UA-11

Sample:	**UA-11**			
Mineral	Bt	Bt	Bt	Bt
Data set/point	43 / 1 .	44 / 1 .	45 / 1 .	55 / 1 .
SiO2	36,232	35,440	35,420	36,235
TiO2	4,553	5,366	5,702	5,109
Cr2O3	0,033	0,144	0,122	0,107
Al2O3	16,557	16,772	16,744	16,617
FeO	16,117	19,040	19,150	17,599
MnO	0,007	0,080	0,000	0,000
MgO	11,928	9,221	9,055	10,164
CaO	0,000	0,000	0,000	0,000
Na2O	0,132	0,169	0,134	0,120
K2O	9,718	9,746	9,769	9,740
Total	95,276	95,979	96,097	95,691
No.O	11,000	11,000	11,000	11,000
Si	2,812	2,784	2,786	2,836
Ti	0,266	0,317	0,337	0,301
Cr	0,002	0,009	0,008	0,007
Al	1,515	1,553	1,552	1,533
Fe3+	0,000	0,000	0,000	0,000
Fe2+	1,046	1,251	1,260	1,152
Mn	0,000	0,005	0,000	0,000
Mg	1,380	1,080	1,062	1,186
Ca	0,000	0,000	0,000	0,000
Na	0,020	0,026	0,020	0,018
K	0,962	0,977	0,980	0,972
Total	8,003	8,001	8,005	8,005
X_{Mg}	0,569	0,463	0,457	0,507

Sample:	**UA-11**								
Position		Rim	Rim	Core	Core	Rim	Core		
Mineral	Grt	Grt	Grt	Grt	Grt	Grt	Grt	Grt	Grt
Data set/point	39 / 1 .	40 / 1 .	41 / 1 .	42 / 1 .	51 / 1 .	53 / 1 .	57 / 1 .	63 / 1 .	64 / 1 .
SiO2	38,234	37,909	38,124	38,065	38,302	37,824	38,114	38,495	38,033
TiO2	0,039	0,029	0,035	0,053	0,060	0,027	0,024	0,058	0,023
Cr2O3	0,042	0,023	0,039	0,006	0,022	0,077	0,051	0,007	0,007
Al2O3	21,748	21,542	21,560	21,447	21,539	21,222	21,705	21,429	21,275
FeO	32,658	32,629	32,658	32,446	32,270	33,694	32,168	32,461	33,404
MnO	1,072	0,997	0,969	1,128	1,012	1,226	0,925	1,118	1,271
MgO	6,029	6,024	5,973	6,050	6,066	5,172	6,825	5,980	5,333
CaO	1,317	1,131	1,180	1,167	1,115	1,114	1,032	1,324	1,105
Na2O	0,008	0,007	0,000	0,000	0,000	0,015	0,008	0,022	0,038
K2O	0,011	0,012	0,002	0,002	0,008	0,000	0,005	0,004	0,003
Total	101,158	100,303	100,542	100,364	100,393	100,371	100,858	100,897	100,491
No.O	12,000	12,000	12,000	12,000	12,000	12,000	12,000	12,000	12,000
Si	2,982	2,982	2,993	2,993	3,009	2,994	2,968	3,011	3,002
Ti	0,002	0,002	0,002	0,003	0,004	0,002	0,001	0,003	0,001
Cr	0,003	0,001	0,002	0,000	0,001	0,005	0,003	0,000	0,000
Al	1,999	1,998	1,995	1,988	1,995	1,980	1,992	1,976	1,979
Fe3+	0,032	0,035	0,012	0,019	0,000	0,026	0,068	0,000	0,019
Fe2+	2,098	2,112	2,133	2,115	2,120	2,204	2,026	2,123	2,186
Mn	0,071	0,066	0,064	0,075	0,067	0,082	0,061	0,074	0,085
Mg	0,701	0,706	0,699	0,709	0,710	0,610	0,792	0,697	0,627
Ca	0,110	0,095	0,099	0,098	0,094	0,094	0,086	0,111	0,093
Na	0,001	0,001	0,000	0,000	0,000	0,002	0,001	0,003	0,006
K	0,001	0,001	0,000	0,000	0,001	0,000	0,001	0,000	0,000
Total	8,000	8,000	8,000	8,001	8,000	8,000	8,000	8,000	8,000
X_{Mg}	0,248	0,248	0,246	0,249	0,251	0,215	0,274	0,247	0,222
Py	0,229	0,231	0,231	0,234	0,233	0,200	0,254	0,228	0,206
Alm	0,686	0,690	0,705	0,697	0,695	0,723	0,651	0,695	0,719
Grss	0,036	0,031	0,033	0,032	0,031	0,031	0,028	0,036	0,031
Spss	0,023	0,022	0,021	0,025	0,022	0,027	0,020	0,024	0,028

Sample:			**UA-11**		
Mineral	Plag	Ksp	Plag	Ksp	Plag
Data set/point	49 / 1 .	50 / 1 .	58 / 1 .	59 / 1 .	60 / 1 .
SiO2	57,755	64,586	58,147	65,261	56,949
TiO2	0,025	0,024	0,000	0,024	0,019
Cr2O3	0,000	0,020	0,000	0,000	0,000
Al2O3	26,927	18,630	26,566	18,496	27,051
FeO	0,047	0,114	0,016	0,036	0,047
MnO	0,003	0,007	0,025	0,000	0,000
MgO	0,000	0,000	0,000	0,019	0,000
CaO	8,949	0,031	8,652	0,029	9,523
Na2O	6,542	1,259	6,881	2,068	6,334
K2O	0,145	15,089	0,170	13,924	0,125
Total	100,392	99,759	100,456	99,856	100,047
No.O	8,000	8,000	8,000	8,000	8,000
Si	2,578	2,979	2,589	2,996	2,554
Ti	0,001	0,001	0,000	0,001	0,001
Cr	0,000	0,001	0,000	0,000	0,000
Al	1,417	1,013	1,394	1,001	1,430
Fe3+	0,000	0,004	0,001	0,001	0,002
Fe2+	0,002	0,000	0,000	0,000	0,000
Mn	0,000	0,000	0,001	0,000	0,000
Mg	0,000	0,000	0,000	0,001	0,000
Ca	0,428	0,002	0,413	0,001	0,458
Na	0,566	0,113	0,594	0,184	0,551
K	0,008	0,888	0,010	0,815	0,007
Total	5,000	5,000	5,001	5,001	5,001
An	0,427	0,002	0,406	0,001	0,451
Ab	0,565	0,112	0,584	0,184	0,542
Ksp	0,008	0,886	0,010	0,815	0,007

Sample:	**UA-11**					
Position		Rim	Core			
Mineral	Sp	Sp	Sp	Crd	Crd	Crd
DataSet/Point	47 / 1 .	61 / 1 .	62 / 1 .	46 / 1 .	48 / 1 .	56 / 1 .
SiO2	0,020	0,027	0,000	48,942	48,887	49,627
Na2O	0,000	0,000	0,000	0,093	0,094	0,044
Al2O3	55,955	56,766	57,018	32,806	32,850	32,870
K2O	0,010	0,007	0,006	0,011	0,009	0,008
CaO	0,002	0,000	0,000	0,022	0,030	0,014
TiO2	0,044	0,047	0,027	0,004	0,055	0,009
FeO	33,276	34,031	34,300	8,816	8,238	8,071
MnO	0,158	0,118	0,101	0,099	0,087	0,068
MgO	4,083	4,277	4,416	8,635	8,772	8,741
Cr2O3	1,186	0,814	0,891	0,000	0,011	0,000
Total	94,733	96,085	96,758	99,429	99,031	99,451
No.O	4,000	4,000	4,000	18,000	18,000	18,000
Si	0,001	0,001	0,000	4,978	4,983	5,040
Na	0,000	0,000	0,000	0,018	0,018	0,009
Al	1,959	1,957	1,952	3,933	3,946	3,934
K	0,000	0,000	0,000	0,001	0,001	0,001
Ca	0,000	0,000	0,000	0,002	0,003	0,002
Ti	0,001	0,001	0,001	0,000	0,004	0,001
Fe^{3+}	0,011	0,020	0,026	0,131	0,098	0,000
Fe^{2+}	0,816	0,812	0,807	0,619	0,604	0,691
Mn	0,004	0,003	0,002	0,009	0,007	0,006
Mg	0,181	0,187	0,191	1,309	1,333	1,323
Cr	0,028	0,019	0,020	0,000	0,000	0,000
Total	3,000	3,000	3,000	11,001	10,999	11,006
X_{Mg}	0,181	0,187	0,192	0,686	0,679	0,688

Estimated effective bulk composition

UA-11.1		**Mole component**	**Molar Volume**		**Estimated Volume**	**Mole Garnet**
			J*bar-1	**Cm3/mol**		
Garnet			11,789	117,89	7,6	0,0645
Almandine	Fe	2,124	11,511	115,11		
Grossular	Ca	0,098	12,535	125,35		
Pyrope	Mg	0,6947	11,318	113,18		
Spessartine	Mn	0,0718	11,792	117,92		
	Al	1,9891				
	Si	2,9927				
Biotite			15,045	150,446667	0,00	0,0000
Al		1,53825	15,432		0,556	
Mg		1,177	14,738		1,323	
Fe		1,17725	14,964		1,0146	
Si		2,8045				
K		0,97275				
H		2				
Silimanite	Sill		4,986	49,86	9,17	0,1839
Plagioclase			10,0425	100,425	0	0,0000
Na		0,6266	10,006			
Ca		0,3568	10,079			
Al		1,3235				
Si		2,6808				
Ksp	Mic		10,892	108,92	0,87	0,0080
K		0,8811				
Na		0,1204				
Al		1,0124				
Si		2,9814				
Spinel			4,0265	40,265	5,92	0,1470
Fe	Herc	0,8117	4,075			
Mg	Sp	0,1862	3,978			
Al		1,9561				
Corderite	Crd		23,516	235,16	50,64	0,2153
Fe	fCrd	0,7126	23,71			
Mg	hCrd	1,3219	23,322			
Al		3,938				
Si		5,000				
Ilmenite	Ilm		3,169	31,69	22,41	0,7072
Sum					99,5036	

UA-11.2	Na2O	MgO	Al2O3	SiO2	K2O	CaO	TiO2	MnO	FeO	H2O
Garnet		0,0448	0,0641	0,1929		0,0063		0,0046	0,1369	
Biotite		0,0000	0,0000	0,0000	0,0000				0,0000	0,0000
Silimanite			0,0920	0,1839						
Plagioclase	0,0000		0,0000	0,0000		0,0000				
Ksp	0,0005		0,0040	0,0238	0,0035					
Spinel		0,0274	0,1438						0,1193	
Corderite		0,2847	0,4240	1,0768					0,1535	
Ilmenite							0,7072		0,7072	
Sum	0,0005	0,3568	0,7279	1,4775	0,0035	0,0063	0,7072	0,0046	1,1169	0,0000

UA-31B

Sample:	**UA-31B**				
Mineral	**Bt**	**Bt**	**Bt**	**Bt**	**Bt**
Data set/point	13/1.	14/1.	15/1.	28/1.	29/1.
SiO2	34,876	35,398	35,244	35,306	34,160
TiO2	2,669	2,605	2,268	1,898	1,857
Cr2O3	0,074	0,059	0,036	0,092	0,142
Al2O3	20,195	19,834	20,209	20,199	21,638
FeO	15,704	15,592	16,014	15,665	15,663
MnO	0,017	0,029	0,000	0,033	0,000
MgO	11,437	11,253	11,161	12,298	11,396
CaO	0,000	0,000	0,000	0,000	0,000
Na2O	0,121	0,111	0,093	0,110	0,116
K2O	9,792	9,966	9,376	9,725	9,730
Total	94,885	94,848	94,401	95,326	94,702
No.O	11,000	11,000	11,000	11,000	11,000
Si	2,692	2,735	2,739	2,699	2,633
Ti	0,155	0,151	0,133	0,109	0,108
Cr	0,004	0,004	0,002	0,006	0,009
Al	1,837	1,807	1,852	1,820	1,966
Fe3+	0,000	0,000	0,000	0,000	0,000
Fe2+	1,014	1,008	1,041	1,001	1,009
Mn	0,001	0,002	0,000	0,002	0,000
Mg	1,316	1,296	1,293	1,401	1,309
Ca	0,000	0,000	0,000	0,000	0,000
Na	0,018	0,017	0,014	0,016	0,017
K	0,964	0,982	0,930	0,948	0,957
Total	8,002	8,002	8,002	8,003	8,007
$\mathbf{X_{Mg}}$	0,565	0,563	0,554	0,583	0,565

Sample:	**UA-31B**										
Mineral	Plag	Plag	Ksp	Ksp	Oli	Ksp	Plag	Plag	Ksp	Plag	Plag
Data set/point	18 / 1 .	19 / 1 .	20 / 1 .	21 / 1 .	22 / 1 .	32 / 1 .	33 / 1 .	34 / 1 .	36 / 1 .	37 / 1 .	38 / 1 .
SiO2	57,962	57,653	64,286	64,655	69,115	64,565	60,036	58,538	64,395	58,823	59,101
TiO2	0,022	0,004	0,036	0,037	0,010	0,038	0,002	0,015	0,037	0,026	0,000
Cr2O3	0,026	0,014	0,000	0,015	0,005	0,035	0,013	0,000	0,010	0,000	0,005
Al2O3	26,349	26,416	18,547	18,681	19,774	18,580	25,341	26,231	18,491	26,181	26,069
FeO	0,076	0,040	0,016	0,060	0,025	0,007	0,071	0,037	0,025	0,010	0,027
MnO	0,000	0,025	0,000	0,000	0,000	0,000	0,000	0,015	0,018	0,000	0,023
MgO	0,000	0,000	0,024	0,000	0,000	0,010	0,003	0,000	0,026	0,000	0,000
CaO	8,429	8,767	0,026	0,045	3,017	0,041	7,325	8,351	0,000	8,182	8,209
Na2O	6,945	6,712	1,293	1,417	8,769	1,310	7,471	6,850	1,353	7,003	7,039
K2O	0,197	0,168	14,905	14,828	0,123	15,032	0,259	0,260	14,984	0,194	0,159
Total	100,007	99,798	99,134	99,738	100,837	99,617	100,522	100,297	99,338	100,419	100,632
No.O	8,000	8,000	8,000	8,000	8,000	8,000	8,000	8,000	8,000	8,000	8,000
Si	2,592	2,586	2,983	2,980	3,063	2,982	2,665	2,612	2,981	2,621	2,627
Ti	0,001	0,000	0,001	0,001	0,000	0,001	0,000	0,001	0,001	0,001	0,000
Cr	0,001	0,000	0,000	0,001	0,000	0,001	0,000	0,000	0,000	0,000	0,000
Al	1,389	1,397	1,014	1,015	1,033	1,011	1,326	1,380	1,009	1,375	1,366
Fe3+	0,003	0,002	0,001	0,002	0,000	0,000	0,001	0,001	0,001	0,000	0,000
Fe2+	0,000	0,000	0,000	0,000	0,001	0,000	0,002	0,000	0,000	0,000	0,001
Mn	0,000	0,001	0,000	0,000	0,000	0,000	0,000	0,001	0,001	0,000	0,001
Mg	0,000	0,000	0,002	0,000	0,000	0,001	0,000	0,000	0,002	0,000	0,000
Ca	0,404	0,421	0,001	0,002	0,143	0,002	0,348	0,399	0,000	0,391	0,391
Na	0,602	0,584	0,116	0,127	0,753	0,117	0,643	0,593	0,121	0,605	0,606
K	0,011	0,010	0,882	0,872	0,007	0,885	0,015	0,015	0,885	0,011	0,009
Total	5,002	5,001	5,001	5,000	5,001	5,001	5,000	5,001	5,001	5,004	5,001
An	0,397	0,415	0,001	0,002	0,159	0,002	0,346	0,397	-0,001	0,388	0,388
Ab	0,592	0,575	0,116	0,127	0,834	0,117	0,639	0,589	0,121	0,601	0,603
Ksp	0,011	0,009	0,882	0,871	0,008	0,881	0,015	0,015	0,880	0,011	0,009

Sample:	**UA-31B**										
Position	Core	Rim	Core	Rim	Rim	Rim		Core			
Mineral	Grt	Grt	Grt	Grt	Grt	Grt	Grt	Grt	Grt	Grt	Grt
Data set/point	1 / 1 .	2 / 1 .	3 / 1 .	4 / 1 .	5 / 1 .	6 / 1 .	7 / 1 .	23 / 1 .	24 / 1 .	25 / 1 .	26 / 1 .
SiO2	37,536	37,351	37,583	37,725	37,319	37,383	37,398	38,349	38,273	37,606	37,508
TiO2	0,039	0,048	0,039	0,011	0,024	0,012	0,042	0,017	0,032	0,032	0,042
Cr2O3	0,000	0,024	0,042	0,052	0,046	0,045	0,052	0,056	0,056	0,045	0,042
Al2O3	21,418	21,427	21,720	21,578	21,472	21,547	21,690	21,445	21,355	21,306	21,247
FeO	32,520	32,165	32,971	34,178	34,486	34,054	33,218	32,239	32,392	33,026	34,031
MnO	0,603	0,681	0,712	0,716	0,770	0,829	0,726	0,702	0,655	0,709	0,807
MgO	6,890	6,669	6,181	5,153	4,940	5,107	5,932	6,599	6,522	5,960	5,448
CaO	1,030	1,012	1,078	1,046	1,134	1,206	1,086	1,141	1,127	1,104	1,034
Na2O	0,001	0,016	0,014	0,000	0,017	0,000	0,011	0,012	0,032	0,007	0,000
K2O	0,000	0,042	0,009	0,004	0,007	0,011	0,006	0,000	0,003	0,011	0,000
Total	100,036	99,433	100,349	100,463	100,216	100,193	100,160	100,559	100,446	99,805	100,158
No.O	12,000	12,000	12,000	12,000	12,000	12,000	12,000	12,000	12,000	12,000	12,000
Si	2,947	2,951	2,953	2,983	2,962	2,964	2,949	2,998	2,998	2,976	2,972
Ti	0,002	0,003	0,002	0,001	0,001	0,001	0,002	0,001	0,002	0,002	0,002
Cr	0,000	0,001	0,003	0,003	0,003	0,003	0,003	0,003	0,003	0,003	0,003
Al	1,982	1,996	2,011	2,011	2,009	2,014	2,016	1,976	1,971	1,988	1,984
Fe3+	0,119	0,101	0,079	0,017	0,065	0,053	0,081	0,023	0,031	0,056	0,063
Fe2+	2,017	2,025	2,087	2,243	2,224	2,205	2,109	2,085	2,090	2,130	2,192
Mn	0,040	0,046	0,047	0,048	0,052	0,056	0,048	0,047	0,043	0,047	0,054
Mg	0,806	0,785	0,724	0,607	0,584	0,603	0,697	0,769	0,761	0,703	0,643
Ca	0,087	0,086	0,091	0,089	0,096	0,102	0,092	0,096	0,095	0,094	0,088
Na	0,000	0,002	0,002	-0,002	0,003	-0,002	0,002	0,002	0,005	0,001	0,000
K	0,000	0,004	0,001	0,000	0,001	0,001	0,001	0,000	0,000	0,001	0,000
Total	8,000	8,000	8,000	8,000	8,000	8,000	8,000	8,000	8,000	8,000	8,000
X_{Mg}	0,274	0,270	0,250	0,212	0,203	0,211	0,241	0,267	0,264	0,243	0,222
Py	0,252	0,248	0,231	0,200	0,188	0,195	0,222	0,253	0,249	0,227	0,207
Alm	0,631	0,638	0,666	0,740	0,715	0,714	0,672	0,685	0,684	0,688	0,706
Grss	0,027	0,027	0,029	0,029	0,031	0,033	0,029	0,031	0,031	0,030	0,028
Spss	0,013	0,014	0,015	0,016	0,017	0,018	0,015	0,015	0,014	0,015	0,017

Sample:	**UA-31B**						
Position	Core	Core	Rim	Rim	Rim		
Mineral	Spl	Spl	Spl	Spl	Spl	Spl	Spl
DataSet/Point	8 / 1 .	9 / 1 .	10 / 1 .	11 / 1 .	12 / 1 .	30 / 1 .	31 / 1 .
SiO2	0,033	0,000	0,041	0,031	0,025	0,006	0,023
Na2O	0,000	0,000	0,000	0,000	0,000	0,000	0,000
Al2O3	56,896	56,706	57,343	57,406	56,456	57,282	57,191
K2O	0,010	0,000	0,020	0,006	0,002	0,004	0,007
CaO	0,000	0,000	0,005	0,005	0,002	0,000	0,017
TiO2	0,044	0,019	0,028	0,077	0,121	0,076	0,029
FeO	34,629	34,023	34,280	33,166	33,887	34,951	34,971
MnO	0,098	0,061	0,074	0,036	0,050	0,057	0,026
MgO	4,031	3,963	4,055	4,294	3,968	3,959	3,957
Cr2O3	0,701	0,653	0,701	0,787	1,012	0,484	0,403
Total	96,443	95,425	96,546	95,808	95,522	96,819	96,623
No.O	4,000	4,000	4,000	4,000	4,000	4,000	4,000
Si	0,001	0,000	0,001	0,001	0,001	0,000	0,001
Na	0,000	0,000	0,000	0,000	0,000	0,000	0,000
Al	1,958	1,970	1,968	1,979	1,962	1,964	1,964
K	0,000	0,000	0,001	0,000	0,000	0,000	0,000
Ca	0,000	0,000	0,000	0,000	0,000	0,000	0,001
Ti	0,001	0,000	0,001	0,002	0,003	0,002	0,001
Fe^{3+}	0,022	0,013	0,013	0,000	0,008	0,021	0,024
Fe^{2+}	0,824	0,825	0,822	0,814	0,828	0,829	0,828
Mn	0,002	0,002	0,002	0,001	0,001	0,001	0,001
Mg	0,175	0,174	0,176	0,187	0,174	0,172	0,172
Cr	0,016	0,015	0,016	0,018	0,024	0,011	0,009
Total	3,000	3,000	3,000	3,002	3,000	3,000	3,000
X_{Mg}	0,176	0,174	0,176	0,187	0,174	0,172	0,172

Sample:	**UA-31B**			
Mineral	Crd	Crd	Crd	Crd
DataSet/Point	16 / 1 .	17 / 1 .	27 / 1 .	35 / 1 .
SiO2	48,311	48,407	49,060	48,779
Na2O	0,156	0,139	0,135	0,135
Al2O3	32,435	32,351	33,161	32,863
K2O	0,004	0,017	0,004	0,016
CaO	0,003	0,014	0,016	0,026
TiO2	0,000	0,000	0,000	0,016
FeO	8,462	8,387	7,296	8,230
MnO	0,007	0,046	0,037	0,038
MgO	8,292	8,303	9,043	8,658
Cr2O3	0,000	0,022	0,000	0,000
Total	97,669	97,685	98,751	98,760
No.O	18,000	18,000	18,000	18,000
Si	5,001	5,010	4,996	4,985
Na	0,031	0,028	0,027	0,027
Al	3,957	3,947	3,980	3,958
K	0,001	0,002	0,000	0,002
Ca	0,000	0,001	0,002	0,003
Ti	0,000	0,000	0,000	0,001
Fe^{3+}	0,076	0,064	0,058	0,100
Fe^{2+}	0,656	0,662	0,563	0,603
Mn	0,001	0,004	0,003	0,003
Mg	1,280	1,281	1,373	1,319
Cr	0,000	0,000	0,000	0,000
Total	11,003	11,000	11,001	11,002
X_{Mg}	0,661	0,659	0,709	0,686

Estimated effective bulk composition

UA-31B.1		**Mole component**	**Molar Volume**		**Estimated Volume**	**Mole Garnet**
			J*bar-1	**Cm3/mol**		
Garnet			11,789	117,89	12,32	0,1045
Almandine	Fe	2,1277	11,511	115,11		
Grossular	Ca	0,0921	12,535	125,35		
Pyrope	Mg	0,6986	11,318	113,18		
Spessartine	Mn	0,048	11,792	117,92		
	Al	1,9963				
	Si	2,9685				
Biotite			15,045	150,447	1,05	0,0070
Al		1,8564	15,432		0,3428	
Mg		1,323	14,738		1,177	
Fe		1,0146	14,964		1,1773	
Si		2,1598				
K		0,9562				
H		2				
Silimanite	Sill		4,986	49,86	3,09	0,0767
Plagioclase			10,0425	100,425	2,76	0,0275
Na		0,5703	10,006			
Ca		0,4328	10,079			
Al		1,4138				
Si		2,5738				
Ksp	Mic		10,892	108,92	2,19	0,0201
K		0,8516				
Na		0,1483				
Al		1,0069				
Si		2,9875				
Spinel			4,0265	40,265	3,09	0,0767
Fe	Herc	0,8242	4,075			
Mg	Sp	0,1758	3,978			
Al						
Corderite	Crd		23,516	235,16	68,71	0,2922
Fe	fCrd	0,6958	23,71			
Mg	hCrd	1,3132	23,322			
Al		3,9604				
Si		4,9981				
Ilmenite	Ilm		3,169	31,69	3,52	0,1111
Sum					12,32	0,1045

UA-31B.2	**Na2O**	**MgO**	**Al2O3**	**SiO2**	**K2O**	**CaO**	**TiO2**	**MnO**	**FeO**	**H2O**
Garnet		0,0730	0,1043	0,3102		0,0096		0,0050	0,2224	
Biotite		0,0092	0,0065	0,0151	0,0033				0,0071	0,0070
Silimanite			0,0767	0,0767						
Plagioclase	0,0078		0,0194	0,0707		0,0119				
Ksp	0,0015		0,0101	0,0601	0,0086					
Spinel		0,0135	0,0755						0,0633	
Corderite		0,3837	0,5786	1,4604					0,2033	
Ilmenite							0,1111		0,1111	
Sum	0,0093	0,4794	0,8711	1,9932	0,0119	0,0215	0,1111	0,0050	0,6072	0,0070

R10-18

Sample:	**R10-18**					
Mineral	Plag	Plag	Plag	Plag	Plag	Plag
Data set/point	89 / 1 .	90 / 1 .	98 / 1 .	105 / 1 .	106 / 1 .	107 / 1 .
SiO2	46,858	46,430	47,653	47,120	46,756	45,420
TiO2	0,000	0,021	0,022	0,000	0,000	0,000
Cr2O3	0,010	0,000	0,000	0,025	0,000	0,045
Al2O3	33,830	33,487	33,860	34,080	33,192	34,533
FeO	0,147	0,333	0,096	0,210	0,082	0,138
MnO	0,000	0,007	0,008	0,006	0,033	0,007
MgO	0,000	0,010	0,000	0,000	0,004	0,000
CaO	18,064	17,568	17,659	17,837	17,636	18,788
Na2O	1,516	1,726	1,715	1,750	1,710	1,142
K2O	0,016	0,033	0,038	0,035	0,039	0,017
Total	100,441	99,615	101,049	101,062	99,453	100,090
No.O	8,000	8,000	8,000	8,000	8,000	8,000
Si	2,147	2,141	2,168	2,141	2,160	2,091
Ti	0,000	0,001	0,001	0,000	0,000	0,000
Cr	0,000	0,000	0,000	0,001	0,000	0,002
Al	1,827	1,820	1,816	1,825	1,808	1,874
Fe3+	0,006	0,013	0,001	0,008	0,003	0,005
Fe2+	0,000	0,000	0,003	0,000	0,000	0,000
Mn	0,000	0,000	0,000	0,000	0,001	0,000
Mg	0,000	0,001	0,000	0,000	0,000	0,000
Ca	0,887	0,868	0,861	0,868	0,873	0,927
Na	0,135	0,154	0,151	0,154	0,153	0,102
K	0,001	0,002	0,002	0,002	0,002	0,001
Total	5,002	5,000	5,003	5,000	5,000	5,001
An	0,867	0,847	0,849	0,848	0,849	0,900
Ab	0,132	0,151	0,149	0,150	0,149	0,099
Ksp	0,001	0,002	0,002	0,002	0,002	0,001

Sample:	**R10-18**							
Position		Core	Rim				Core	Rim
Mineral	Oamp	Amp	Amp	Oamp	Oamp	Oamp	Amp	Amp
Data set/point	88 / 1 .	91 / 1 .	92 / 1 .	93 / 1 .	96 / 1 .	97 / 1 .	99 / 1 .	100 / 1 .
SiO2	55,201	46,063	52,043	54,698	54,607	54,565	45,972	47,068
TiO2	0,068	1,731	0,680	0,075	0,053	0,081	1,975	1,808
Cr2O3	0,064	0,280	0,116	0,021	0,058	0,042	0,349	0,283
Al2O3	0,370	9,211	4,473	0,431	0,688	0,489	9,325	8,573
FeO	22,069	12,816	11,697	21,103	21,828	22,823	12,752	12,497
MnO	0,550	0,189	0,205	0,553	0,671	0,583	0,153	0,216
MgO	18,940	13,447	16,518	19,312	18,690	18,468	13,196	13,888
CaO	0,705	11,530	11,503	0,904	1,069	0,534	11,547	11,554
Na2O	0,036	1,008	0,424	0,013	0,061	0,022	1,040	0,866
K2O	0,007	0,829	0,244	0,000	0,005	0,014	0,881	0,698
Total	98,009	97,104	97,901	97,111	97,731	97,621	97,190	97,450
No.O	22,000	22,000	22,000	22,000	22,000	22,000	22,000	22,000
Si	6,975	6,701	7,315	6,956	6,947	6,931	6,701	6,792
Ti	0,006	0,189	0,072	0,007	0,005	0,008	0,216	0,196
Cr	0,006	0,032	0,013	0,002	0,006	0,004	0,040	0,032
Al	0,055	1,579	0,741	0,065	0,103	0,073	1,602	1,458
Fe3+	2,332	0,575	0,849	2,244	2,322	2,424	0,458	0,590
Fe2+	0,000	0,984	0,526	0,000	0,000	0,000	1,096	0,918
Mn	0,059	0,023	0,024	0,060	0,072	0,063	0,019	0,026
Mg	3,567	2,916	3,460	3,660	3,544	3,496	2,867	2,987
Ca	0,095	1,797	1,732	0,123	0,146	0,073	1,803	1,786
Na	0,009	0,284	0,116	0,003	0,015	0,005	0,294	0,242
K	0,001	0,154	0,044	0,000	0,001	0,002	0,164	0,128
Total	13,105	15,235	14,891	13,119	13,161	13,080	15,261	15,157
$\mathbf{X_{Mg}}$	0,605	0,652	0,716	0,620	0,604	0,591	0,648	0,665

Sample:	**R10-18**						
Position	Core	Rim				Rim	Core
Mineral	Opx	Opx	Opx	Opx	Opx	Opx	Opx
Data set/point	86 / 1 .	87 / 1 .	94 / 1 .	102 / 1 .	103 / 1 .	150 / 1 .	151 / 1 .
SiO2	52,498	52,681	52,588	52,217	52,669	51,948	51,963
TiO2	0,079	0,097	0,093	0,115	0,089	0,076	0,107
Cr2O3	0,028	0,075	0,033	0,057	0,039	0,043	0,095
Al2O3	0,625	0,560	0,635	0,739	0,491	0,684	0,676
FeO	26,264	26,349	26,612	26,595	26,757	26,563	26,264
MnO	0,672	0,754	0,705	0,674	0,700	0,730	0,666
MgO	19,594	19,367	19,742	19,585	19,889	19,218	19,500
CaO	0,830	0,729	0,771	0,803	0,569	0,781	0,793
Na2O	0,027	0,002	0,000	0,000	0,000	0,000	0,015
K2O	0,000	0,005	0,008	0,004	0,010	0,004	0,012
Total	100,617	100,617	101,186	100,788	101,214	100,047	100,091
No.O	3,000	3,000	3,000	3,000	3,000	3,000	3,000
Si	1,965	1,981	1,985	1,976	1,981	1,986	1,965
Ti	0,004	0,004	0,003	0,003	0,002	0,003	0,004
Cr	0,001	0,001	0,001	0,001	0,002	0,001	0,001
Al	0,034	0,028	0,029	0,024	0,021	0,028	0,034
Fe3+	0,028	0,004	0,000	0,017	0,011	0,000	0,028
Fe2+	0,827	0,820	0,823	0,825	0,814	0,827	0,827
Mn	0,023	0,022	0,020	0,021	0,022	0,021	0,023
Mg	1,087	1,106	1,105	1,109	1,121	1,098	1,087
Ca	0,032	0,031	0,036	0,023	0,025	0,035	0,032
Na	0,000	0,003	0,000	0,000	0,000	0,001	0,000
K	0,000	0,000	0,000	0,000	0,000	0,000	0,000
Total	4,000	4,000	4,002	4,000	4,000	4,001	4,000
Enst	0,543	0,553	0,552	0,555	0,561	0,543	0,553
Ferr	0,413	0,410	0,412	0,413	0,407	0,413	0,410

Sample:	**R10-18**							
Position	Core	Rim	Core	Rim	Rim	Core	Rim	Core
Mineral	Opx	Opx	Opx	Opx	Opx	Opx	Opx	Opx
Data set/point	152 / 1 .	153 / 1 .	154 / 1 .	155 / 1 .	156 / 1 .	152 / 1 .	153 / 1 .	157 / 1 .
SiO2	51,546	52,081	52,331	51,875	52,208	52,580	51,546	52,580
TiO2	0,130	0,131	0,122	0,090	0,077	0,106	0,130	0,106
Cr2O3	0,019	0,031	0,050	0,047	0,074	0,035	0,019	0,035
Al2O3	0,753	0,633	0,652	0,533	0,463	0,627	0,753	0,627
FeO	26,812	25,892	25,956	26,437	26,010	26,193	26,812	26,193
MnO	0,722	0,668	0,621	0,648	0,693	0,656	0,722	0,656
MgO	19,125	19,503	19,543	19,535	19,828	19,500	19,125	19,500
CaO	0,793	0,764	0,881	0,573	0,627	0,876	0,793	0,876
Na2O	0,000	0,045	0,000	0,000	0,000	0,009	0,000	0,009
K2O	0,001	0,000	0,000	0,004	0,003	0,000	0,001	0,000
Total	99,900	99,748	100,155	99,741	99,983	100,581	99,900	100,581
No.O	3,000	3,000	3,000	3,000	3,000	3,000	3,000	3,000
Si	1,965	1,981	1,985	1,976	1,981	1,986	1,965	1,986
Ti	0,004	0,004	0,003	0,003	0,002	0,003	0,004	0,003
Cr	0,001	0,001	0,001	0,001	0,002	0,001	0,001	0,001
Al	0,034	0,028	0,029	0,024	0,021	0,028	0,034	0,028
Fe3+	0,028	0,004	0,000	0,017	0,011	0,000	0,028	0,000
Fe2+	0,827	0,820	0,823	0,825	0,814	0,827	0,827	0,827
Mn	0,023	0,022	0,020	0,021	0,022	0,021	0,023	0,021
Mg	1,087	1,106	1,105	1,109	1,121	1,098	1,087	1,098
Ca	0,032	0,031	0,036	0,023	0,025	0,035	0,032	0,035
Na	0,000	0,003	0,000	0,000	0,000	0,001	0,000	0,001
K	0,000	0,000	0,000	0,000	0,000	0,000	0,000	0,000
Total	4,000	4,000	4,002	4,000	4,000	4,001	4,000	4,001
Enst	0,543	0,553	0,552	0,555	0,561	0,543	0,553	0,549
Ferr	0,413	0,410	0,412	0,413	0,407	0,413	0,410	0,414

Sample:	**R10-18**					
Mineral	Bt	Bt	Bt	Bt	Bt	Bt
Data set/point	97 / 1 .	101 / 1 .	104 / 1 .	108 / 1 .	109 / 1 .	110 / 1 .
SiO2	37,518	37,109	37,668	37,463	37,162	37,252
TiO2	5,683	5,334	4,688	4,502	4,331	5,107
Cr2O3	0,312	0,349	0,349	0,323	0,303	0,386
Al2O3	14,252	14,274	14,489	14,264	14,313	14,385
FeO	15,403	15,186	15,304	15,640	15,608	15,474
MnO	0,057	0,042	0,078	0,072	0,051	0,033
MgO	0,000	0,000	0,000	0,000	0,000	0,000
CaO	13,508	13,643	14,048	13,909	14,013	13,741
Na2O	0,000	0,000	0,000	0,069	0,000	0,000
K2O	0,201	0,178	0,162	0,194	0,188	0,191
Total	9,615	9,691	9,520	9,408	9,346	9,587
No.O	11,000	11,000	11,000	11,000	11,000	11,000
Si	2,872	2,856	2,876	2,875	2,865	2,856
Ti	0,327	0,309	0,269	0,260	0,251	0,294
Cr	0,019	0,021	0,021	0,020	0,018	0,023
Al	1,286	1,295	1,304	1,290	1,301	1,300
Fe3+	0,000	0,000	0,000	0,000	0,000	0,000
Fe2+	0,986	0,977	0,977	1,004	1,006	0,992
Mn	0,004	0,003	0,005	0,005	0,003	0,002
Mg	1,541	1,565	1,598	1,591	1,610	1,570
Ca	0,000	0,000	0,000	0,006	0,000	0,000
Na	0,030	0,026	0,024	0,029	0,028	0,028
K	0,939	0,951	0,927	0,921	0,919	0,938
Total	8,004	8,002	8,001	8,000	8,002	8,003
$\mathbf{X_{Mg}}$	0,610	0,616	0,621	0,613	0,615	0,613

NI-123

Sample:	**NI-123**					
Mineral	Ms	Ms	Ms	Bt	Bt	Bt
Data set/point	115 / 1 .	117 / 1 .	128 / 1 .	114 / 1 .	116 / 1 .	126 / 1 .
SiO2	46,830	45,617	46,024	34,868	35,027	34,334
TiO2	1,360	1,277	0,912	3,525	2,713	3,176
Cr2O3	0,000	0,047	0,007	0,003	0,014	0,023
Al2O3	32,791	35,339	35,812	18,527	18,093	18,934
FeO	1,763	1,175	1,157	21,495	20,983	20,870
MnO	0,020	0,004	0,031	0,372	0,364	0,337
MgO	1,207	0,681	0,732	7,364	7,872	7,055
CaO	0,000	0,000	0,000	0,000	0,000	0,000
Na2O	0,219	0,451	0,502	0,083	0,060	0,119
K2O	10,952	10,740	10,705	9,980	9,761	9,953
Total	95,144	95,332	95,881	96,218	94,886	94,801
No.O	11,000	11,000	11,000	11,000	11,000	11,000
Si	3,147	3,048	3,050	2,749	2,787	2,742
Ti	0,069	0,064	0,045	0,209	0,162	0,191
Cr	0,000	0,003	0,000	0,000	0,001	0,001
Al	2,598	2,784	2,798	1,722	1,697	1,782
Fe3+	0,000	0,000	0,000	0,000	0,000	0,000
Fe2+	0,099	0,066	0,064	1,417	1,396	1,394
Mn	0,001	0,000	0,002	0,025	0,024	0,023
Mg	0,000	0,000	0,000	0,865	0,934	0,840
Ca	0,121	0,068	0,072	0,000	0,000	0,000
Na	0,000	0,000	0,000	0,013	0,009	0,018
K	0,029	0,058	0,064	1,004	0,991	1,014
Total	0,939	0,915	0,905	8,004	8,002	8,004
X_{Mg}	0,550	0,508	0,530	0,379	0,401	0,376

Sample:	**NI-123**						
Mineral	Ksp	Plag	Ksp	Ksp	Ksp	Plag	Plag
Data set/point	113 / 1 .	120 / 1 .	127 / 1 .	130 / 1 .	131 / 1 .	132 / 1 .	133 / 1 .
SiO2	63,559	61,015	64,281	64,570	64,556	61,294	60,649
TiO2	0,019	0,000	0,009	0,003	0,017	0,000	0,003
Cr2O3	0,000	0,035	0,000	0,003	0,008	0,000	0,000
Al2O3	18,247	24,134	18,565	18,599	18,455	24,770	24,880
FeO	0,007	0,028	0,032	0,002	0,023	0,024	0,020
MnO	0,000	0,030	0,000	0,019	0,049	0,000	0,006
MgO	0,006	0,000	0,004	0,005	0,000	0,000	0,000
CaO	0,000	6,140	0,000	0,037	0,000	6,683	6,874
Na2O	1,001	7,961	0,676	1,320	1,145	7,799	7,599
K2O	15,736	0,377	16,115	14,873	15,281	0,306	0,358
Total	98,576	99,720	99,682	99,430	99,534	100,876	100,387
No.O	8,000	8,000	8,000	8,000	8,000	8,000	8,000
Si	2,967	2,723	2,974	2,987	2,987	2,709	2,695
Ti	0,001	0,000	0,000	0,000	0,001	0,000	0,000
Cr	0,000	0,001	0,000	0,000	0,000	0,000	0,000
Al	1,004	1,270	1,013	1,014	1,007	1,291	1,303
Fe3+	0,000	0,000	0,001	0,000	0,001	0,000	0,000
Fe2+	0,000	0,001	0,000	0,000	0,000	0,001	0,001
Mn	0,000	0,001	0,000	0,001	0,002	0,000	0,000
Mg	0,000	0,000	0,000	0,000	0,000	0,000	0,000
Ca	0,000	0,294	0,000	0,002	0,000	0,316	0,327
Na	0,091	0,689	0,061	0,118	0,103	0,668	0,655
K	0,937	0,021	0,951	0,878	0,902	0,017	0,020
Total	5,000	5,000	5,000	5,000	5,002	5,002	5,002
An	0,000	0,292	0,000	0,002	0,000	0,316	0,327
Ab	0,088	0,686	0,060	0,119	0,101	0,667	0,653
Ksp	0,912	0,021	0,940	0,880	0,899	0,017	0,020

Sample:	**NI-123**					
Position					Rim	
Mineral	Grt	Grt	Grt	Grt	Grt	Grt
Data set/point	111 / 1 .	112 / 1 .	118 / 1 .	119 / 1 .	121 / 1 .	122 / 1 .
SiO2	36,477	36,553	37,104	37,302	36,238	36,676
TiO2	0,013	0,000	0,000	0,001	0,012	0,002
Cr2O3	0,007	0,051	0,012	0,013	0,013	0,000
Al2O3	20,942	20,887	20,853	20,873	20,468	20,851
FeO	30,779	28,428	29,308	30,543	28,516	29,063
MnO	7,952	10,411	9,924	8,376	11,237	10,295
MgO	2,763	2,189	2,274	2,799	2,009	2,225
CaO	1,262	1,385	1,205	1,140	1,264	1,275
Na2O	0,003	0,043	0,013	0,003	0,006	0,000
K2O	0,000	0,028	0,000	0,000	0,000	0,006
Total	100,199	99,974	100,691	101,050	99,762	100,393
No.O	12,000	12,000	12,000	12,000	12,000	12,000
Si	2,944	2,964	2,989	2,986	2,955	2,965
Ti	0,001	0,000	0,000	0,000	0,001	0,000
Cr	0,000	0,003	0,001	0,001	0,001	0,000
Al	1,992	1,996	1,980	1,970	1,968	1,987
Fe3+	0,117	0,084	0,043	0,057	0,119	0,082
Fe2+	1,960	1,844	1,932	1,988	1,825	1,883
Mn	0,544	0,715	0,677	0,568	0,776	0,705
Mg	0,332	0,265	0,273	0,334	0,244	0,268
Ca	0,109	0,120	0,104	0,098	0,110	0,110
Na	0,001	0,007	0,002	0,000	0,001	0,000
K	0,000	0,003	0,000	0,000	0,000	0,001
Total	8,001	8,001	8,001	8,001	8,001	8,001
$\mathbf{X_{Mg}}$	0,138	0,121	0,122	0,140	0,112	0,120
Py	0,104	0,084	0,089	0,108	0,076	0,086
Alm	0,614	0,588	0,630	0,643	0,571	0,602
Grss	0,034	0,038	0,034	0,032	0,035	0,035
Spss	0,170	0,228	0,221	0,184	0,243	0,225

NO-08

Sample:	**NO-08**					
Mineral	Grt	Grt	Grt	Grt	Grt	Grt
Data set/point	138 / 1 .	139 / 1 .	140 / 1 .	141 / 1 .	143 / 1 .	149 / 1 .
SiO2	37,256	37,508	37,436	37,407	37,492	37,256
TiO2	0,000	0,001	0,020	0,000	0,000	0,000
Cr2O3	0,000	0,032	0,001	0,000	0,026	0,000
Al2O3	21,001	21,008	20,840	21,021	20,953	21,001
FeO	33,858	33,227	33,255	33,491	33,628	33,858
MnO	4,451	4,186	4,146	4,646	4,385	4,451
MgO	2,784	3,009	2,919	2,444	3,027	2,784
CaO	1,473	1,496	1,496	1,488	1,323	1,473
Na2O	0,000	0,042	0,083	0,038	0,016	0,000
K2O	0,013	0,000	0,040	0,010	0,006	0,013
Total	100,835	100,508	100,236	100,543	100,856	100,835
No.O	12,000	12,000	12,000	12,000	12,000	12,000
Si	2,986	3,007	3,010	3,009	2,999	2,986
Ti	0,000	0,000	0,001	0,000	0,000	0,000
Cr	0,000	0,002	0,000	0,000	0,002	0,000
Al	1,984	1,985	1,975	1,993	1,976	1,984
Fe3+	0,045	0,006	0,020	0,000	0,029	0,045
Fe2+	2,224	2,222	2,216	2,253	2,221	2,224
Mn	0,302	0,284	0,282	0,317	0,297	0,302
Mg	0,333	0,360	0,350	0,293	0,361	0,333
Ca	0,126	0,129	0,129	0,128	0,113	0,126
Na	0,000	0,006	0,013	0,006	0,002	0,000
K	0,000	0,000	0,004	0,001	0,001	0,000
Total	8,001	8,000	8,000	8,001	8,001	8,001
X_{Mg}	0,128	0,139	0,135	0,115	0,119	0,138
Py	0,108	0,118	0,114	0,096	0,102	0,119
Alm	0,725	0,731	0,721	0,742	0,752	0,729
Grss	0,041	0,042	0,042	0,042	0,041	0,037
Spss	0,099	0,094	0,092	0,104	0,099	0,098

Sample:	**NO-08**			
Mineral	Bt	Bt	Bt	Bt
Data set/point	134 / 1 .	136 / 1 .	146 / 1 .	147 / 1 .
SiO2	35,506	35,610	35,149	36,219
TiO2	1,636	1,660	1,694	1,796
Cr2O3	0,049	0,000	0,043	0,000
Al2O3	19,505	19,294	19,144	19,639
FeO	19,064	19,521	19,662	18,871
MnO	0,079	0,088	0,034	0,041
MgO	9,903	9,634	9,718	9,779
CaO	0,000	0,000	0,000	0,000
Na2O	0,171	0,185	0,169	0,186
K2O	9,285	9,406	9,259	9,193
Total	95,197	95,398	94,871	95,723
No.O	11,000	11,000	11,000	11,000
Si	2,766	2,775	2,754	2,808
Ti	0,096	0,097	0,100	0,105
Cr	0,003	0,000	0,003	0,000
Al	1,791	1,772	1,768	1,795
Fe3+	0,000	0,000	0,000	0,000
Fe2+	1,242	1,272	1,288	1,223
Mn	0,005	0,006	0,002	0,003
Mg	1,150	1,119	1,135	1,130
Ca	0,000	0,000	0,000	0,000
Na	0,026	0,028	0,026	0,028
K	0,923	0,935	0,925	0,909
Total	8,000	8,005	8,001	8,001
$\mathbf{X_{Mg}}$	0,481	0,468	0,468	0,480

Sample:	**NO-08**			
Mineral	Plag	Plag	Plag	Plag
Data set/point	135 / 1 .	137 / 1 .	142 / 1 .	145 / 1 .
SiO2	60,155	60,304	59,696	60,998
TiO2	0,000	0,000	0,000	0,000
Cr2O3	0,000	0,028	0,000	0,003
Al2O3	25,162	25,018	24,894	24,576
FeO	0,113	0,048	0,000	0,016
MnO	0,000	0,011	0,033	0,014
MgO	0,000	0,000	0,000	0,000
CaO	7,179	6,922	6,886	6,291
Na2O	7,640	7,690	7,921	8,173
K2O	0,104	0,098	0,084	0,103
Total	100,353	100,120	99,513	100,174
No.O	8,000	8,000	8,000	8,000
Si	2,673	2,685	2,669	2,706
Ti	0,000	0,000	0,000	0,000
Cr	0,000	0,001	0,000	0,000
Al	1,318	1,313	1,312	1,285
Fe3+	0,000	0,000	0,000	0,001
Fe2+	0,004	0,002	0,000	0,000
Mn	0,000	0,000	0,001	0,001
Mg	0,000	0,000	0,000	0,000
Ca	0,342	0,330	0,330	0,299
Na	0,658	0,664	0,687	0,703
K	0,006	0,006	0,005	0,006
Total	5,000	5,001	5,002	5,000
An	0,340	0,330	0,323	0,297
Ab	0,654	0,664	0,672	0,698
Ksp	0,006	0,006	0,005	0,006